NASA TECHNICAL NOTE

NASA TN D-3920

NASA TN D-3920

FREE JET IMPINGEMENT NORMAL TO A CURVED SURFACE IN A VACUUM

by Leonard V. Clark

Langley Research Center
Langley Station, Hampton, Va.

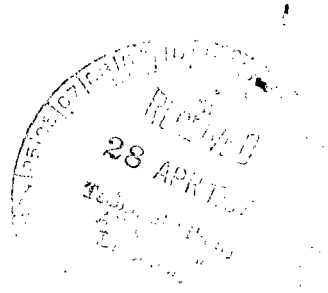

NATIONAL AERONAUTICS AND SPACE ADMINISTRATION • WASHINGTON, D. C. • APRIL 1967

Completed - 23 May 68 - Ltr

ERRATA

NASA Technical Note D-3920

FREE JET IMPINGEMENT NORMAL TO A CURVED SURFACE IN A VACUUM

By Leonard V. Clark

April 1967

Page 10: Equation (10) is in error. It should read

$$\frac{p_s}{p_c} = \frac{K+2}{2}\left[\frac{h + R(1 - \cos\omega)}{r_e}\right]^{-2} \frac{F}{p_c A_e}(\cos\theta)^{K+2}\left[\cos(\theta + \omega)\right]^2 \qquad (10)$$

Page 16: Equation (20) is in error. It should read

$$\frac{p_s}{p_{stag}} = (\cos\theta)^{K+2}\left[\cos(\theta + \omega)\right]^2\left[1 + \frac{R}{h}(1 - \cos\omega)\right]^{-2} \qquad (20)$$

Note: Equation (20) was used to provide a theoretical comparison with experimental data in figures 31, 32, and 33 (pp. 58 to 60). Applying this corrected equation to the experimental data of these figures improves the comparison slightly at large values of ω.

NASA-Langley, 1968

Issued 3-19-68

NASA TN D-3920

FREE JET IMPINGEMENT NORMAL TO A CURVED SURFACE IN A VACUUM

By Leonard V. Clark

Langley Research Center
Langley Station, Hampton, Va.

NATIONAL AERONAUTICS AND SPACE ADMINISTRATION

For sale by the Clearinghouse for Federal Scientific and Technical Information
Springfield, Virginia 22151 – CFSTI price $3.00

FREE JET IMPINGEMENT NORMAL TO A CURVED SURFACE IN A VACUUM*

By Leonard V. Clark
Langley Research Center

SUMMARY

An experimental investigation of highly underexpanded exhaust jets impinging normal to a curved surface was conducted in the Langley 55-foot vacuum cylinder. The investigation included measurements of impingement pressures and of various bow-shock characteristics. The curved surfaces were semicircular cylinders and impingement pressures were measured both along and around the cylinders which were located at various distances from the exhaust jets. Three nozzles were used with unheated nitrogen and helium; thus, six different sonic and hypersonic jets could be studied. The tests were conducted at pressure altitudes at or above 200,000 feet (61 km). The experimental data are compared with available theory to determine the applicability of analytical methods for predicting exhaust-jet impingement pressures for a range of conditions.

The results of this investigation verify previous experience and analysis and indicate that Roberts' simplified analysis is as good as the more cumbersome method of characteristics plus Newtonian analysis for determining impingement pressures resulting from underexpanded exhaust jets.

INTRODUCTION

Exhaust jets are finding many useful applications in space at the present time such as attitude control of spacecraft and spacecraft propulsion. The expansion of these jets because of the low ambient pressure in space may complicate such operations as staging, rendezvous, and docking, and even a lunar landing. During orbital rendezvous of vehicles with space stations, for example, the vehicle will necessarily maneuver in many directions. The possibility of the exhaust from thrust or control systems being directed toward the station is not unlikely. If the exhaust impinges upon the station, it may provide a sufficient force to change the stations' orbital characteristics. During a lunar

*The information presented herein is based upon a thesis entitled "An Investigation of Highly Underexpanded Exhaust Jets Impinging Normal to a Curved Surface" submitted by Leonard V. Clark in partial fulfillment of the requirements for the degree of Master of Science in Engineering Mechanics, Virginia Polytechnic Institute, Blacksburg, Virginia, March 1966.

landing, a vehicle like the Apollo lunar module (LM) must brake its approach velocity by using retrograde rockets. One of the problems to be considered in this instance is the exhaust plume interference with the landing radar system as the LM maneuvers in closing with the lunar surface. These and other problems are summarized in reference 1.

The characteristics of exhaust jets depend to some extent upon the ratio of jet-exit pressure to ambient pressure. When the ambient pressure is less than the jet-exit pressure, some expansion takes place outside the jet nozzle. A jet operating under this condition is generally referred to as an underexpanded jet. The character of underexpanded free jets is well known as evidenced by references 2 and 3, two of many published works. However, a knowledge of the character of impinging jets has only recently become important and is less well known. There are few published experimental papers and the adequacy of available theory for predicting impingement pressures has not been widely demonstrated. The studies of references 4 to 6 were concerned with experimentally determining impingement pressures on flat plates oriented parallel to or at slight angles to the jet exhaust axis. The applicability of an analysis using the method of characteristics and Newtonian flow theory (hereinafter called characteristics plus Newtonian analysis) was demonstrated in reference 5 for jets at one location parallel to a plate and using nitrogen and helium. The studies of references 7 and 8 were concerned with experimentally determining impingement pressures on flat plates oriented normal to the jet-exhaust axis. Variables, such as distance of the jet away from the plate, jet-exit Mach number, nozzle contour, and the ratio of jet-exit pressure to ambient pressure, were studied. The applicability of a characteristics plus Newtonian analysis and an approximate analysis developed by Roberts in references 9 and 10 was demonstrated in reference 8.

An examination of available literature revealed little information regarding the influence of either scale effect of jet size relative to the surface or surface shape on the distribution of impingement pressures. The present study was undertaken to determine the applicability of available theory for predicting impingement pressures for a range of these conditions. Impingement pressures were measured on several semicircular cylinders having different curvature for several underexpanded sonic and hypersonic exhaust jets. The jet axis was maintained perpendicular to the surface longitudinal axis of symmetry to provide data directly comparable with theory. The experiments were conducted in the Langley 55-foot vacuum cylinder and included a shadowgraph study of the exhaust-impingement region on one of the surfaces for the different jets from which certain bow-shock characteristics were measured.

SYMBOLS

The units used for the physical quantities defined in this paper are given both in the U.S. Customary Units and in the International System of Units (SI). Factors relating the two systems are given in reference 11.

A	area
d	diameter
dA	differential area
F	thrust
h	distance measured along jet axis from jet exit to surface
K	constant given by equation (11)
l	distance measured along model surface in axial direction from jet-axis impingement point
M	Mach number
p	static pressure
q	dynamic pressure
r	radial distance measured from jet axis
R	gas constant
s	distance measured along model surface in circumferential direction from jet-axis impingement point
T	temperature
V	velocity
x	distance measured along jet axis from jet exit
α	streamline inclination angle measured from jet axis

γ	ratio of specific heats
δ	initial expansion of exhaust at nozzle exit measured between jet axis and tangent to jet boundary
Δ	bow-shock standoff distance along jet axis
θ	azimuthal angle measured from jet center line at jet exit
θ_e	nozzle-exit half-angle
ν	Prandtl-Meyer expansion angle
ρ	density of exhaust gas
ω	angle measured from jet axis at model center of curvature

Subscripts:

a	jet axis
B	bow-shock bowl
c	nozzle settling chamber
e	nozzle exit
m	model
max	maximum
N	normal
r	shock recovery conditions
s	surface
stag	jet-axis impingement point (stagnation)
T	tangential

1 denotes a particular point in the exhaust flow field

∞ vacuum chamber conditions (ambient)

APPARATUS AND PROCEDURE

Test Setup and Procedure

The experimental investigation was conducted in the Langley 55-foot (16.7 m) vacuum cylinder with the test setup shown in figure 1. High-pressure unheated gas was supplied to the nozzle from a bottle farm located outside the cylinder with the nozzle-chamber pressure not regulated. Nozzle-chamber pressures measured during the experiments ranged from 340 to 1630 psia (2.34×10^6 to 11.2×10^6 N/m^2) and the vacuum-chamber pressure prior to initiation of jet-exhaust flow was between 0.050 to 0.155 torr (6.67 to 20.6 N/m^2). These nozzle-chamber pressures are realistic of those for present launch-vehicle propulsion systems while nozzle-chamber pressures of approximately 100 psia (0.689×10^6 N/m^2) are realistic for operation of exhaust jets for spacecraft control and propulsion. The vacuum-chamber pressure would correspond to an altitude above the earth of approximately 200,000 feet (61 km). Figure 1 shows the general arrangement of the nozzle, quick-acting valve, impingement surface, shadowgraph light source, mirrors, and 70-mm sequence camera.

The impingement surfaces, semicircular cylinders, were mounted perpendicular to the nozzle axial center line. Surface pressure distributions were measured both along and around the cylinders which were located at various distances from the six different exhaust jets used in this investigation. A solenoid valve located in the gas supply line a short distance from the nozzle permitted the nozzle to be operated remotely. In addition, the test nozzle was mounted on a movable carriage; this mounting permitted the distance between the nozzle and the surface to be varied remotely. These features made vacuum-chamber repressurization necessary only for model or nozzle changes. The duration of a typical test at a particular jet height was about 3 seconds during which time the vacuum chamber pressure increased by about 0.150 torr (20.0 N/m^2). For a subsequent test, the nozzle height was changed and the volume of gas exhausted into the vacuum chamber from the previous test was evacuated by pumps which were kept in continuous operation.

Impingement Surfaces

The cylindrical impingement surfaces are shown dimensionally in figure 2. The locations of the static-pressure orifices along and around the surface of the cylinders are indicated in figure 2. Also shown is the coordinate system l, ω at the center of

which the jet-exhaust axis was alined. The static-pressure orifices were 0.038 inch (0.0965 cm) in diameter.

Test Nozzles

The investigation was conducted with three nozzles which are shown dimensionally in figure 3. Using two gases with each of the nozzles actually permitted six different exhaust jets to be studied. One of the nozzles was a converging $(M_e = 1.0)$ nozzle whereas the other two nozzles were converging-diverging conical nozzles with an area ratio of 25 with an exit half-angle of 15^o. The two converging-diverging nozzles differed only in size, one being twice as large as the other. The nominal design exit Mach number of the converging-diverging nozzles was 5.0 with nitrogen and 7.09 with helium. The investigation reported in reference 6 used a similar converging-diverging nozzle with air and showed by a static-pressure measurement in the expansion wall near the nozzle exit that the jet actually had an indicated Mach number of 4.79 instead of the inviscid design value of 5. In addition, measurements of the initial turning angle of the exhaust flow at the nozzle exit δ obtained from schlieren photographs at known values of the ratio of nozzle chamber pressure to ambient pressure indicated an effective nozzle-exit half-angle δ of 26.5^o instead of the inviscid design value of 15^o.

The calculated exhaust initial turning angle for the jets used in this study for various values of the ratio of jet-exit pressure to ambient pressure is shown in figure 4. This angle was computed by using the approach discussed in reference 1 for the properties of nitrogen and helium ascertained from the compressible flow tables of references 12 and 13. Also shown in the figure is the maximum possible turning angle for each of the nozzles which occurs at an infinite pressure ratio. The figure indicates that even at the finite operating pressure ratios of the present tests, the jets were not too far from being fully expanded.

Instrumentation

Nozzle-chamber pressure was measured by a 2000-psia $(13.8 \times 10^6\ N/m^2)$ capacity pressure transducer located in the nozzle-settling chamber as shown in figure 3. The vacuum-chamber ambient pressure was measured before and after the short test period by a thermopile-type pressure gage that had been calibrated with a McLeod gage. The impingement surface was equipped with static-pressure orifices which were connected to strain-gage diaphragm-type absolute pressure gages by short lengths of plastic tubing. The orifice on the jet axis was connected to a 10-psia $(68.9 \times 10^3\ N/m^2)$ capacity gage. The surrounding four orifices were connected to 5-psia $(34.5 \times 10^3\ N/m^2)$ capacity gages. The next orifice in each row was connected to a 3-psia $(20.7 \times 10^3\ N/m^2)$ capacity gage and the remaining orifices were connected to 1-psia $(6.89 \times 10^3\ N/m^2)$ capacity gages.

All pressures were recorded during the tests on an oscillograph. Nozzle position was indicated on the same oscillograph by the output of a potentiometer. During the tests the pressure gages were operating anywhere from 10 to 100 percent of the gage rating and it is estimated that the overall accuracy of the data is ±2 percent.

The response time of the various pressure gages is of importance because of the short test time. In figure 5 are presented the nozzle-chamber and surface stagnation pressure history for a portion of a typical test. For the present tests the impingement pressure data were selected at a time when a constant ratio of surface to nozzle-chamber pressure existed. This time ranged from 0.3 second for the gage measuring stagnation pressure (fig. 5) to 0.7 second for the outermost gages.

During some of the tests, shadowgraphs of the jet exhaust in the vicinity of the impingement surface were obtained by using the system depicted in figure 1. For this system a beam of light produced by a commercial, 25-watt zirconium concentrated-arc, point source located at the focus of an 18-inch-diameter (0.457 m) parabolic mirror was adjusted to be parallel to the impingement surface. This beam was intercepted by another 18-inch-diameter (0.457 m) parabolic mirror located on the other side of the vacuum chamber and was directed into a lensless 70-mm sequence camera. Both the light source and camera were contained in pressure boxes which were vented to atmospheric pressure and equipped with glass viewing ports.

ANALYSIS

The experimental data obtained during the present tests were compared with the results obtained from two methods of approximate analysis. Both methods use Newtonian flow theory to get the impingement pressure; however, the properties of the jet exhaust are obtained differently. One uses the method of characteristics whereas the other uses a simplified integral method. A good discussion of Newtonian flow theory is given in reference 14.

Characteristics Plus Newtonian Analysis

In this method the flow properties of the exhaust are calculated by the method of characteristics, and then the surface pressures are estimated by Newtonian theory. A discussion of the method of characteristics may be found in reference 15 which also provides a computer program for calculating the characteristic network for any jet operating in an underexpanded condition. This particular program yields jet-exhaust boundary coordinates and several additional internal parameters in the flow field, one of which is the local Mach number. To determine impingement pressures, plots of constant Mach number contours and constant-flow-inclination contours within the exhaust plume

were required for use with Newtonian theory. A computer program to interpolate between consecutive points in the characteristic net to obtain these contours was available only for Mach number contours (ref. 16). Available calculated contours were utilized, where possible, for expediency. For example, reference 8 contains the Mach number contours for a sonic jet and an $M_e = 4.79$, $\theta_e = 26.5^o$ jet for air ($\gamma = 1.4$). These contours, shown in figure 6, were considered to be applicable for the nitrogen jets of the present study as the properties of nitrogen and air (79-percent nitrogen) are very similar. They were computed for a specific ratio of nozzle-chamber pressure to ambient pressure; however, as noted in reference 8 the contours are unaffected by additional increases in pressure ratio. In figure 6(b) can be seen the leading characteristic line as determined from the nozzle-exit Mach number by the method detailed in reference 2. The leading characteristic line serves as a dividing line between the internal flow region where the flow characteristics are determined by the nozzle contour and the external flow region where the flow characteristics are determined by the ratio of jet-exit pressure to ambient pressure. For conical nozzles the leading characteristic line is curved and the flow in the internal region is radial and axisymmetric. The constant Mach number contours for an $M_e = 7.09$, $\theta_e = 15^o$ helium jet were obtained by using the computer programs in references 15 and 16 and are given in figure 7. The flow-inclination contours for the nitrogen jets shown in figure 8 were calculated for but are not presented in reference 8. These contours are seen to be approximately equal to azimuthal angles measured from the jet axis at the jet exit.

Values of p, p_r, and q at any point in the jet-exhaust flow field may now be found from the isentropic relations tabled, as a function of Mach number, in references 12 and 13 for air and helium after which surface pressures are obtained by using Newtonian flow theory, a shock layer coincident with the surface being assumed. By utilizing the nomenclature shown in sketch (1) which depicts a typical jet exhaust streamline V_1 impinging upon a body with a circular cross section,

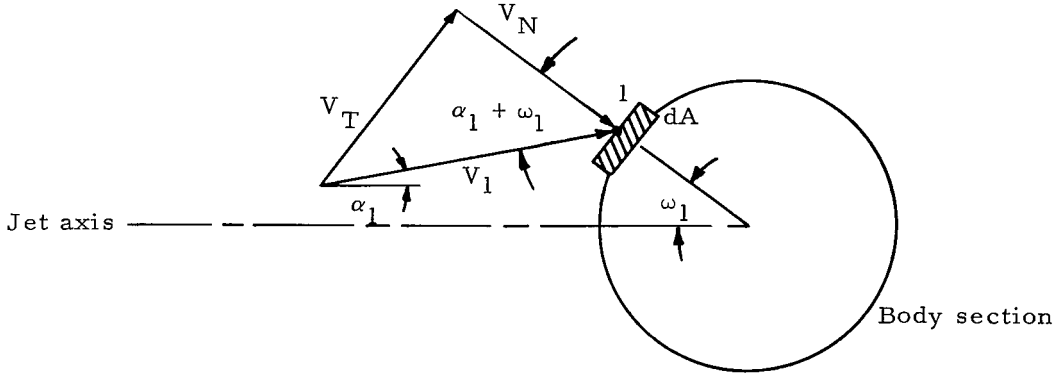

Sketch (1)

the impingement pressure is obtained from Newtonian theory as

$$p_s = 2q_1\left[\cos\left(\alpha_1 + \omega_1\right)\right]^2 + p_1 \tag{1}$$

where

$$q_1 = \frac{1}{2}\rho_1 V_1^{\,2} \tag{2}$$

Along the model longitudinal axis, the geometry simplifies the impingement pressure equation to

$$p_s = 2q_1\left(\cos\,\alpha_1\right)^2 + p_1 \tag{3}$$

At the jet axis the impingement pressure equation would further simplify to

$$p_{stag} = 2q_a + p_a \tag{4}$$

The static pressure p_1 may generally be neglected when the Mach number of the incident flow is very great as this term is much smaller than q_1 for large M_1. This statement means that the actions exerted by the fluid particles upon each other in the impinging flow are small in comparison with the actions exerted by the same particles on the body surface when the flow is highly supersonic. Even the flow from a sonic jet becomes highly supersonic downstream of the nozzle exit as it expands to the vacuum; thus the surface pressure at the jet axis may be written

$$p_{stag} = 2q_a \qquad \left(M_a >> 1\right) \tag{5}$$

Another approach based upon Newtonian flow theory is given in reference 17 where it is assumed that the surface pressure at a point is equal to the bow-shock recovery pressure for the local flow Mach number at that point multiplied by the cosine squared of the streamline impingement angle. Thus, for the curved surfaces, the impingement pressure may be written as

$$p_s = p_{r,1}\left[\cos\left(\alpha_1 + \omega_1\right)\right]^2 \tag{6}$$

The surface pressure along the model axis then becomes

$$p_s = p_{r,1}\left(\cos\,\alpha_1\right)^2 \tag{7}$$

and the surface stagnation pressure is given by

$$p_{stag} = p_{r,a} \tag{8}$$

To apply Newtonian theory along the jet axis requires only a plot of the axial variation of the flow-field Mach number for the particular jet. Figure 9 shows the calculated axial variation of Mach number for some of the present jets. Included is the variation for an $M_e = 5$, $\theta_e = 15^o$ air jet which was obtained from reference 8. A comparison of jet-axis impingement pressures obtained from the two approaches using a characteristics plus Newtonian flow analysis (eq. (5) and eq. (8)) is afforded by figure 10. In this figure calculated values are plotted for various values of Mach number for air and helium. The figure shows that surface pressure is expected to decrease with increasing flow Mach number and that both approaches give about the same results.

Analysis of Roberts

In this method the flow properties of the exhaust are calculated by an approximate integral method, and then the surface pressures are estimated by Newtonian theory. This method is developed in references 9 and 10 and considers two distinct cases of flow: (1) flow where the leading characteristic intersects the jet axis somewhere downstream (called typical exhaust flow) and (2) flow where the leading characteristic does not intersect the jet axis (called spherical source flow). The two flow cases are distinguished according to reference 9 by whether or not

$$\nu_e + 2\theta_e \geqq \nu_{max} = 90^o\left(\sqrt{\frac{\gamma + 1}{\gamma - 1}} - 1\right) \tag{9}$$

This equation is graphically represented in figure 11 and delineates the maximum jet-exit Mach number for which the leading characteristic of a given conical nozzle can intersect the jet axis.

Typical exhaust flow.- For this flow case the governing impingement pressure equation when the jet is far from the curved surface is given by the method of reference 10 as

$$\frac{p_s}{p_c} = \frac{K + 2}{2}\left(\frac{h}{r_e}\right)^{-2} \frac{F}{p_c A_e}(\cos\theta)^{K+2}\left[\cos(\theta + \omega)\right]^2 \tag{10}$$

where

$$K = \gamma(\gamma - 1)M_e^2 \tag{11}$$

* See errata

F is the jet thrust, and θ is the azimuthal angle measured from the jet axis which locates a particular point in the flow field. This equation has the restriction that $M_e^2 >> 1$; and, in addition, the assumption was made that the exhaust gas velocity is constant and equal to V_{max} where

$$V_{max} = \sqrt{\frac{2\gamma}{\gamma - 1} RT_c} \tag{12}$$

which is not exactly true near the jet exit. Along the model longitudinal axis of symmetry, the impingement pressure equation would simplify to

$$\frac{p_s}{p_c} = \frac{K + 2}{2}\left(\frac{h}{r_e}\right)^{-2} \frac{F}{p_c A_e}(\cos \theta)^{K+4} \tag{13}$$

At the jet axis, the impingement pressure equation would further simplify to

$$\frac{p_{stag}}{p_c} = \frac{K + 2}{2}\left(\frac{h}{r_e}\right)^{-2} \frac{F}{p_c A_e} \tag{14}$$

When the jet is close to the impingement surface, reference 9 gives the surface pressure as

$$\frac{p_{stag}}{p_c} = \frac{F}{p_c A_e} = \frac{\rho_e V_e^2 + p_e}{p_c} \tag{15}$$

The equations for impingement pressures for the different jet positions relative to the surface (eqs. (14) and (15)) are seen to coincide at

$$\frac{h}{r_e} = \sqrt{\frac{K + 2}{2}} \tag{16}$$

which is taken as the limit of applicability of equation (14).

Spherical flow.- For this flow case reference 9 gives an asymptotic equation for the density distribution of the exhaust gas along the jet axis but does not present any equations for determining impingement pressures. By removing the restriction on the jet height ratio that $\frac{h}{r_e} >> 1$ and using Newtonian theory with this density distribution, the equation which gives surface stagnation pressure for spherical flow jets becomes

$$\frac{p_{stag}}{p_c} = \left(1 + \frac{2\gamma}{K}\right)^{-1/2}\left(\frac{2\gamma}{\gamma - 1}\right)\left(1 + \frac{\gamma - 1}{2} M_e^2\right)^{-\frac{1}{\gamma-1}}\left(1 + \frac{h}{r_e} \sin \theta_e\right)^{-2} \tag{17}$$

The other assumption made during the derivation of the equation of axial density distribution for these jets was that the exhaust gas velocity is constant and equal to V_{max}.

RESULTS AND DISCUSSION

Impingement Pressure Data

Experimentally determined pressure distributions both around and along the various curved models resulting from the different impinging jets of the present study are given in figures 12 to 19 for several representative jet heights. Figures 12 to 15 show pressure distributions around the cylinders and figures 16 to 19 show the associated pressure distributions along the cylinders.

Effect of Jet Distance From Surface

The data of figures 12 to 15 show that the distribution of impingement pressures is generally symmetric about the jet-axis impingement point and that surface pressures increase as the jet approaches the surface. There was some nozzle misalinement for one configuration (data of fig. 12(a)) which was corrected for subsequent tests. The variation of the axial impingement pressure with jet distance from the surface, which is generally the maximum surface pressure, as obtained from figures 12 to 15 is summarized in figures 20 to 24.

$M_e = 5$ nitrogen jet.- Figure 20 is a summary of the experimental data for both sizes of the $M_e = 5$ nitrogen jet and includes analytical estimates as well as experimental data from references 7 and 8 for the same Mach number jet by using air impinging a flat plate. Axial impingement pressure depends on the ratio of the distance of the jet from the surface to the jet-exit size (jet height ratio) since the data from three different sized jets fall along a common path. Axial impingement pressure does not depend upon the shape of the surface since the data from four different curved surfaces and a flat plate fall along the same common path. Analytical estimates from characteristics plus Newtonian analysis (eqs. (5) and (8)) utilizing the appropriate axial Mach number distribution from figure 9 agree very well with the experimental data especially when the jets are close to the surface. This analysis slightly underestimates the decrease of surface stagnation pressure for jets at large distances from the surface. For the analysis based on Roberts' approach, the equations for a typical exhaust flow case are applicable. (See fig. 11.) When the jet is within a couple of jet-exit diameters from the surface, the axial impingement pressure is given by equation (15) and at further distances from the surface, the axial impingement pressure is given by equation (14). This analysis agrees very well with the experimental data when the jet is 4 to 10 exit diameters from the surface.

Noted on this and subsequent similar figures is the theoretical value of surface pressure for close distances of the particular jet as obtained from equation (15).

The previous experimental data of figure 20 are presented again in figure 21, but the jets are considered to have an exit Mach number of 4.79 with an exit half-angle of 26.5°. From inviscid theory for this Mach number, the two sizes of supersonic nozzle would have effective exit diameters of 0.568 in. (1.44 cm) and 1.14 in. (2.88 cm) which shifts the experimental data slightly. The equations for a typical exhaust flow case are still applicable for the analysis of Roberts and are seen to agree with the experimental data as well as before. This slight change in jet-exit Mach number does not significantly affect the pressure estimates of the analysis of Roberts. The characteristics plus Newtonian pressure estimates, however, change considerably and no longer agree with the data.

The method of characteristics solution for properties in the jet flow field depends not only on the jet-exit Mach number but also on the nozzle-exit half-angle. Increasing this half-angle from 15° to 26.5° changes the calculated properties in the jet flow field considerably and consequently the impingement pressures estimated by using these properties. The effective nozzle-exit half-angle for the $M_e = 5$ jet that was calculated during the investigation of reference 6 probably resulted from a local effect. Most of the gases issuing from the nozzle are affected only by its geometric characteristics. The analysis of Roberts neglects this expansion angle as it considers most of the mass and momentum of the jet concentrated near the jet axis.

$M_e = 7.09$ helium jet.- Figure 22 is a summary of the experimental data for both sizes of the $M_e = 7.09$ helium jet and includes analytical estimates. Characteristics plus Newtonian pressure estimates using the appropriate axial Mach number distribution for this jet appear to underestimate the surface stagnation pressures. For the analysis of Roberts, the spherical flow equation is applicable. (See fig. 11.) This analysis also underestimates the pressures and is seen to coincide with one of the characteristics plus Newtonian analyses. For small values of jet height ratio, this analysis should underpredict surface stagnation pressures because of the assumption that $V = V_{max}$ which is not exactly true near the exit.

Figure 23 shows the surface stagnation-pressure variation with distance for both a stationary and a moving $M_e = 7.09$ helium jet. The small inflection in the data trend is possibly a result of some internal-shock phenomenon in the jet plume. The data for the moving jet $\left(0.54\ d_e/\text{sec}\right)$ were taken to determine whether this easier test technique might be an acceptable method for obtaining impingement pressures over a range of distances. The data for the stationary jet are the same as shown in the previous figure for the smaller nozzle. The moving jet appears to provide an expeditious means to obtain

impingement pressures over a range of distances provided the continuously decreasing ratio of jet-exit pressure to ambient pressure can be overlooked. This pressure ratio does not influence the jet exhaust along the jet axis from the jet exit to the intersection of the leading characteristic with the axis. For the $M_e = 7.09$ helium jet, the leading characteristic never intersects the jet axis and thus the axial impingement pressures could be determined by using a moving nozzle at any distance as long as the jet remains underexpanded. The off-axis distribution, however, depends on the pluming of the jet which changes with pressure ratio.

Sonic jets.- Figure 24 is a summary of the experimental data for both sonic jets and includes analytical estimates as well as experimental data of references 7 and 8 for a sonic air jet impinging on a flat plate. Pressure estimates from characteristics plus Newtonian analyses slightly underestimate the experimental data for the sonic nitrogen jet. The analysis of Roberts also underestimates the impingement pressures for this jet. This method is not considered to be applicable for low Mach number jets because of the assumption that $M_e^2 >> 1$; however, it was applied to determine its possible usefulness in this range. Two empirical equations which seemed to fair the data are also presented in the figure. For the sonic helium jet, the data agree very well with an inverse square variation with jet distance. Again, the analysis of Roberts underestimates the surface stagnation pressures for this jet.

Effect of Jet Mach Number

Figure 25 summarizes the measured surface stagnation-pressure data for the jets of the present study. The figure indicates that at a given height ratio, the sonic jets cause significantly higher stagnation pressures and hence higher overall impingement pressures than supersonic jets with the same gas and jet-chamber pressure.

Effect of Exhaust Gas Properties

Figure 26 summarizes the measured surface stagnation-pressure data for the sonic jets. The helium jet theoretically produces only about 2.5-percent more thrust than the nitrogen jet but experimentally causes about 25-percent higher stagnation pressures for the same height ratio and jet-chamber pressure.

Effect of Surface Curvature

Pressure distributions along cylinders.- Figures 27 to 30 summarize the distribution of impingement pressures along the axis of symmetry of the cylinders compared with an analysis for a jet exhaust impinging a flat surface. The comparison of the experimental data with the analysis of Roberts is made by using the equation

$$\frac{p_s}{p_{stag}} = (\cos \theta)^{K+4} \tag{18}$$

which is the ratio of equation (13) to equation (14). The comparison with a characteristics plus Newtonian analysis is made by using the equation

$$\frac{p_s}{p_{stag}} = \frac{p_{r,1}}{p_{r,a}}\left(\cos \alpha_1\right)^2 \tag{19}$$

which is the ratio of equation (7) to equation (8).

Figure 27 is a summary of the impingement pressures for the small $M_e = 5$ nitrogen jet. The data are plotted against l/h, which is equivalent to $\tan \theta$, without the multitude of data points occurring at the jet axis ($l/h = 0$). There is some data spread for the range of jet distances and model sizes represented; however, the analysis of Roberts appears to agree with the data very well. Apparently, the surface curvature of the cylindrical models does not appreciably affect the distribution of impingement pressures along the cylinder axis. The characteristics plus Newtonian analysis is shown for two jet heights, a bow shock coincident with the surface being assumed, and does not agree particularly well with the experimental data obtained by using the flow characteristics of an $M_e = 4.79$, $\theta_e = 26.5^\circ$ jet.

Figure 28 is a summary of the data for the large $M_e = 5$ nitrogen jet. The analysis of Roberts agrees with the data nearly as well as that for the smaller jet.

Figure 29 is a summary of the data for both sizes of the $M_e = 7.09$ helium jet. The characteristics plus Newtonian analysis is shown for two jet heights and does agree somewhat with the data, but it appears that an empirical equation for which the impingement pressure varies as the $\cos \theta$ raised to some power would be more applicable.

Figure 30 is a summary of the data for both sonic jets. Included for comparison with the sonic nitrogen jet data are data taken from reference 7 for a sonic air jet $\left(d_e = 0.50 \text{ in. } (1.27 \text{ cm})\right)$ impinging onto a flat surface. These data agree very well and are overestimated by the analysis of Roberts. The characteristics plus Newtonian pressure estimates for the two selected jet heights were identical and slightly underestimate the experimental data. The experimental data for the sonic helium jet are also overestimated by the analysis of Roberts.

Pressure distributions around cylinders.- Figures 31 to 33 show pressure distributions around the cylinders at two jet heights for the different jets together with calculations based on the analysis of Roberts by using the equation

$$\frac{p_s}{p_{stag}} = (\cos\theta)^{K+2}\left[\cos(\theta + \omega)\right]^2 \tag{20}$$

which is the ratio of equation (10) to equation (14). This equation is easily applied since choosing a value of angular position on a given cylinder for a particular jet height uniquely determines the angle θ from geometry as

$$\theta = \tan^{-1}\frac{R\sin\omega}{h + R(1 - \cos\omega)} \tag{21}$$

Figure 31 which shows pressure distributions for the small nitrogen jet and different cylinders compared with the analysis indicates that experimental agreement with the analysis depends upon jet height and surface curvature. The analysis of Roberts underestimates the fall-off of impingement pressure with increasing angular position at both jet heights for the smallest cylinder, which has the highest surface curvature. For the next largest cylinder, the analysis underestimates the pressure fall-off at only the higher jet height. The analysis and experimental data agree very well at both jet heights for the other cylinders.

Figure 32 presents similar data for the large $M_e = 5$ nitrogen jet and again indicates much better agreement between analysis and experiment for the lower jet heights. This analysis underestimates the pressure fall-off for the higher jet height for all the cylinders.

Figure 33 shows the distribution of impingement pressures around one of the cylinders for the sonic jets at two representative jet heights compared with analysis. The characteristics plus Newtonian analysis agrees very well with the data for the nitrogen jet whereas the analysis of Roberts underestimates the fall-off of these pressures. The analysis of Roberts also underestimates the pressure fall-off with increasing angular position for the helium jet.

The data from the supersonic helium jet are compared with a characteristics plus Newtonian analysis in figure 34 by using the equation

$$\frac{p_s}{p_{stag}} = \frac{p_{r,1}}{p_{r,a}}\left[\cos\left(\alpha_1 + \omega_1\right)\right]^2 \tag{22}$$

which is the ratio of equation (6) to equation (8). This analysis indicates some agreement although underestimating the fall-off of impingement pressure with increasing angular position on the surface.

* See errata

Effect of the Ratio of Jet-Exit Pressure to Ambient Pressure

The experimental data were obtained at finite values of the ratio of jet-exit pressure to ambient pressure and it is of interest to determine the effect of this pressure ratio. Although the pressure ratios at which the present tests were conducted (see fig. 4) were far from being infinite, the jets were not foo far from being fully expanded. Figure 35 presents the impingement pressure distribution around one of the cylinders for the large $M_e = 5$ nitrogen jet at a particular value of jet height for three values of pressure ratio. The figure indicates that varying the pressure ratio by a factor of 3 did not have an appreciable effect on the impingement pressures. The data of reference 8 are in agreement that significant variations in the ratio of jet-exit pressure to ambient pressure at fairly large values of pressure ratio do not influence the magnitude of impingement pressures.

Bow-Shock Characteristics

Shadowgraphs were taken of the exhaust impingement region of one of the cylinders for five different jets from which certain bow-shock characteristics were measured. The shadowgraphs were taken in a plane perpendicular to the cylinder axis to determine the influence of surface curvature. Representative shadowgraphs are presented in figures 36 to 38 for various distances of the jets above the cylinder surface. The figures indicate that surface curvature has a decided influence upon the shape of the bow shock. When a jet exhaust impinges upon a flat surface, a bowl-shaped bow shock is formed which curves away from the surface (see ref. 18); however, the shape of the bow shock for a curved surface depends upon the jet, its distance from the surface, and the degree of surface curvature. The bow shock is fairly flat when the jets are close to the surface and curves toward the surface as the distance between the jets and surface increases with the exception of the $M_e = 7.09$ helium jet. The bow shock for this jet has no inclination to follow the curvature of the surface as the jet is moved away from the surface. An explanation for this effect is not apparent; however, this jet is one wherein the exhaust leading characteristic never intersects the jet axis.

The relationship of nozzle size to shock size is shown in figure 39 which is a plot of the shock bowl diameters taken from the shadowgraphs of figure 36 for the two sizes of $M_e = 5$ nitrogen jet. The data are limited because the shock becomes larger than the region being photographed but indicate that the size of the shock is probably directly proportional to the nozzle size. An empirical equation which fairs the limited data gives the shock size as being equal to twice the distance of the jet from the surface. The size of the bow shock should perhaps be expected to increase with increasing ratio of jet-exit pressure to ambient pressure since the size of the exhaust plume increases with increasing pressure ratio. This condition was shown in reference 18 to exist for an

$M_e = 5$ nitrogen jet exhausting onto a flat plate, although the shock characteristics, both size and standoff distance, appeared to approach constant values for pressure ratios greater than approximately 100.

The variation of bow-shock standoff distance at the jet axis, as determined from the shadowgraphs, is shown in figures 40 to 42. The shock standoff distance for the supersonic jets appears to approach a limit with increasing jet distance. The location of the bow-shock wave has been suggested as being useful for more closely predicting impingement pressures. (See ref. 8.) The bow shock was considered to be coincident with the surface for the present study because the usefulness of the analysis should depend upon a minimum of information having to be determined.

CONCLUSIONS

An experimental study has been made of the impingement of underexpanded jets onto various curved surfaces in a vacuum environment and the results have been compared with available analyses. The study suggests the following conclusions:

1. The magnitude of axial impingement pressure depends on the exit Mach number of the jet and the jet height ratio but not on the shape of the impingement surface. The characteristics plus Newtonian analysis adequately predicts this pressure and its variation with jet distance from the surface for a range of exhaust jets. The analysis of Roberts is easier to apply and predicts this pressure and its variation with jet distance from the surface for a range of exhaust jets equally well, provided $M_e^2 \gg 1$ (where M_e is the nozzle-exit Mach number).

2. A realistic estimate of the axial impingement pressure and its variation with jet distance for sonic jets is given by an empirical equation which states that the ratio of surface stagnation pressure to nozzle-chamber pressure is equal to the inverse square variation of the ratio of distance to jet-exit diameter.

3. At the same height ratio, sonic jets produce significantly higher axial impingement pressures than do supersonic jets with the same gas and jet-chamber pressure.

4. Sonic helium jets produce slightly higher axial impingement pressures than do sonic nitrogen jets at the same height ratio and jet-chamber pressure.

5. The distribution of impingement pressures depends upon the exit Mach number of the jet, the jet height ratio, and the shape of the surface. The characteristics plus Newtonian analysis reasonably predicts for a range of exhaust jets the distribution of impingement pressures on both planar and curved surfaces. The analysis of Roberts is easier to apply and provides about the same degree of accuracy for predicting impingement pressures on these surfaces provided $M_e^2 \gg 1$.

6. There is no significant difference between the distribution of impingement pressures along the longitudinal axis of symmetry of curved surfaces and those along a flat plate.

Langley Research Center,
National Aeronautics and Space Administration,
Langley Station, Hampton, Va., November 21, 1966,
124-08-05-09-23.

REFERENCES

1. Vick, Allen R.; Cubbage, James M.; and Andrews, Earl H., Jr.: Rocket Exhaust Plume Problems and Some Recent Related Research. Presented at a Specialist's Meeting on "The Fluid Dynamic Aspects of Space Flight" (Marseille, France), AGARD, Apr. 20-24, 1964.

2. Love, Eugene S.; Grigsby, Carl E.; Lee, Louise P.; and Woodling, Mildred J.: Experimental and Theoretical Studies of Axisymmetric Free Jets. NASA TR R-6, 1959. (Supersedes NACA RM L54L31 by Love and Grigsby, RM L55J14 by Love, RM L56G18 by Love, Woodling, and Lee, and TN 4195 by Love and Lee.)

3. Adamson, Thomas C., Jr.: The Structure of the Rocket Exhaust Plume Without Reaction at Various Altitudes. 4613-45-T (Contract SD-91), Inst. Sci. and Technol., Univ. of Michigan, June 1963.

4. Bauer, R. C.; and Schlumpf, R. L.: Experimental Investigation of Free Jet Impingement on a Flat Plate. AEDC-TN-60-223, U.S. Air Force, Mar. 1961.

5. Margolin, E. L.; and Welch, Eugene: Final Report - Single Nozzle Jet Plume Test in the Rocket Nozzle Test Facility. SID 63-426, North American Aviation, Inc., May 6, 1963.

6. Vick, Allen R.; and Andrews, Earl H., Jr.: An Experimental Investigation of Highly Underexpanded Free Jets Impinging Upon a Parallel Flat Surface. NASA TN D-2326, 1964.

7. Stitt, Leonard E.: Interaction of Highly Underexpanded Jets With Simulated Lunar Surfaces. NASA TN D-1095, 1961.

8. Vick, Allen R.; and Andrews, Earl H., Jr.: An Investigation of Highly Underexpanded Exhaust Plumes Impinging Upon a Perpendicular Flat Surface. NASA TN D-3269, 1966.

9. Roberts, Leonard; and South, Jerry C., Jr.: Comments on Exhaust Flow Field and Surface Impingement. AIAA J., vol. 2, no. 5, May 1964, pp. 971-974.

10. Roberts, Leonard: The Action of a Hypersonic Jet on a Dust Layer. Paper No. 63-50, Inst. Aerospace Sci., Jan. 1963.

11. Mechtly, E. A.: The International System of Units – Physical Constants and Conversion Factors. NASA SP-7012, 1964.

12. Ames Research Staff: Equations, Tables, and Charts for Compressible Flow. NACA Rept. 1135, 1953. (Supersedes NACA TN 1428.)

13. Mueller, James N.: Equations, Tables, and Figures for Use in the Analysis of Helium Flow at Supersonic and Hypersonic Speeds. NACA TN 4063, 1957.

14. Guiraud, Jean-Pierre: Topics in Hypersonic Flow Theory. Sudaer No. 154 (Contract AF 49(638)965), Dept. of Aeron. Astronaut., Standford Univ., May 1963.

15. Vick, Allen R.; Andrews, Earl H., Jr.; Dennard, John S.; and Craidon, Charlotte B.: Comparisons of Experimental Free-Jet Boundaries With Theoretical Results Obtained With the Method of Characteristics. NASA TN D-2327, 1964.

16. Andrews, Earl H., Jr.; Vick, Allen R.; and Craidon, Charlotte B.: Theoretical Boundaries and Internal Characteristics of Exhaust Plumes From Three Different Supersonic Nozzles. NASA TN D-2650, 1965.

17. Eastman, Donald W.; and Radtke, Leonard P.: Flow Field of an Exhaust Plume Impinging on a Simulated Lunar Surface. AIAA J. (Tech. Notes and Comments), vol. 1, no. 6, June 1963, pp. 1430-1431.

18. Land, Norman S.; and Clark, Leonard V.: Experimental Investigation of Jet Impingement on Surfaces of Fine Particles in a Vacuum Environment. NASA TN D-2633, 1965.

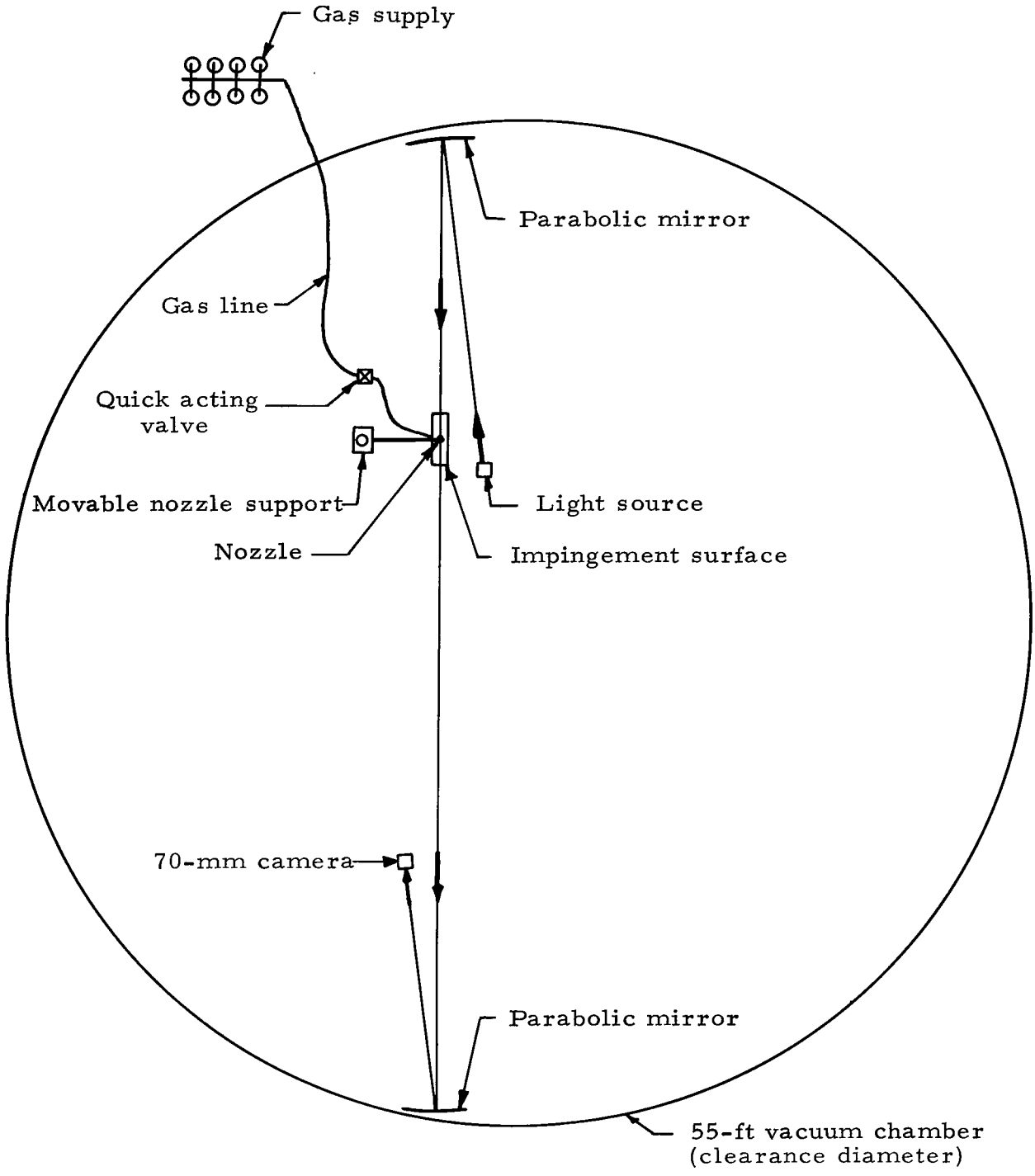

(a) Plan view of test setup in 55-foot vacuum cylinder.

Figure 1.- General layout of test setup.

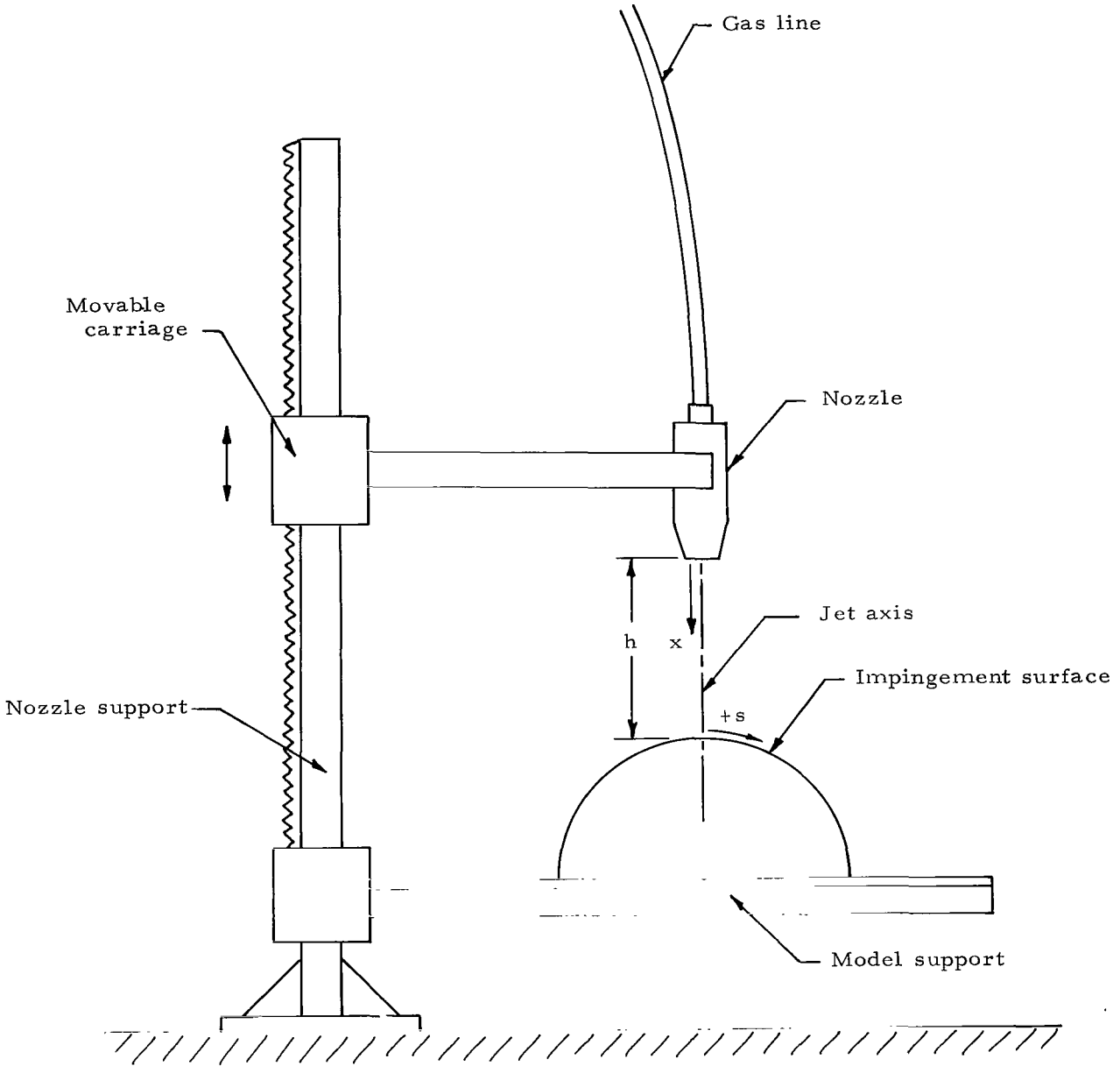

(b) Elevation view of model and nozzle setup.

Figure 1.- Concluded.

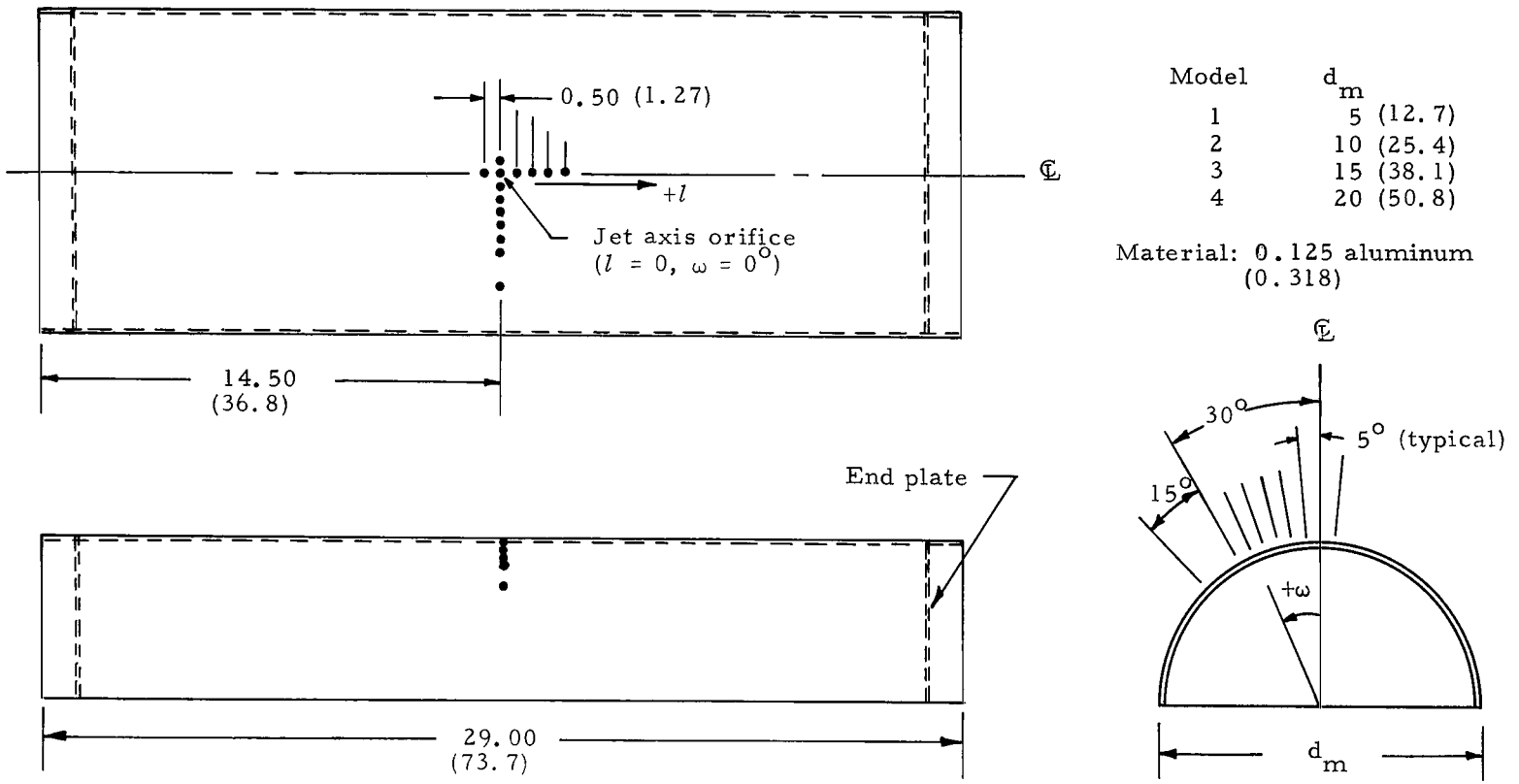

Figure 2.- Drawing of cylindrical models showing static-pressure orifice locations. All linear dimensions are given in inches and parenthetically in centimeters.

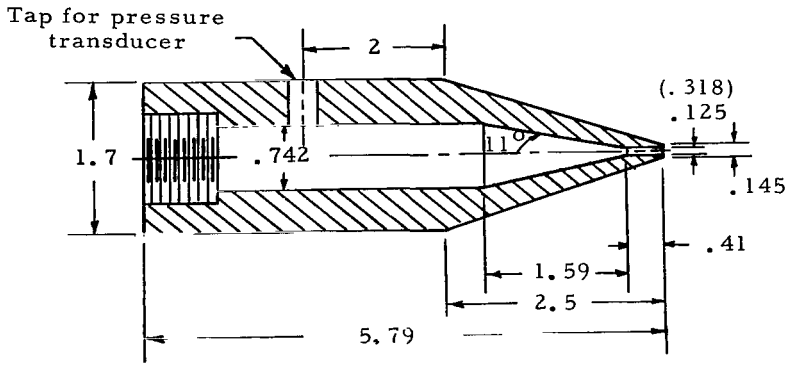

(a) Convergent nozzle.

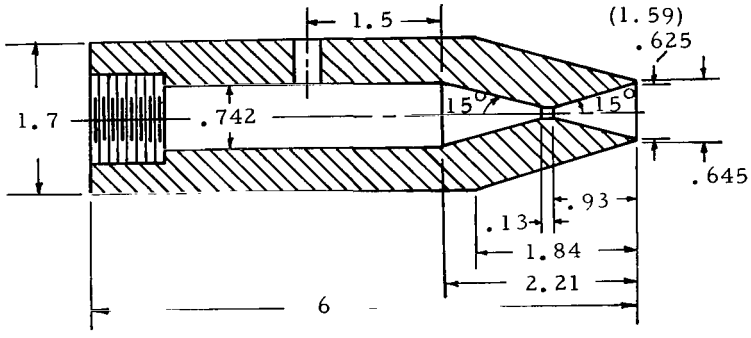

(b) Convergent-divergent nozzle, d_e = 0.625 (1.59).

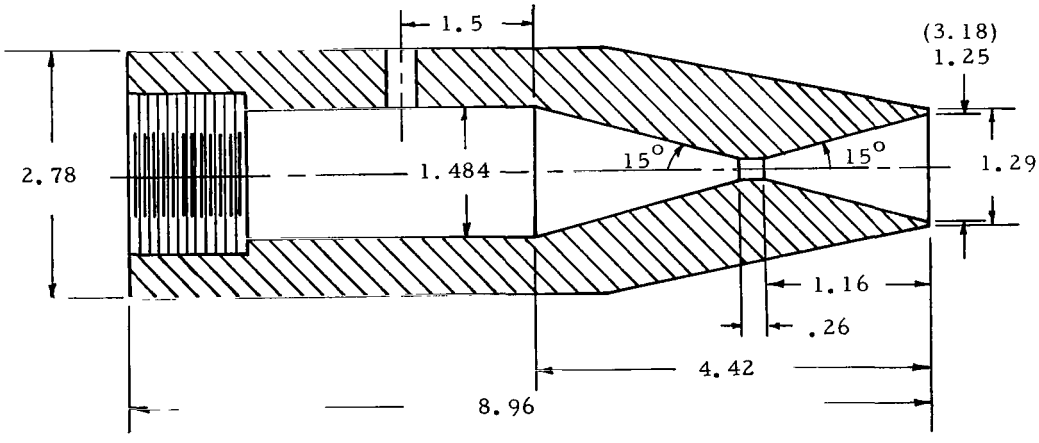

(c) Convergent-divergent nozzle, d_e = 1.25 (3.18).

Figure 3.- Section drawing of test nozzles. Linear dimensions are given in inches and parenthetically in centimeters. Because of space limitations conversions to the S.I. system of units are presented for only a few representative dimensions.

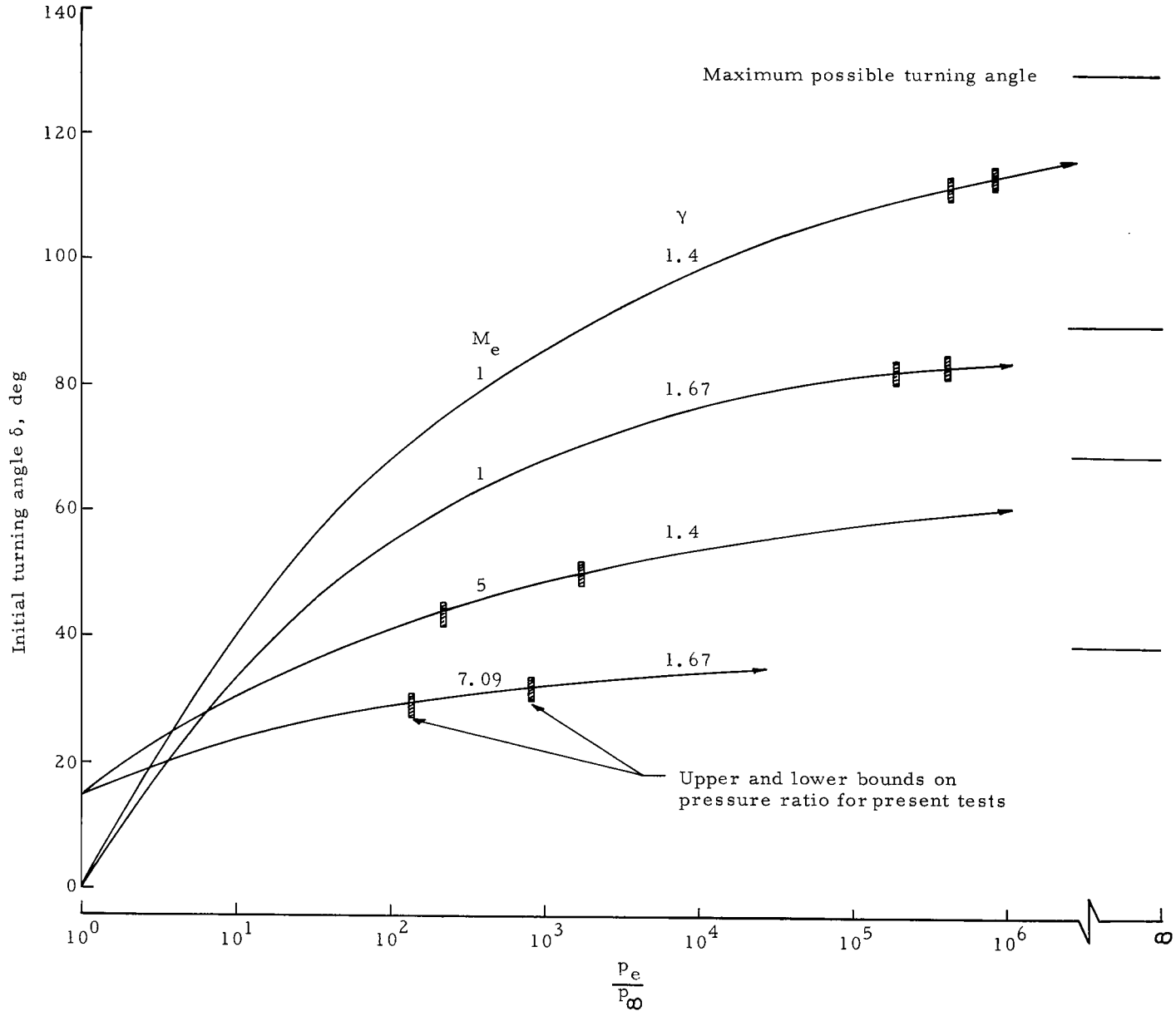

Figure 4.- Variation of initial turning angle of exhaust flow with pressure ratio for nozzles used in the present tests.

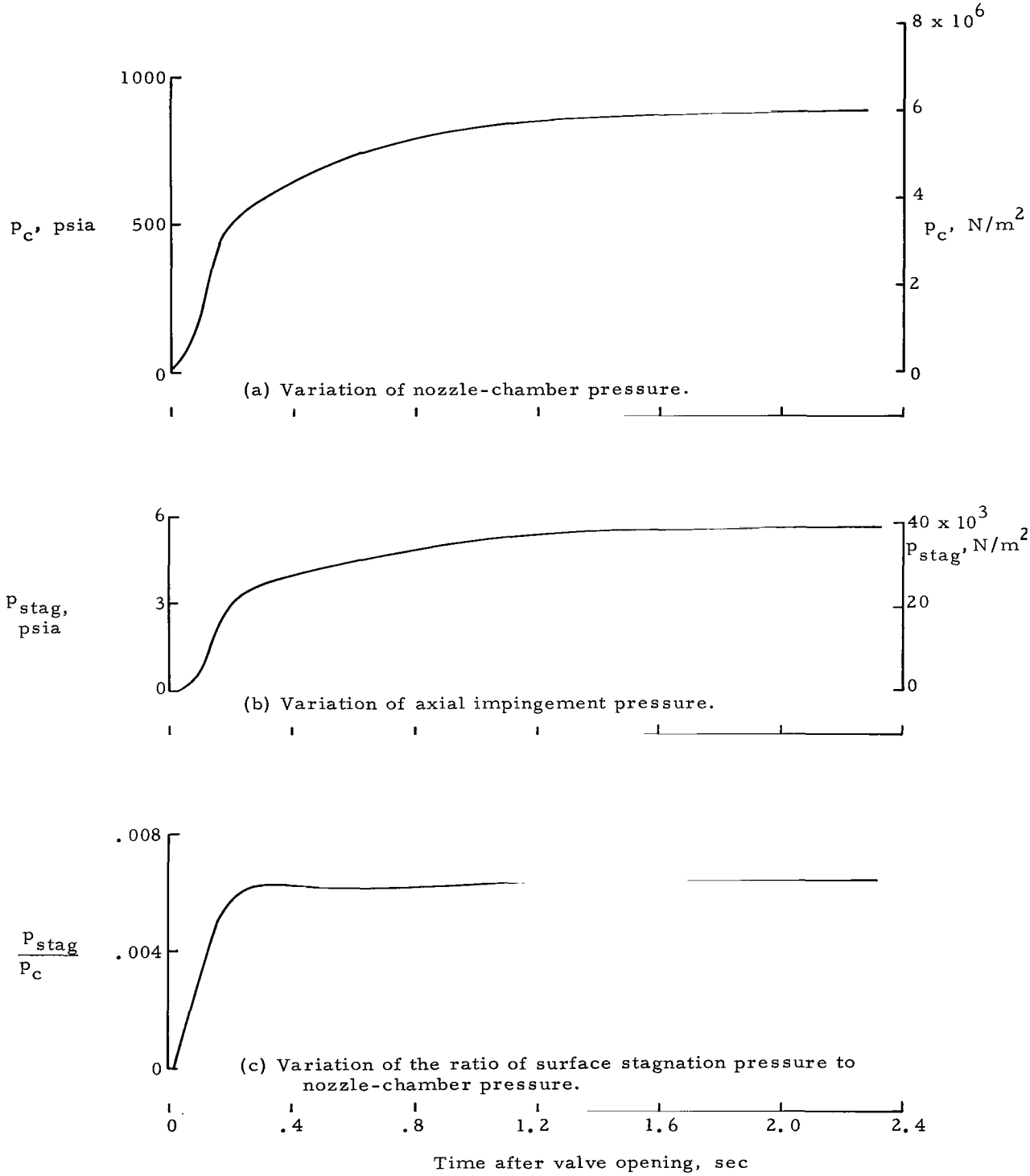

Figure 5.- Gage response during a typical test.

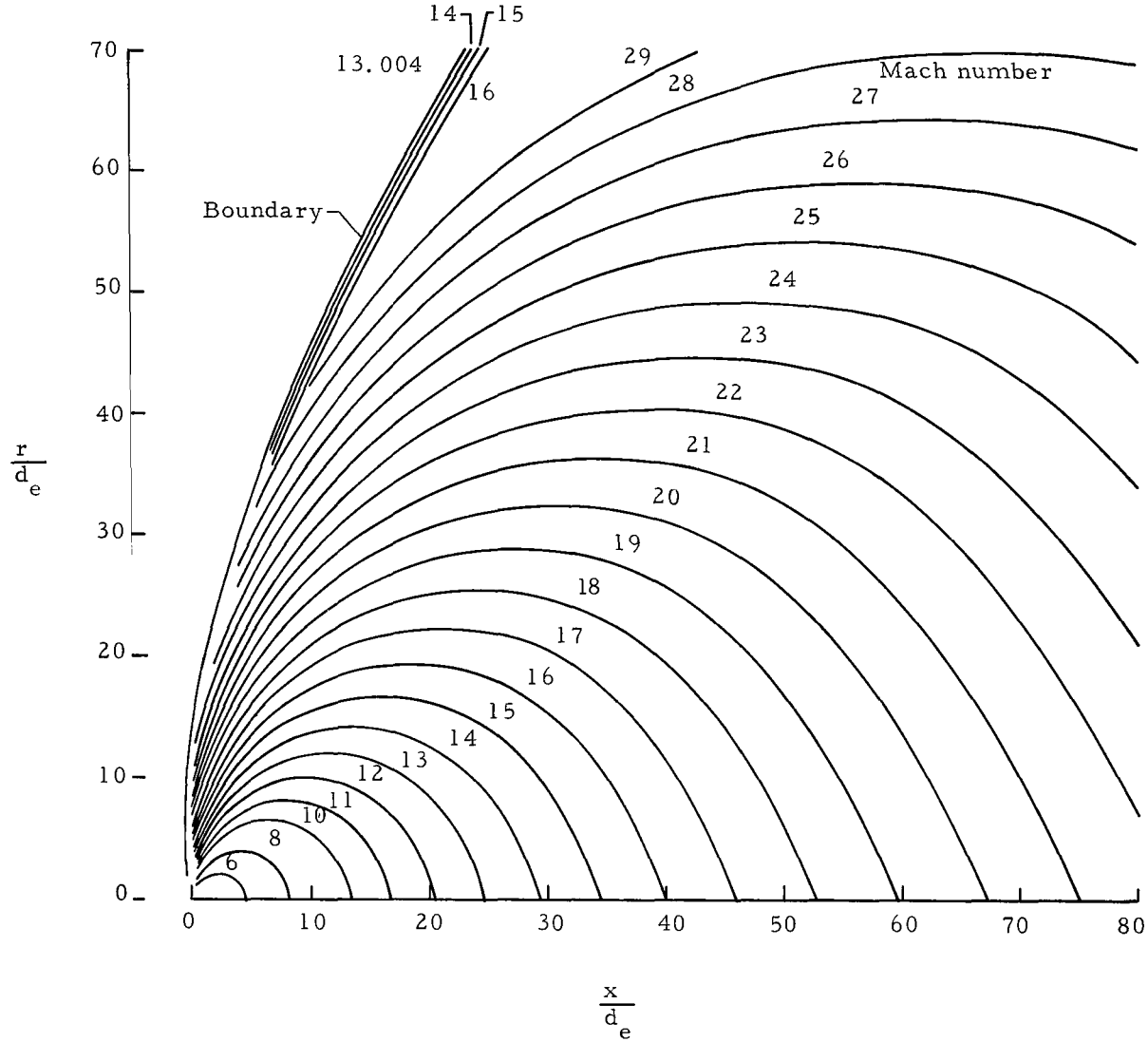

(a) $M_e = 1.0$.

Figure 6.- Theoretically calculated contour lines of constant Mach number within nozzle exhaust plume for a jet using air. $p_c/p_\infty = 250 \times 10^3$ (from ref. 8).

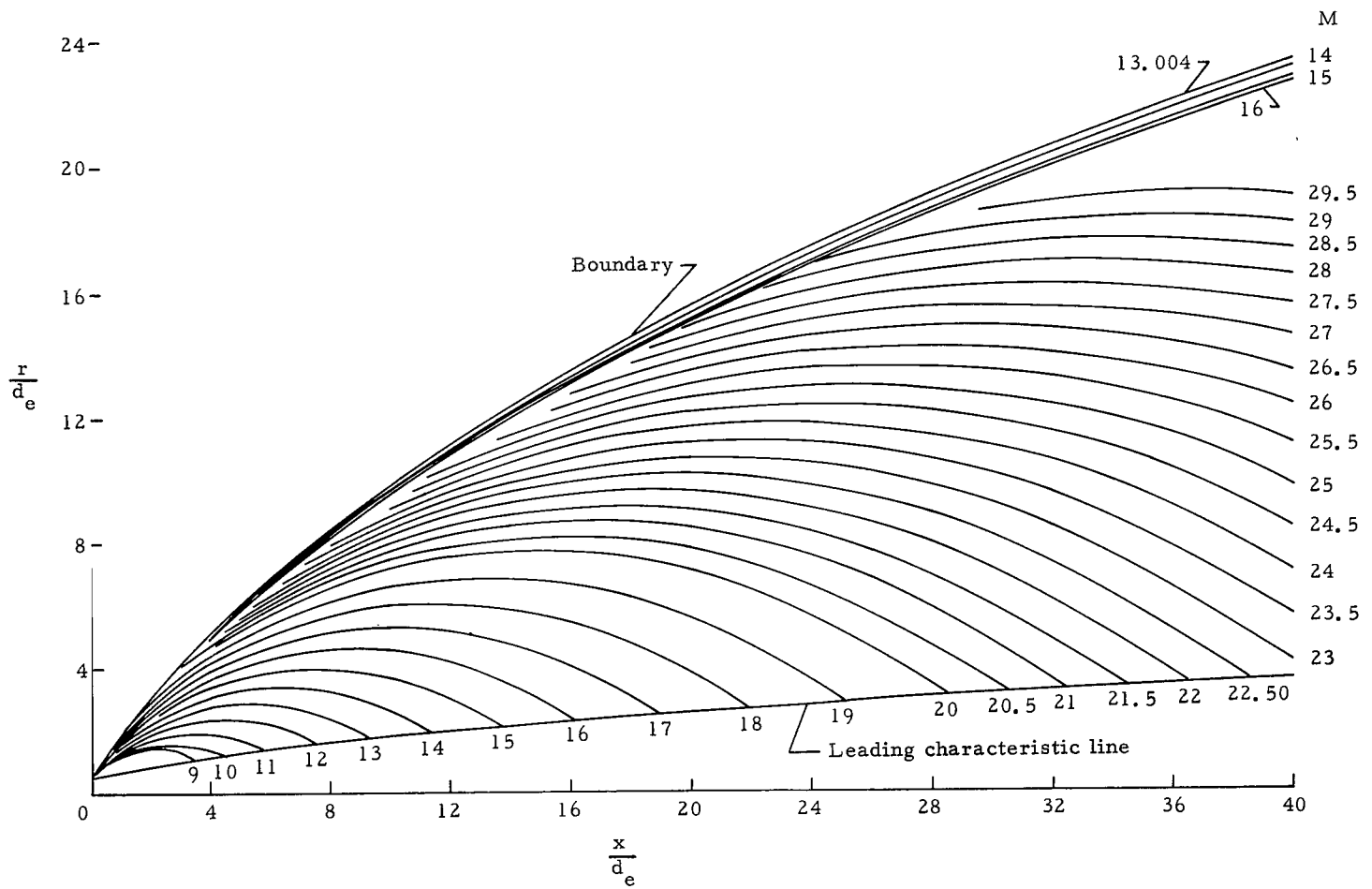

(b) $M_e = 4.79$; $\theta_e = 26.5^0$.

Figure 6.- Concluded.

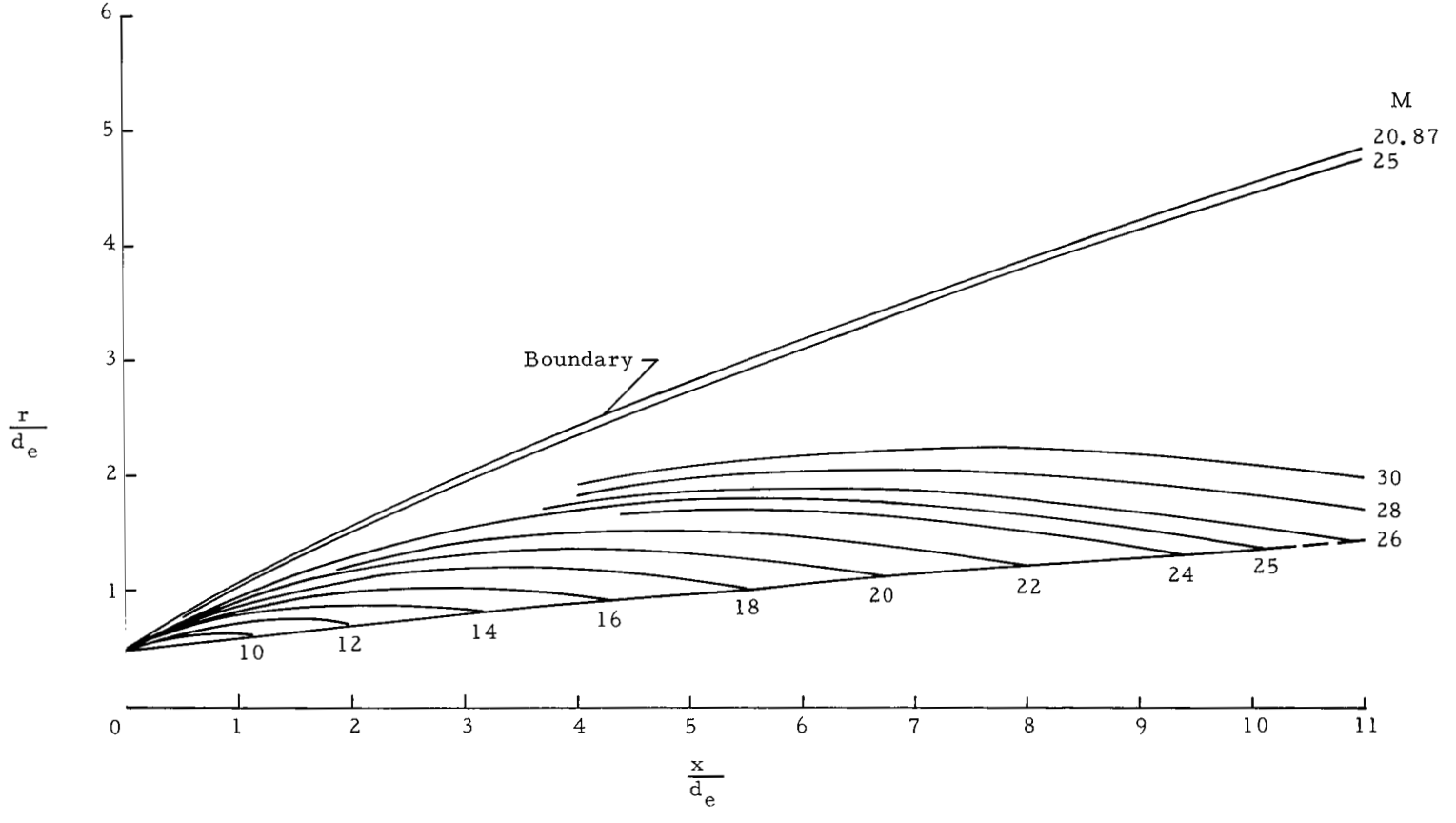

Figure 7.- Theoretically calculated contour lines of constant Mach number within nozzle exhaust plume for an $M_e = 7.09$, $\theta_e = 15^0$ jet using helium. $p_c/p_\infty = 258 \times 10^3$.

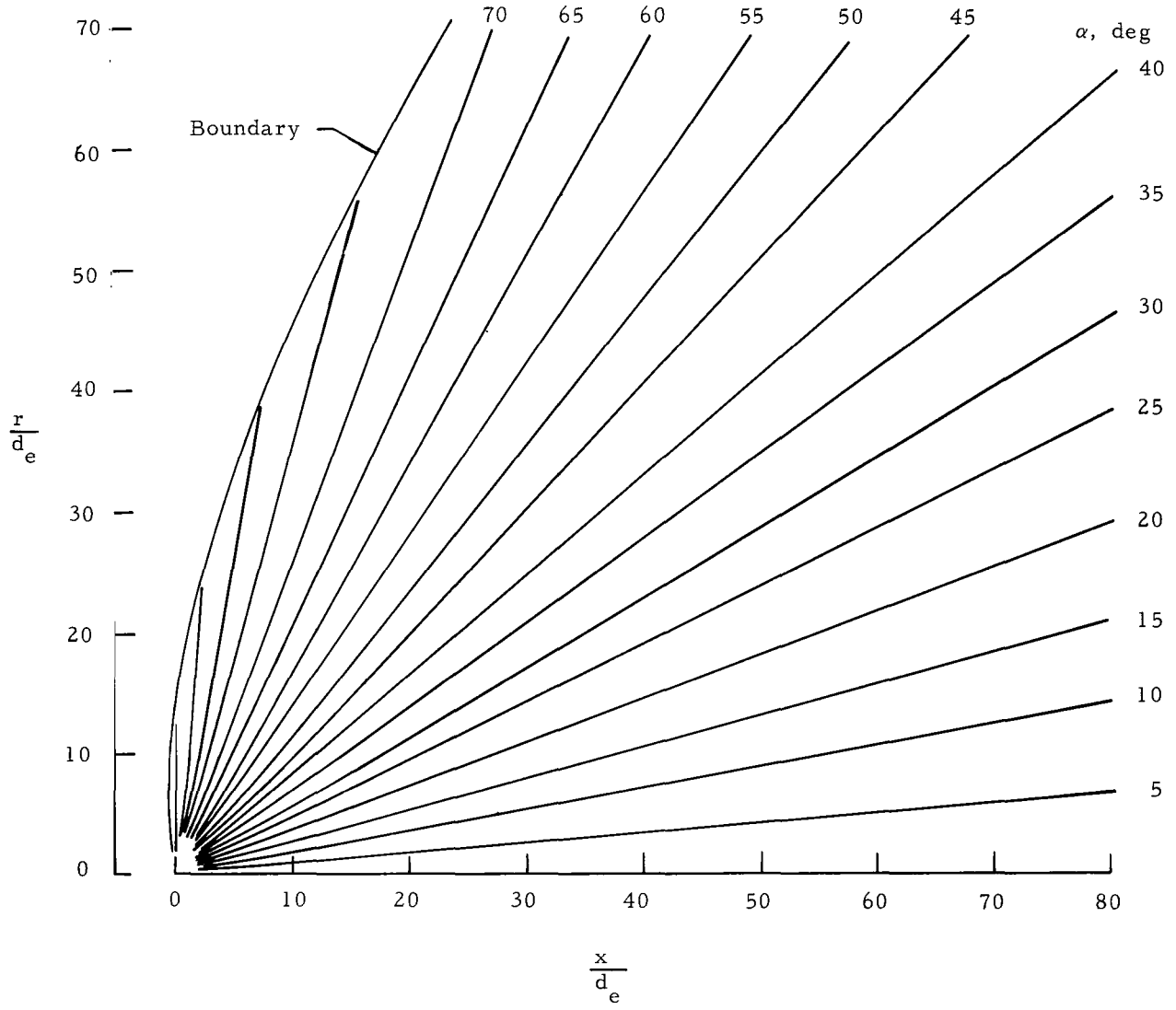

(a) $M_e = 1.0$.

Figure 8.- Constant lines of flow direction within nozzle exhaust plume for a jet using air. (Unpublished data of ref. 8.)

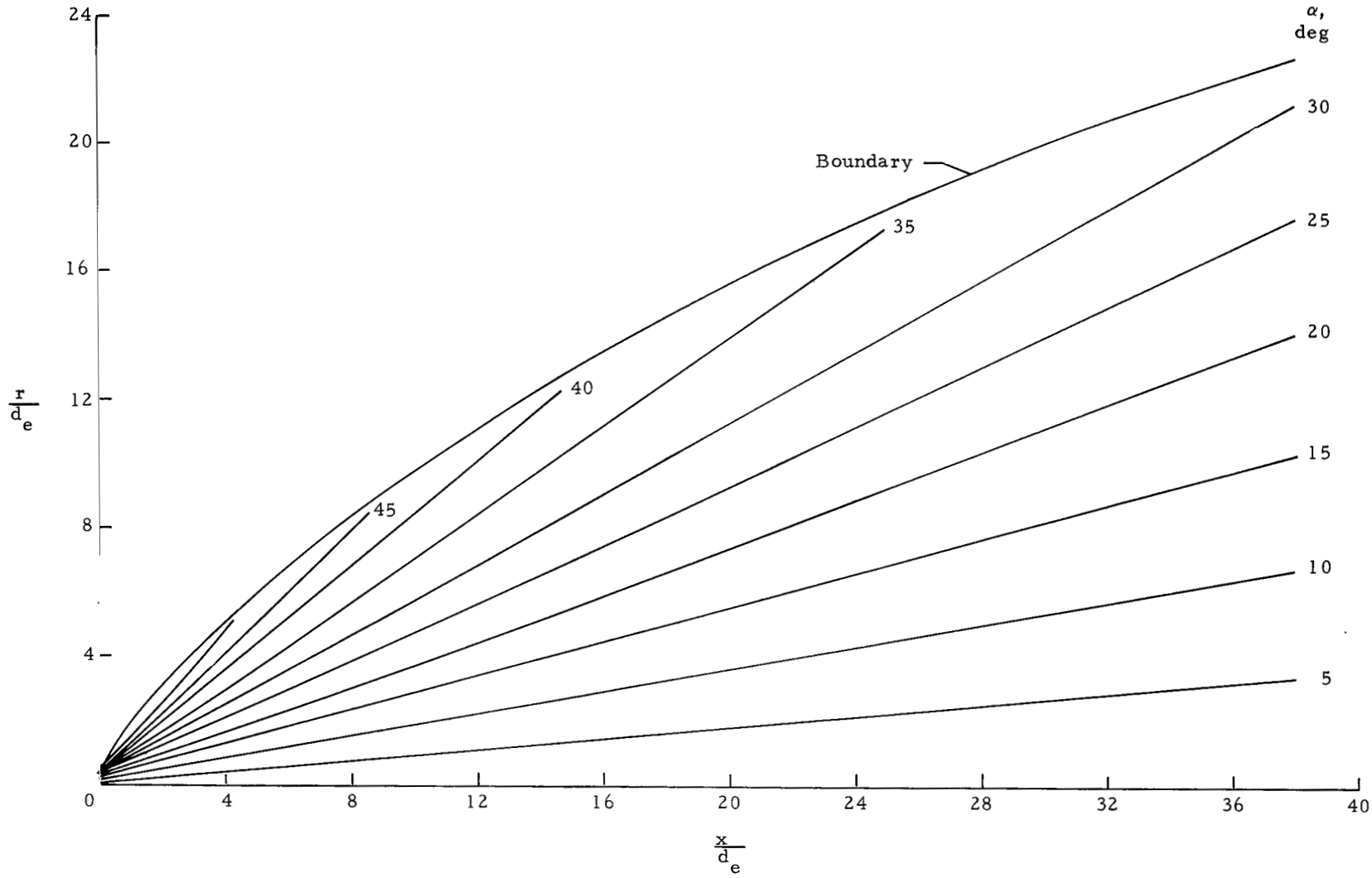

(b) $M_e = 4.79$; $\theta = 26.5^0$.

Figure 8.- Concluded.

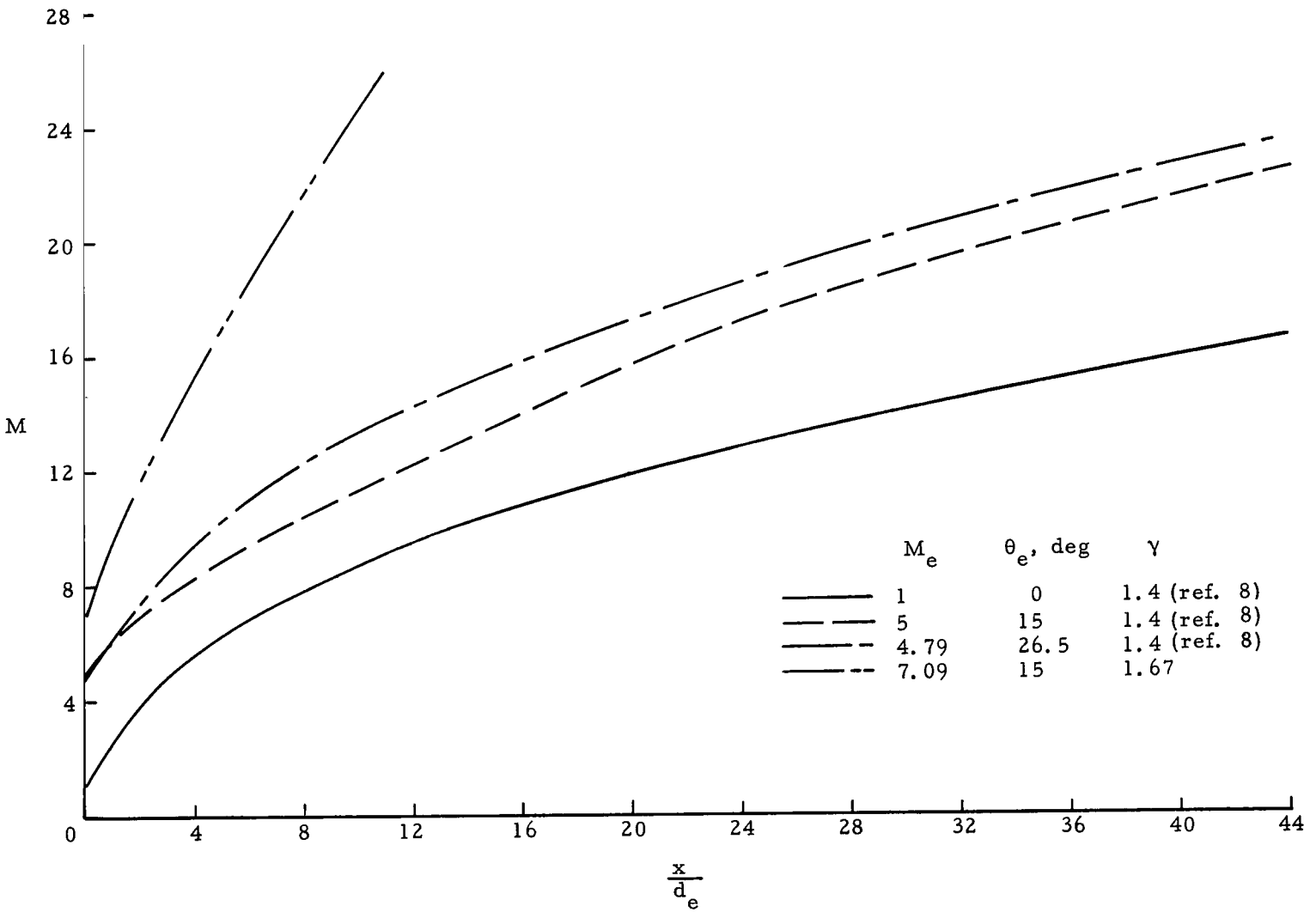

Figure 9.- Calculated jet axis Mach number distribution for the exhaust jets of the present study.

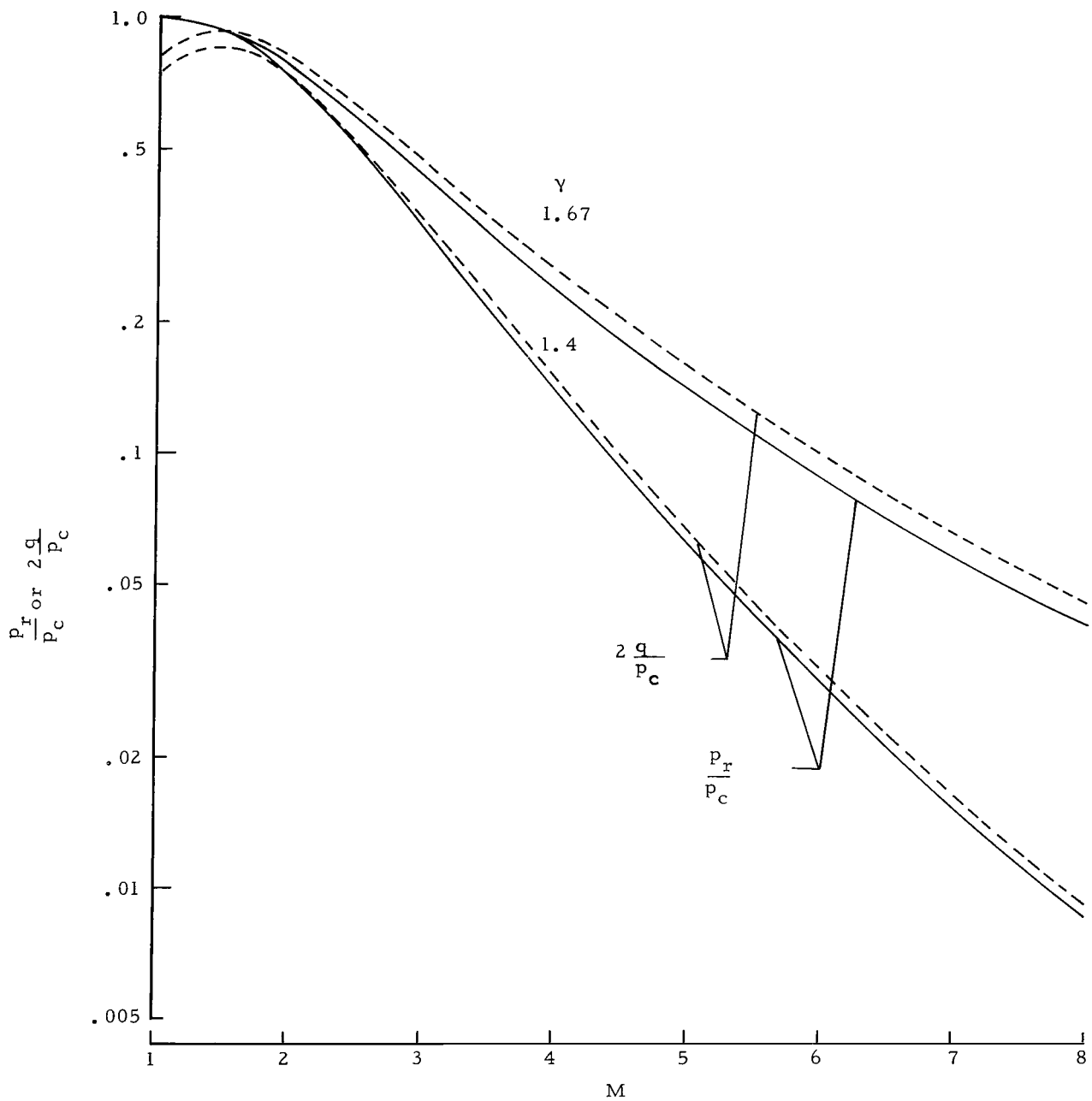

Figure 10.- Variation of surface stagnation pressure with local Mach number by using a method of characteristics plus Newtonian flow analysis.

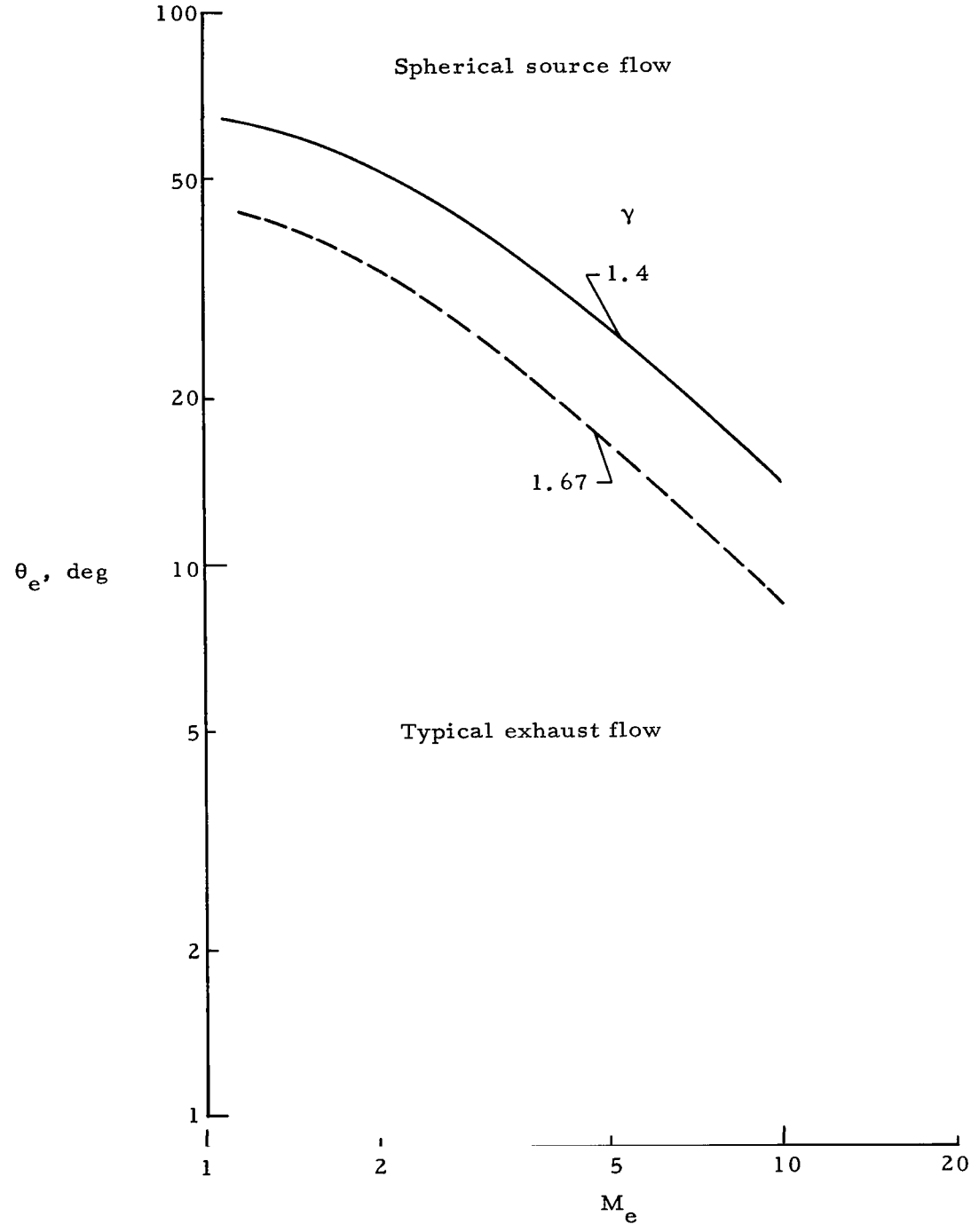

Figure 11.- Flow regimes for conical nozzles delineating the maximum jet-exit Mach number for which the leading characteristic can intersect the jet axis.

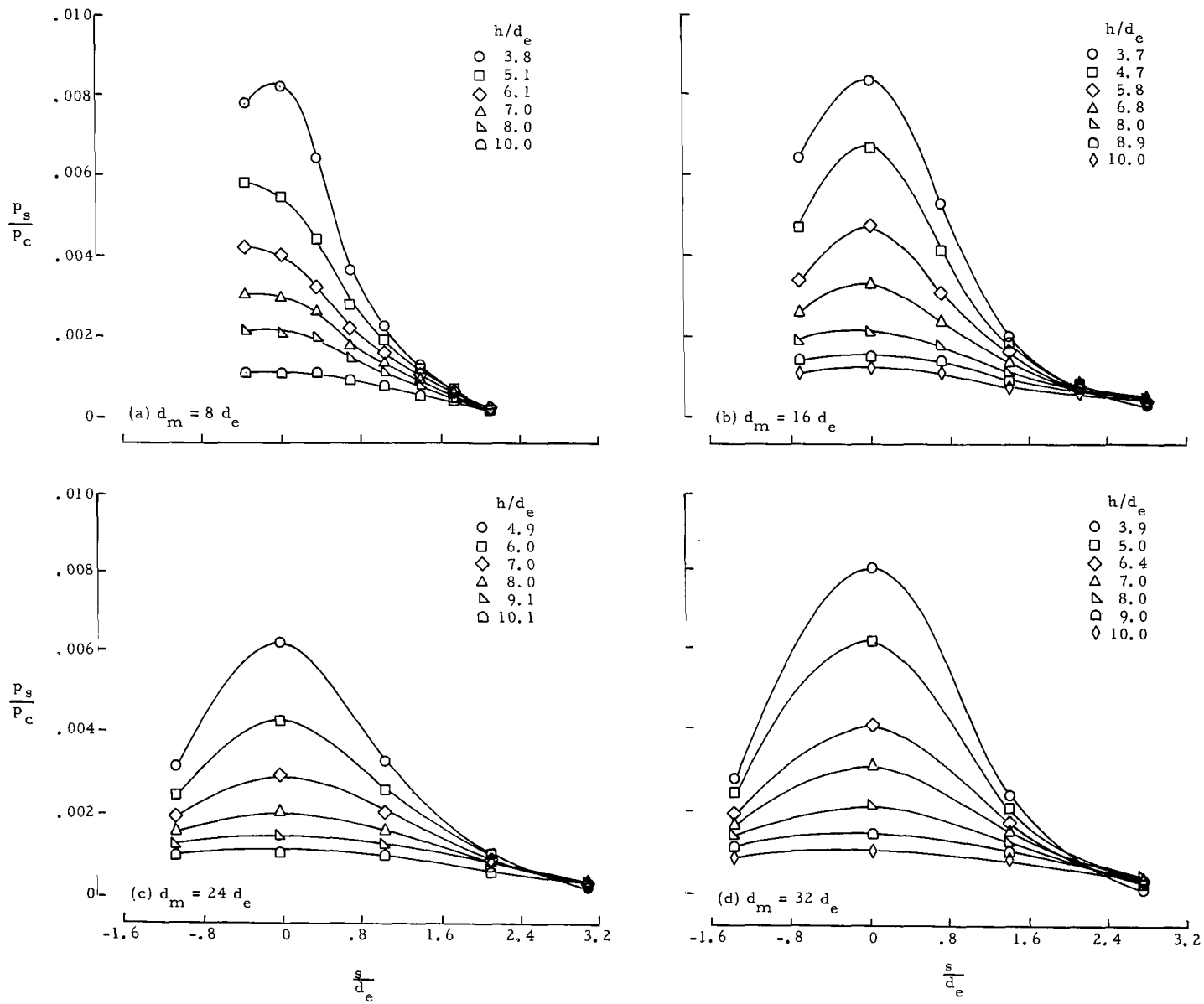

Figure 12.- Distribution of impingement pressures around cylinders for $M_e = 5$ nitrogen jet having $d_e = 0.625$ in. (1.59 cm).

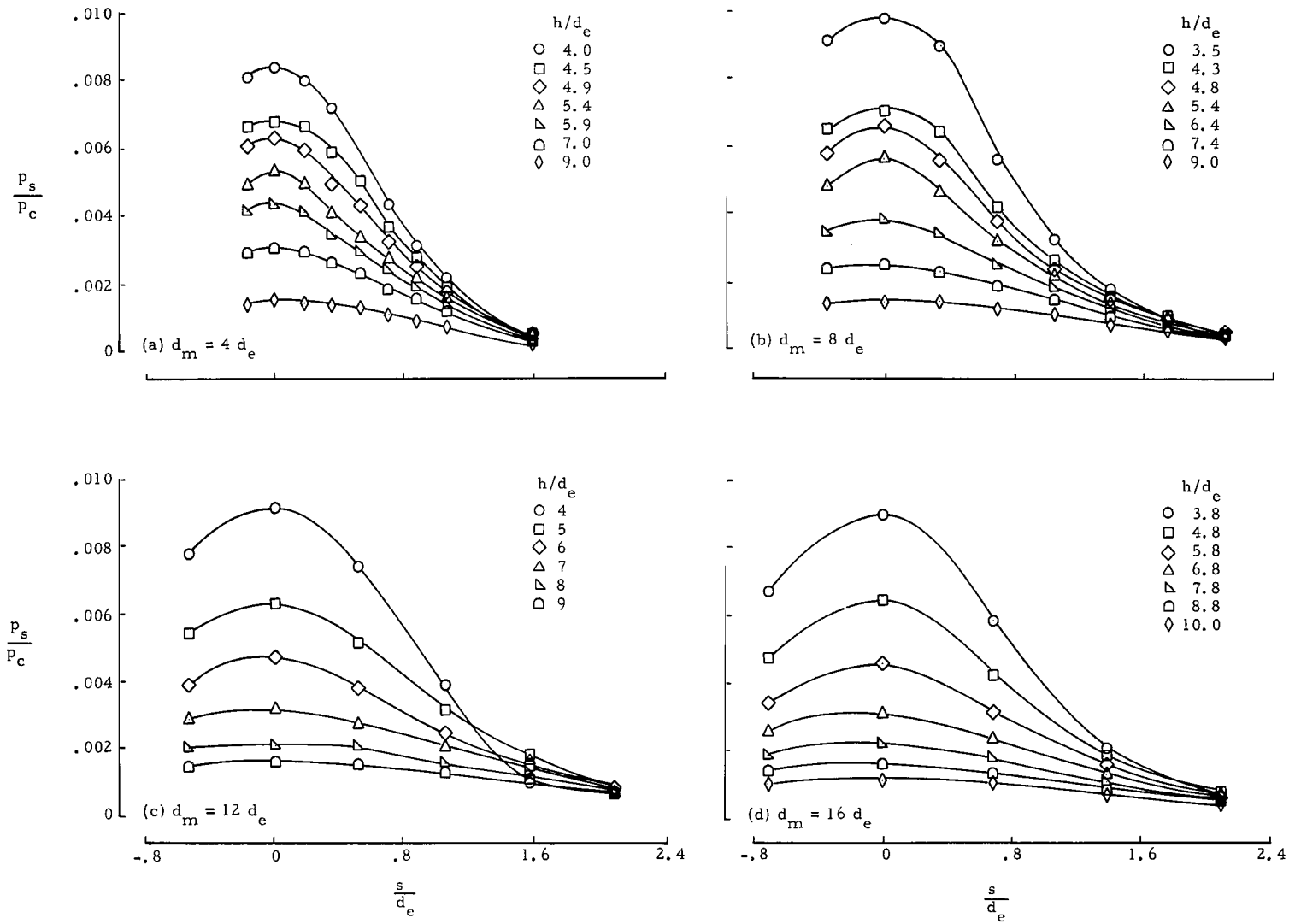

Figure 13.- Distribution of impingement pressures around cylinders for $M_e = 5$ nitrogen jet having $d_e = 1.25$ in. (3.18 cm).

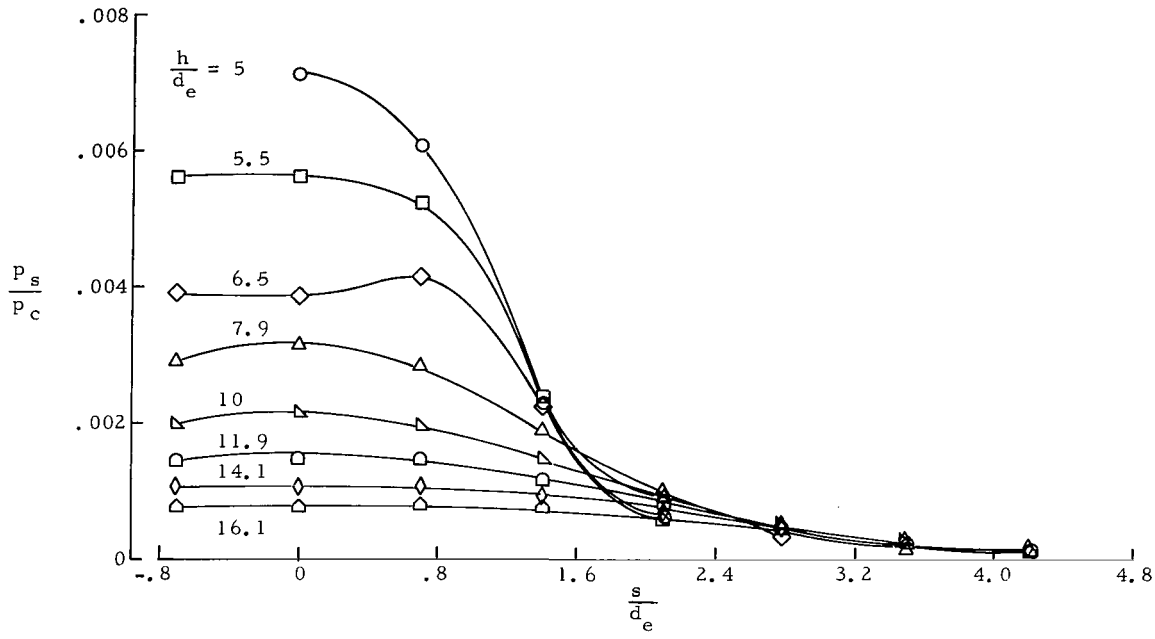

(a) d_e = 0.625 in. (1.59 cm).

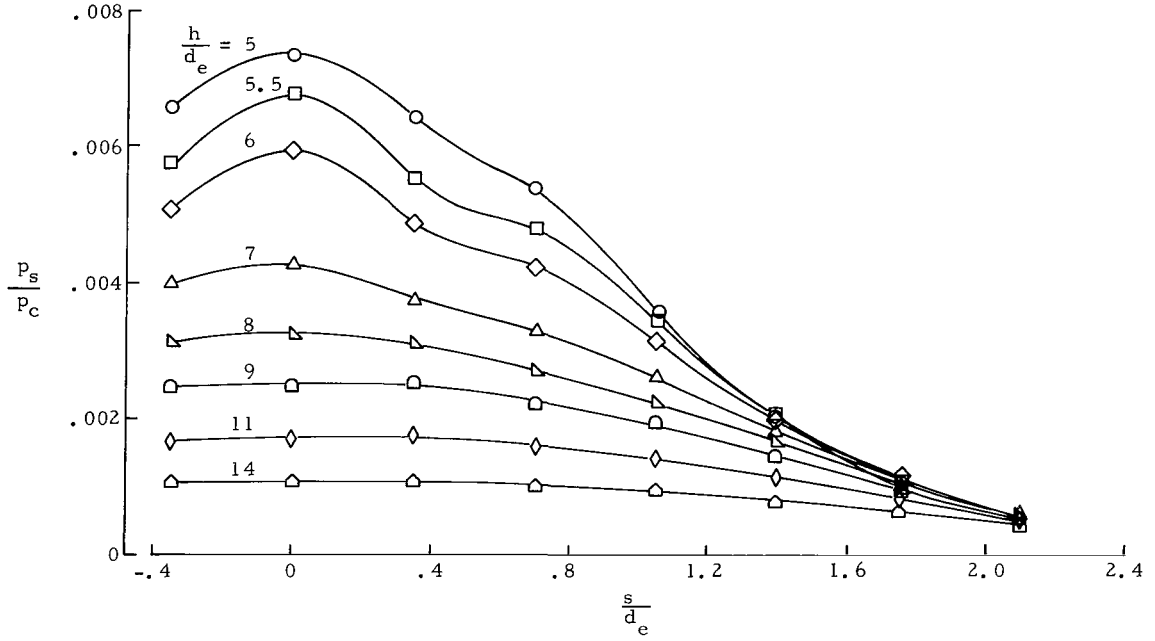

(b) d_e = 1.25 in. (3.18 cm).

Figure 14.- Distribution of impingement pressures around d_m = 10-in. (25.4-cm) cylinder for M_e = 7.09 helium jets.

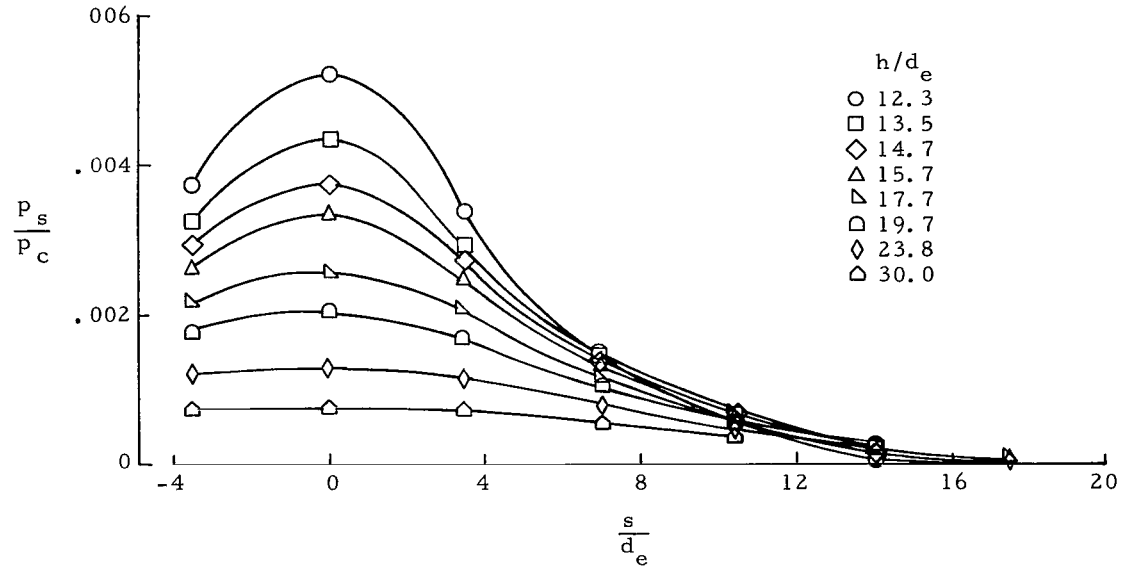

(a) γ = 1.4.

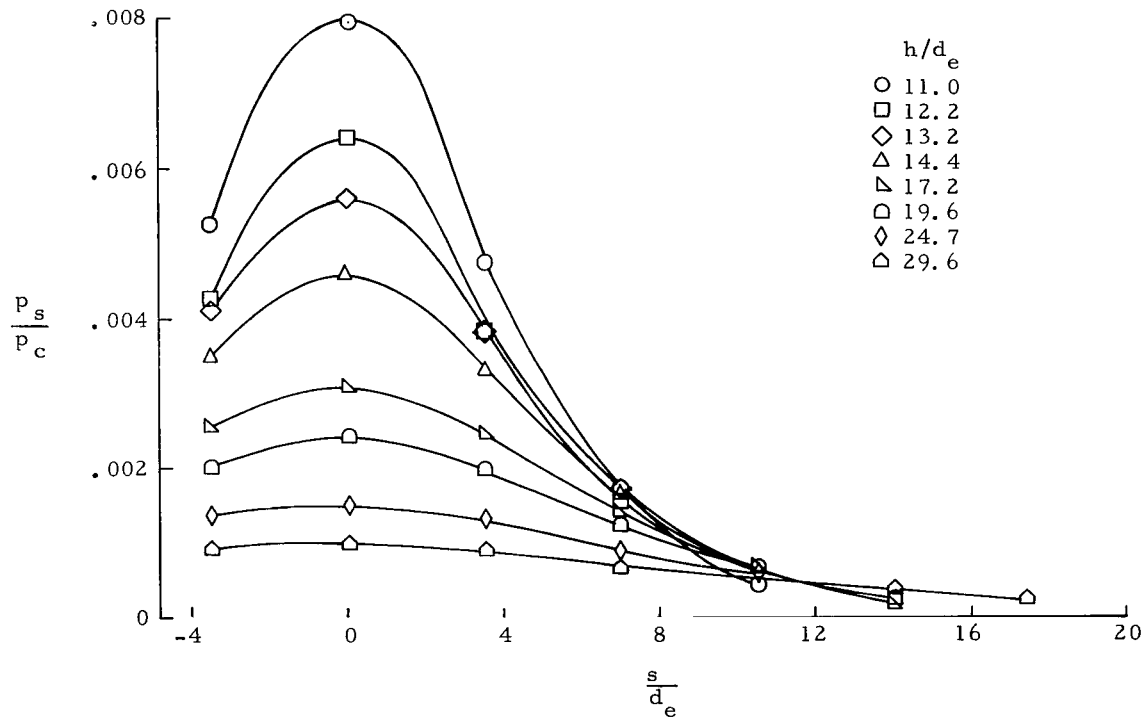

(b) γ = 1.67.

Figure 15.- Distribution of impingement pressures around d_m = 10-in. (25.4-cm) cylinder for sonic jets.

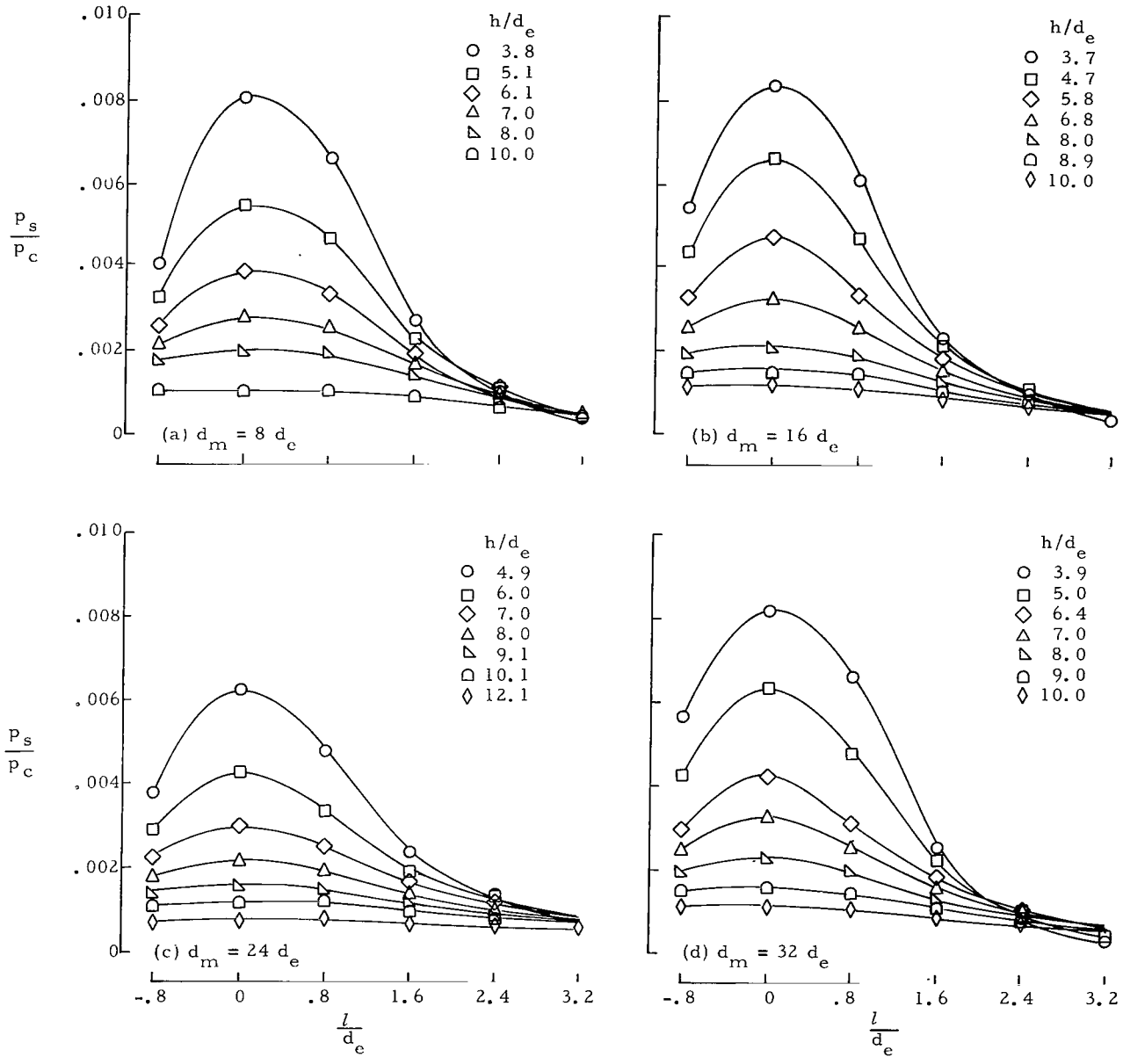

Figure 16.- Distribution of impingement pressures along cylinders for $M_e = 5$ nitrogen jet having $d_e = 0.625$ in. (1.59 cm).

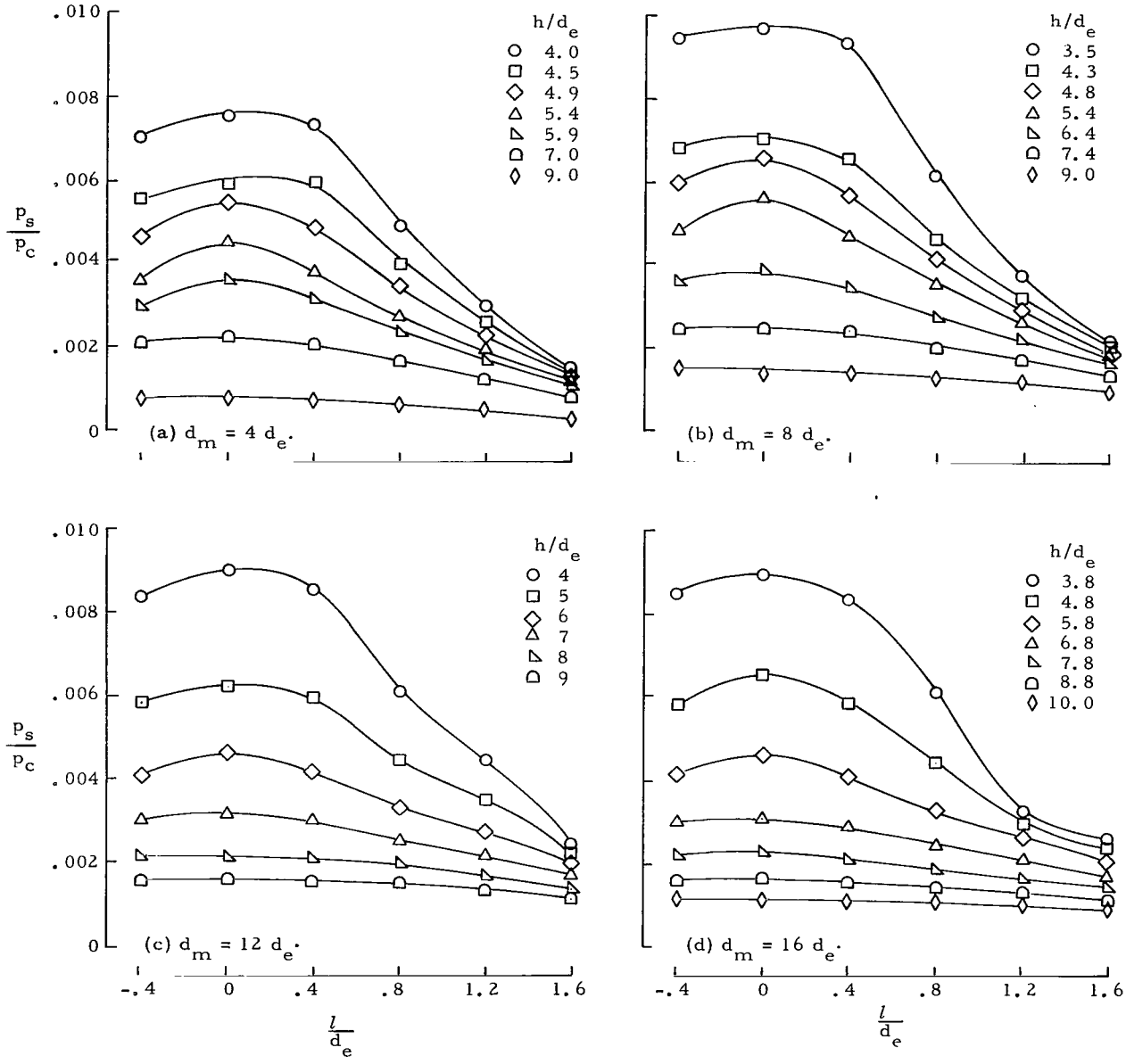

Figure 17.- Distribution of impingement pressures along cylinders for $M_e = 5$ nitrogen jet having $d_e = 1.25$ in. (3.18 cm).

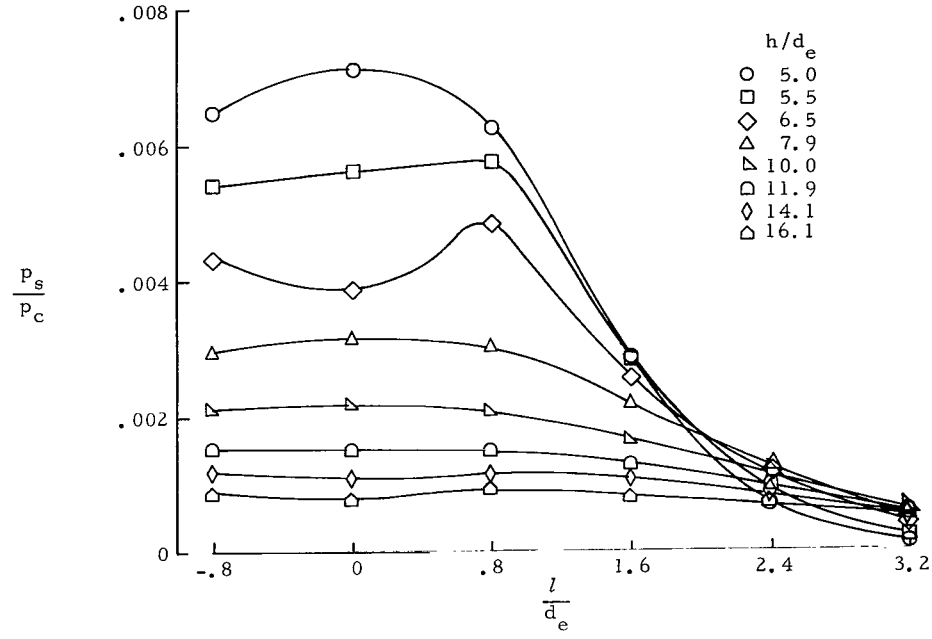

(a) d_e = 0.625 in. (1.59 cm).

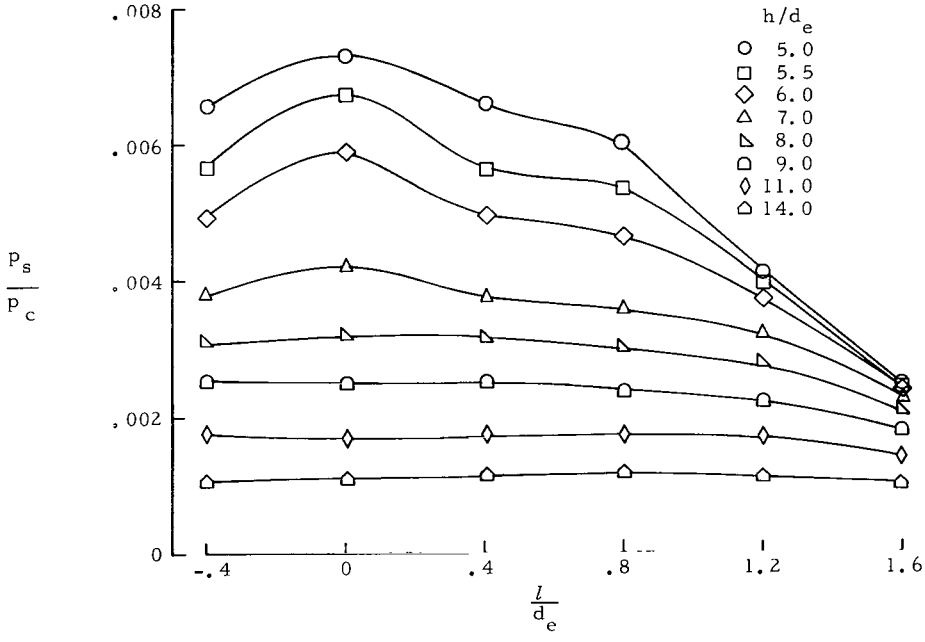

(b) d_e = 1.25 in. (3.18 cm).

Figure 18.- Distribution of impingement pressures along d_m = 10-in. (25.4-cm) cylinder for M_e = 7.09 helium jets.

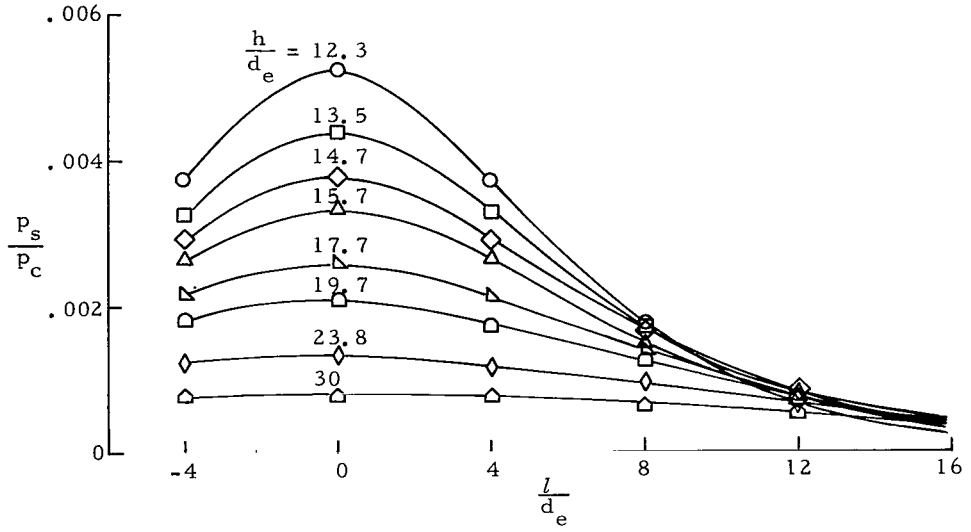

(a) γ = 1.4.

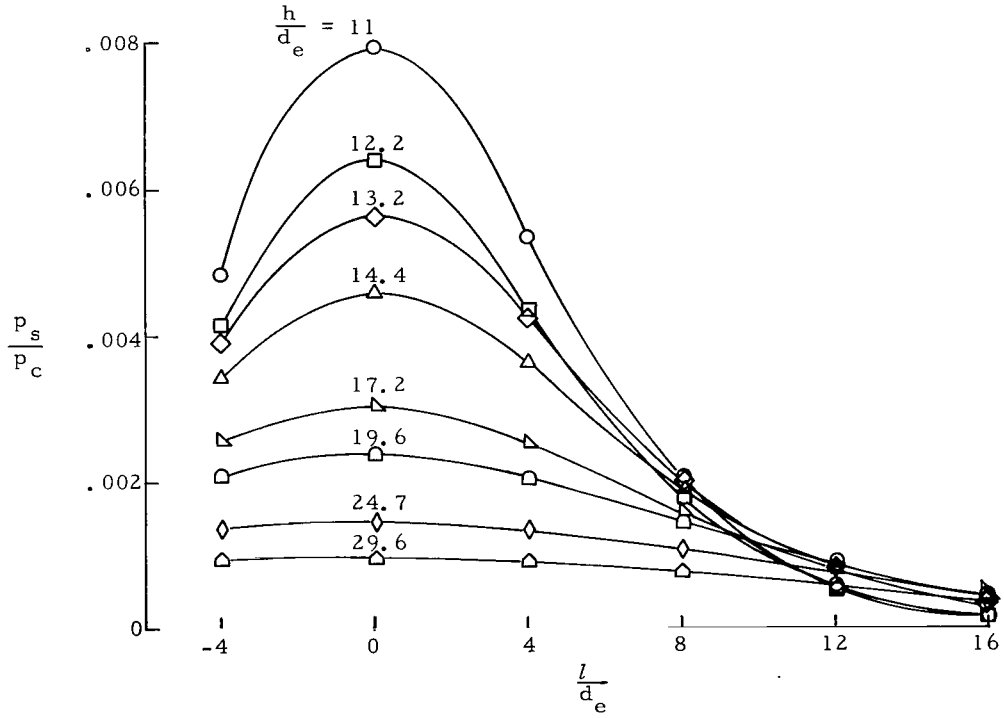

(b) γ = 1.67.

Figure 19.- Distribution of impingement pressures along d_m = 10-in. (25.4-cm) cylinder for sonic jets.

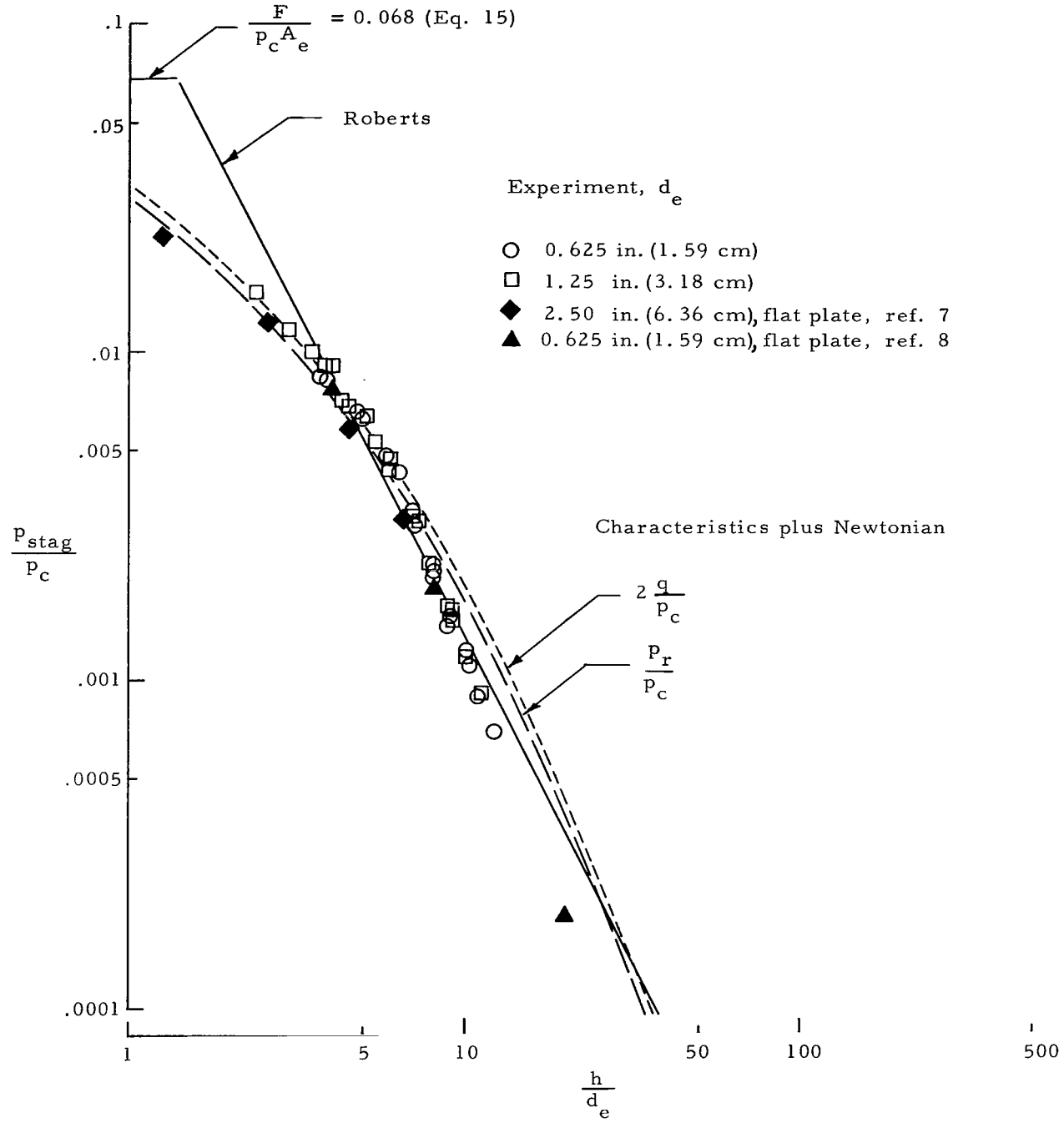

Figure 20.- Effect of jet height on surface stagnation pressure for $M_e = 5$, $\theta_e = 15^0$ jets using nitrogen.

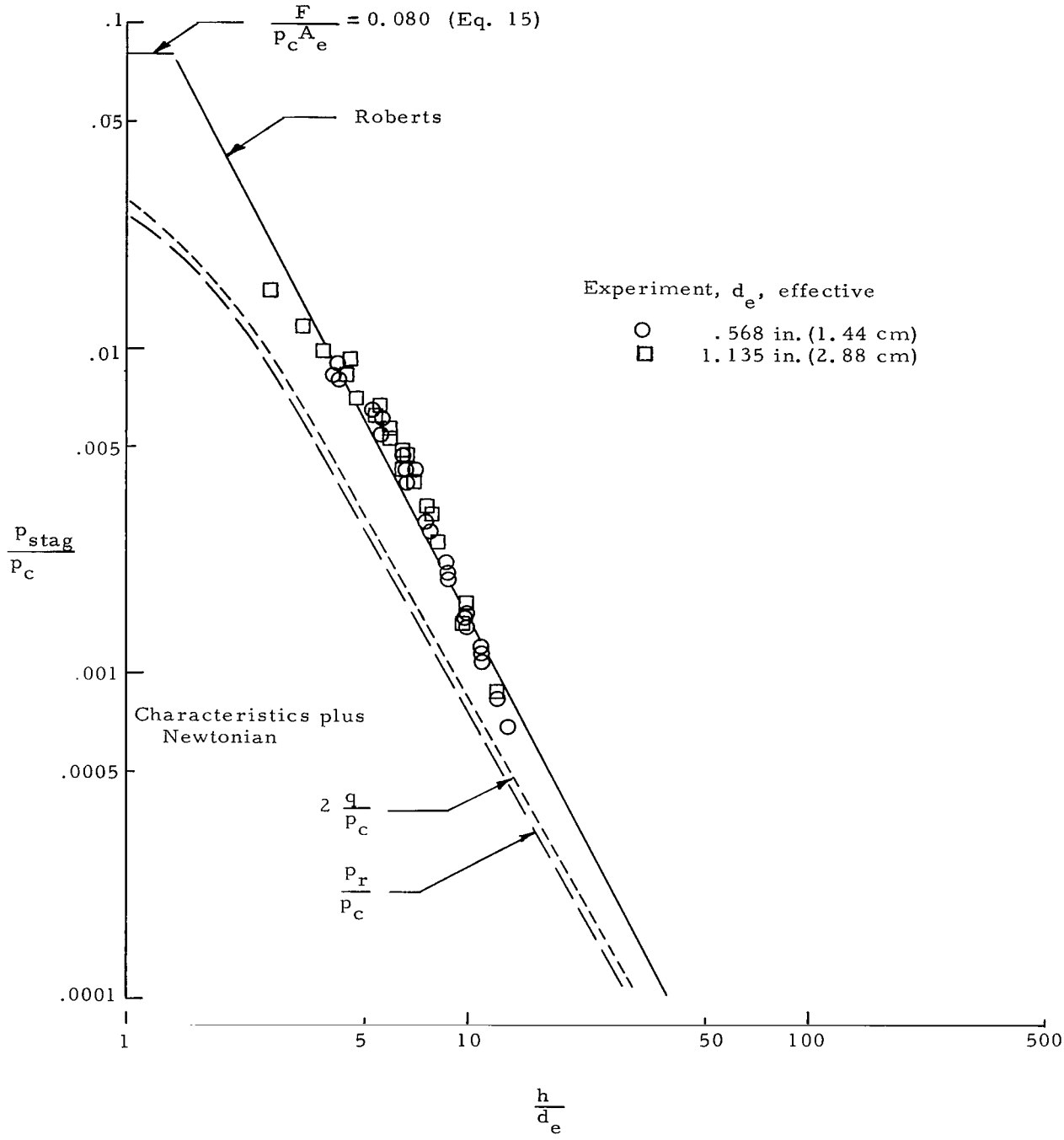

Figure 21.- Effect of jet height on surface stagnation pressure for $M_e = 4.79$, $\theta_e = 26.5^0$ jets using nitrogen.

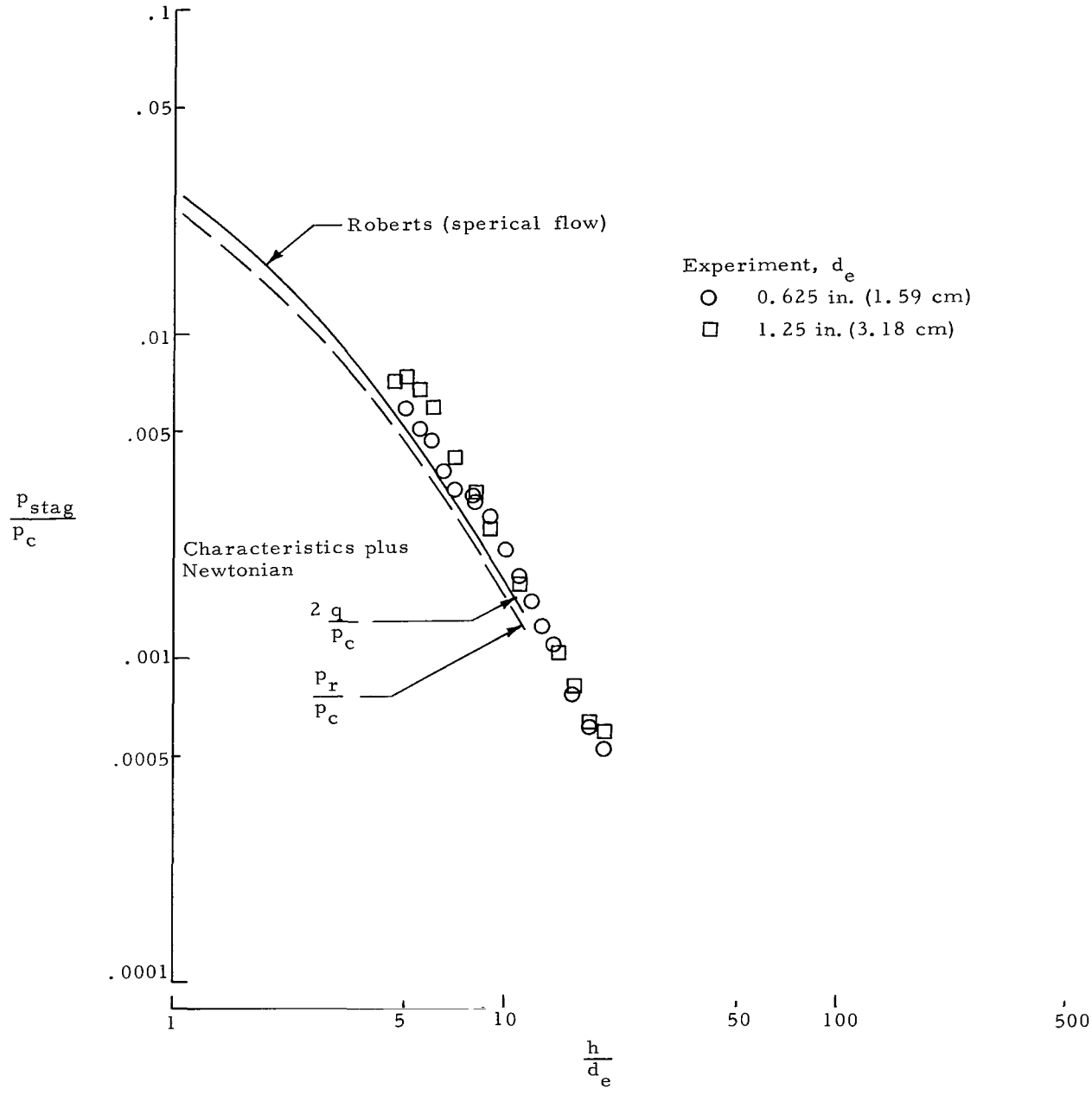

Figure 22.- Effect of jet height on surface stagnation pressure for $M_e = 7.09$, $\theta_e = 15^0$ jets using helium.

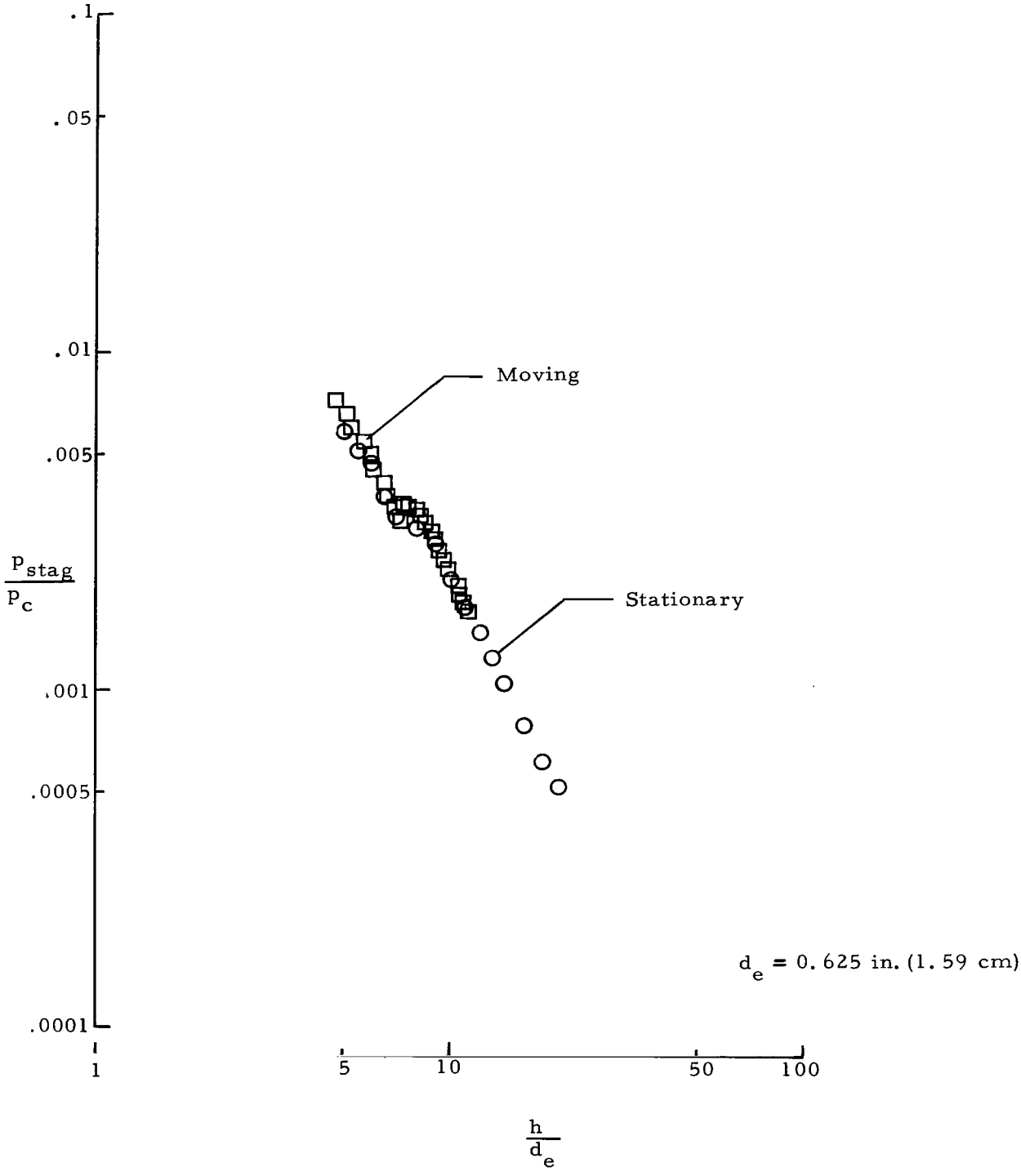

Figure 23.- Comparison of axial impingement pressures for stationary and moving M_e = 7.09 jet using helium.

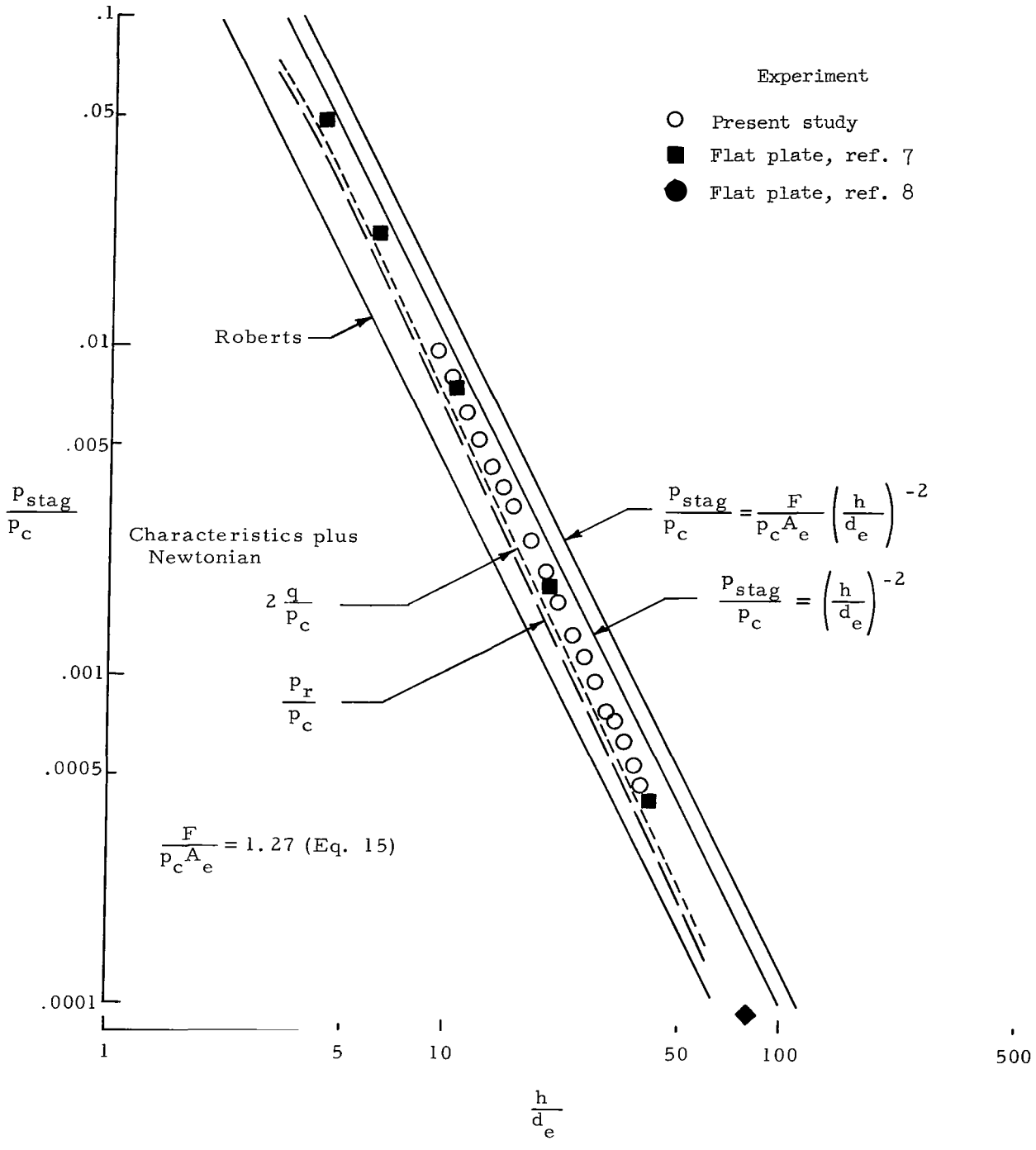

(a) Nitrogen, $\gamma = 1.4$.

Figure 24.- Effect of jet height on surface stagnation pressure for sonic jets.

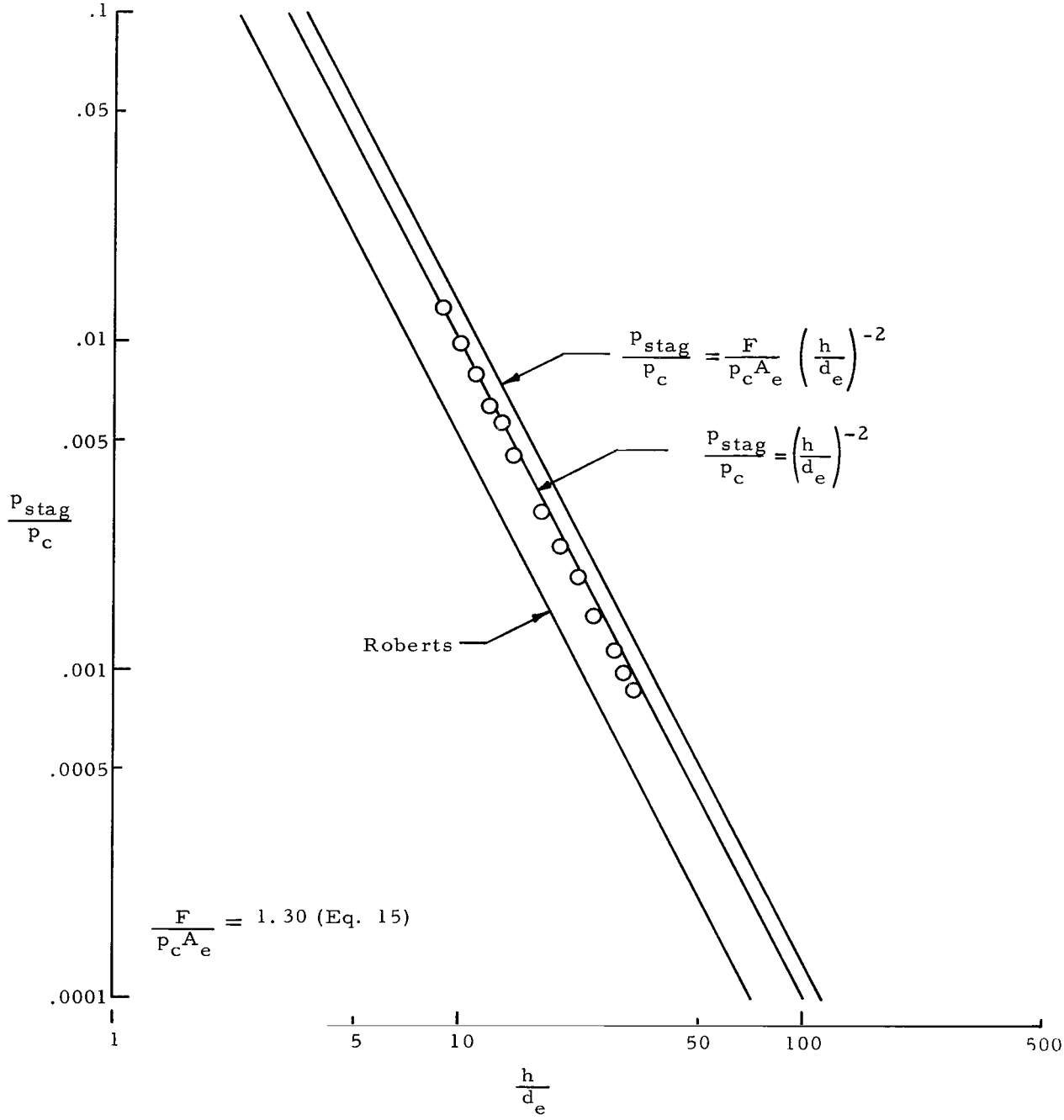

(b) Helium, $\gamma = 1.67$.

Figure 24.- Concluded.

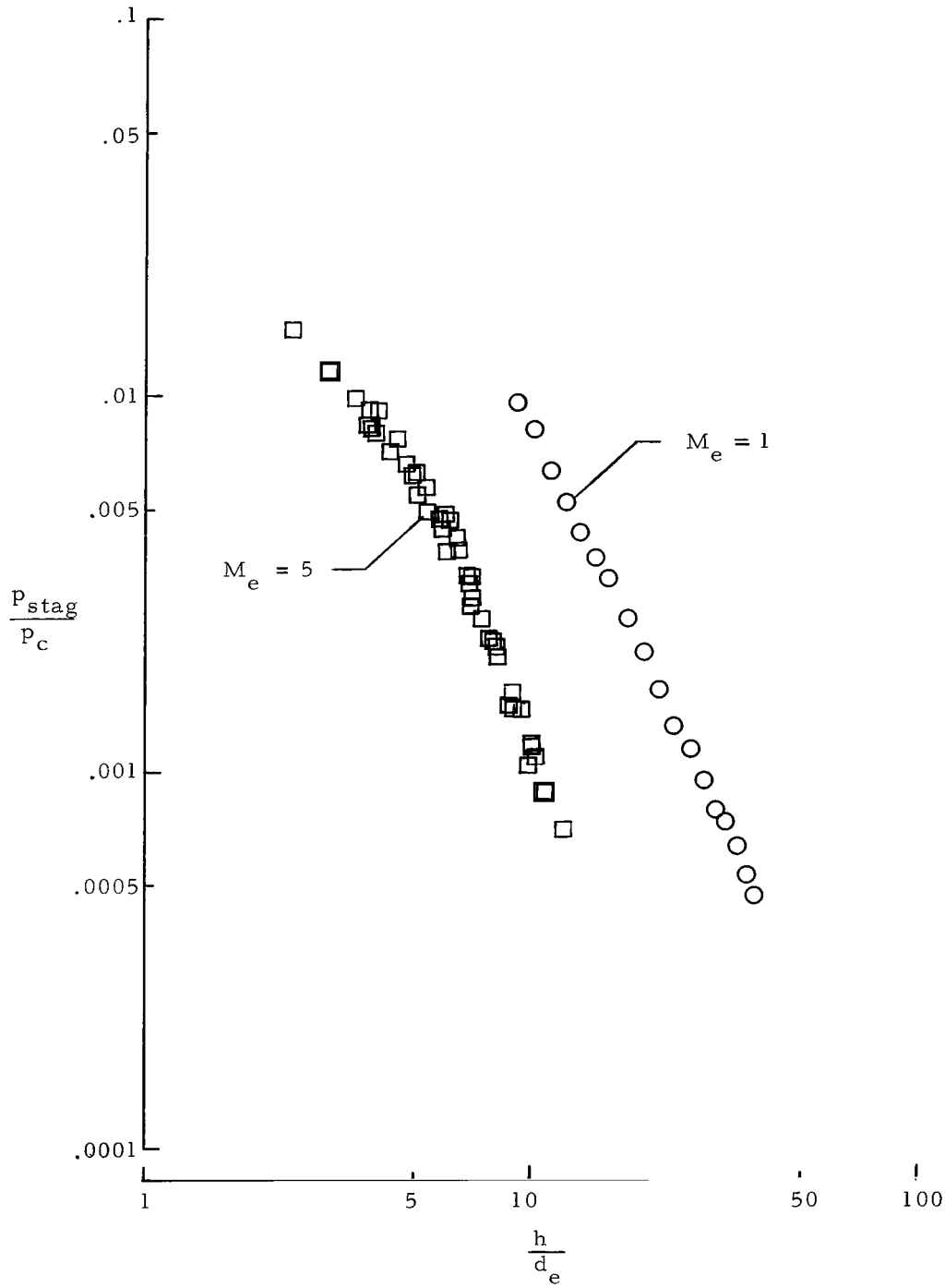

(a) Nitrogen, $\gamma = 1.4$.

Figure 25.- Effect of jet-exit Mach number on surface stagnation pressure.

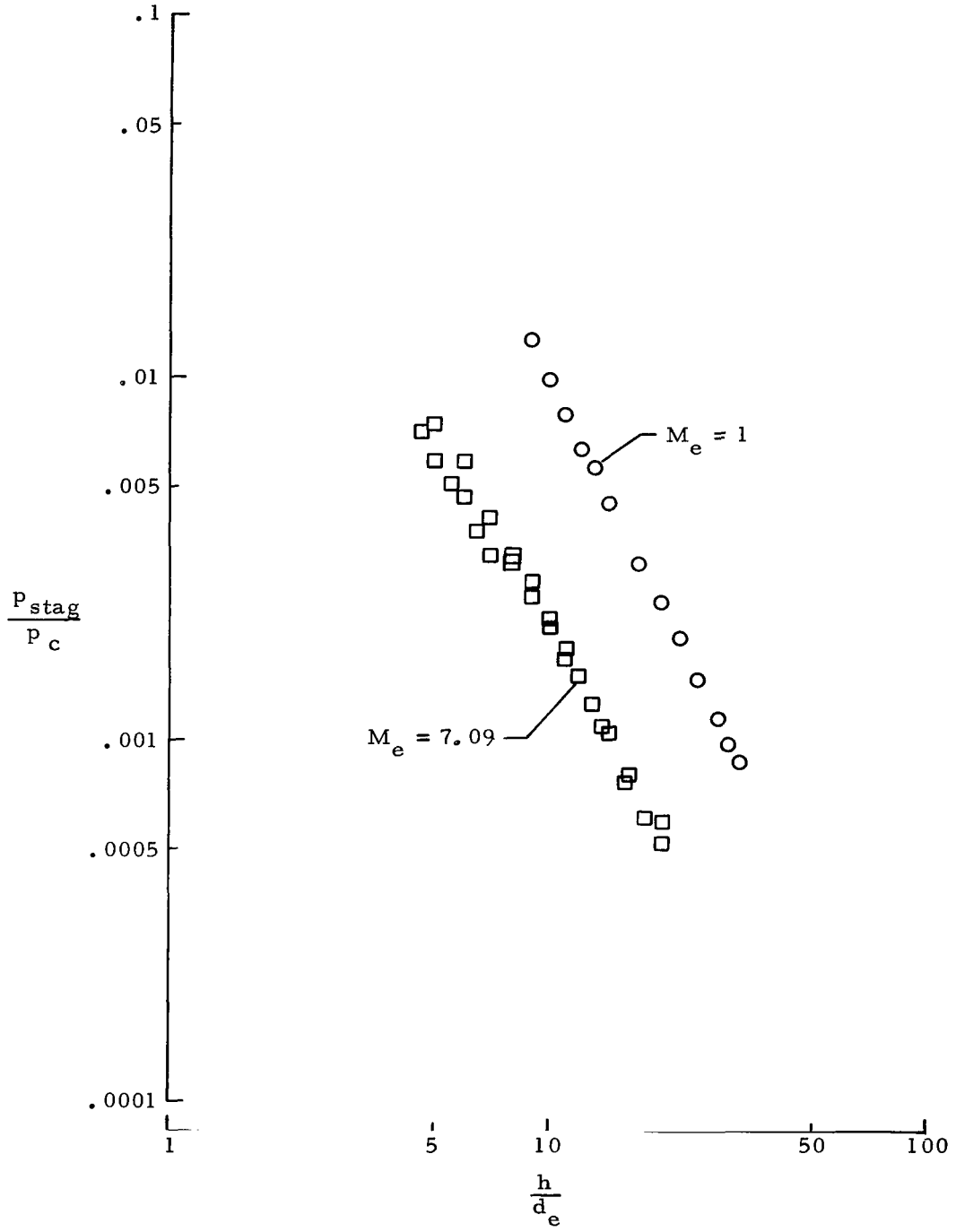

(b) Helium, $\gamma = 1.67$.

Figure 25.- Concluded.

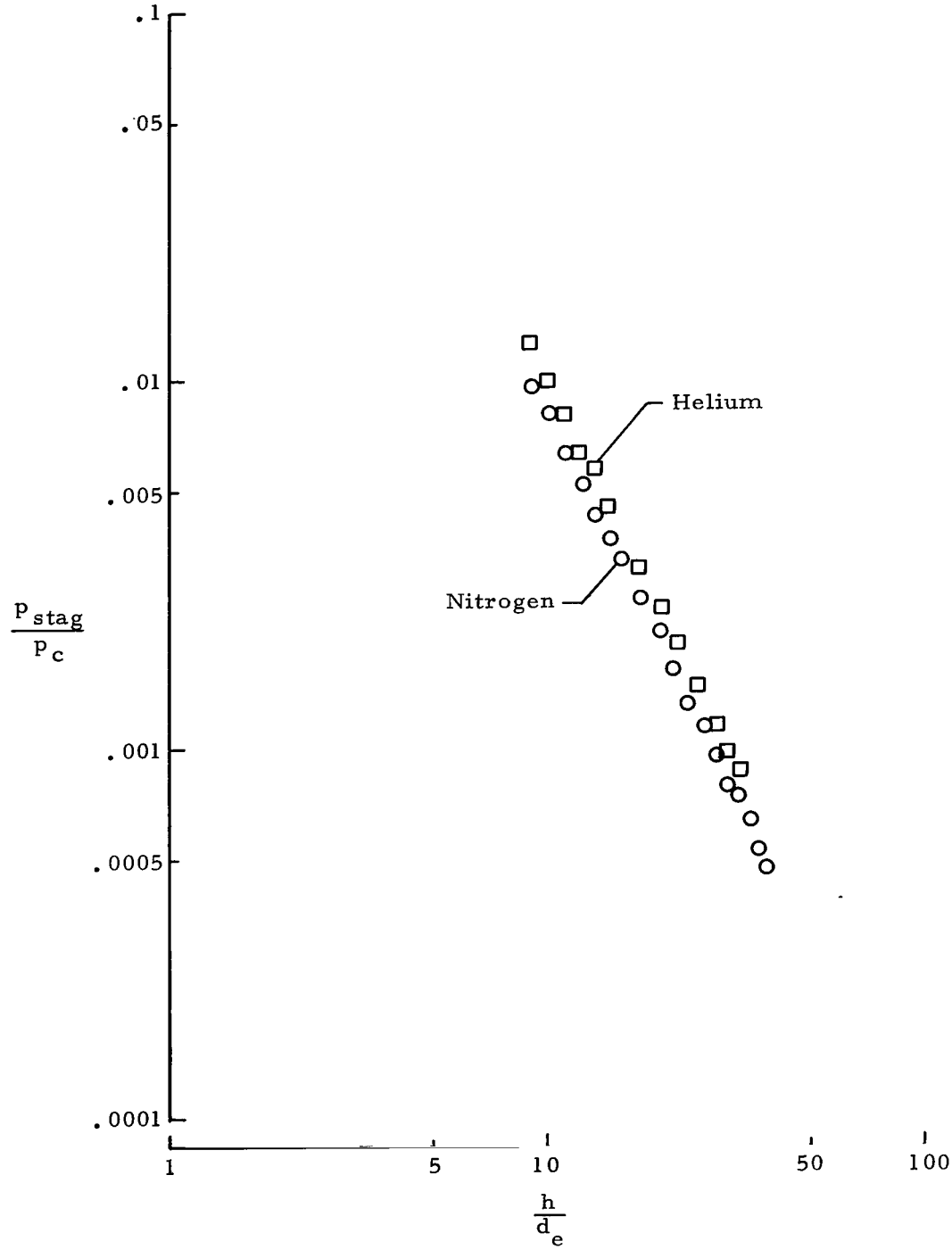

Figure 26.- Effect of exhaust gas properties on surface stagnation pressure for sonic jets.

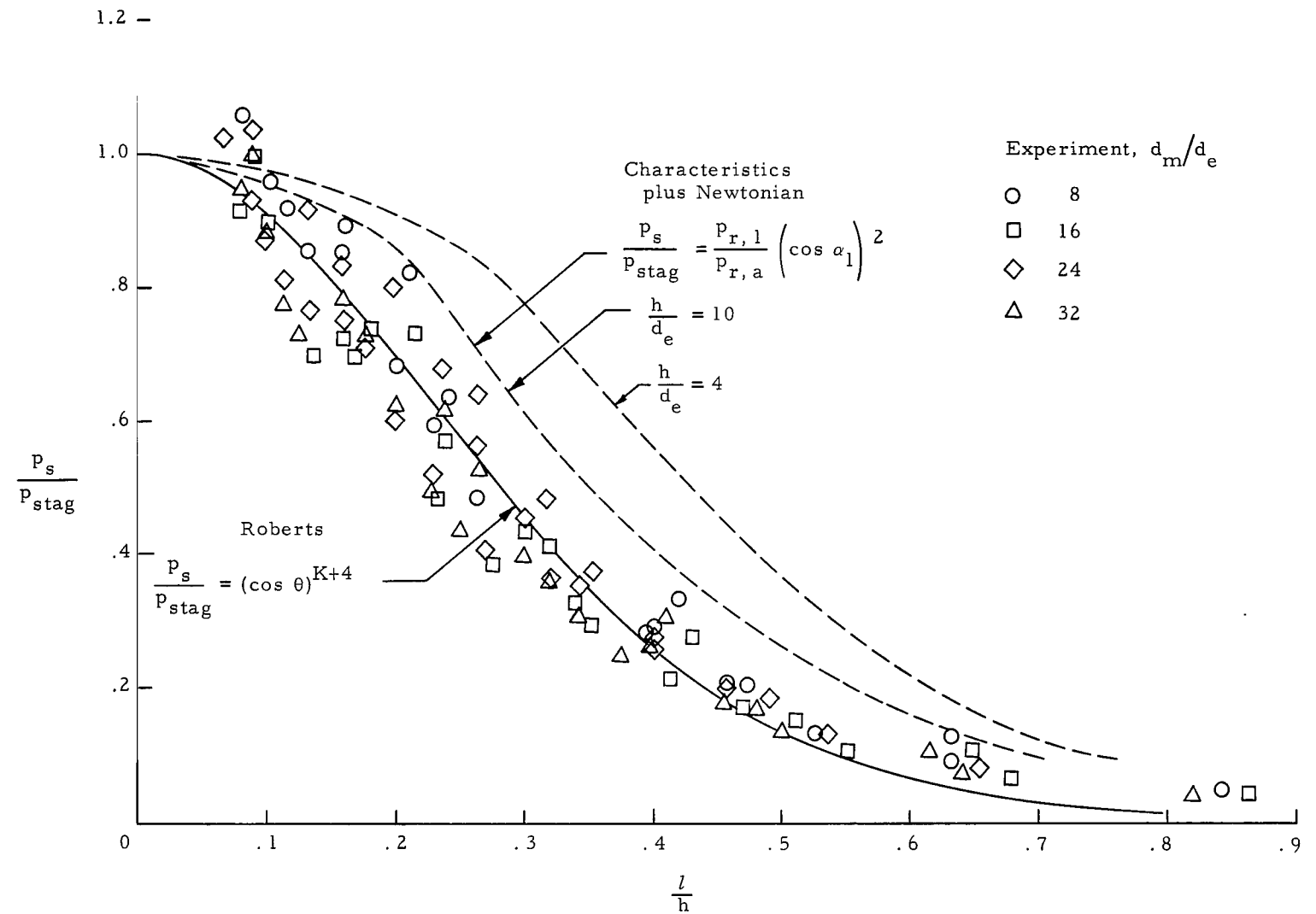

Figure 27.- Summary of distribution of impingement pressures along cylinders for $M_e = 5$ nitrogen jet having $d_e = 0.625$ in. (1.59 cm).

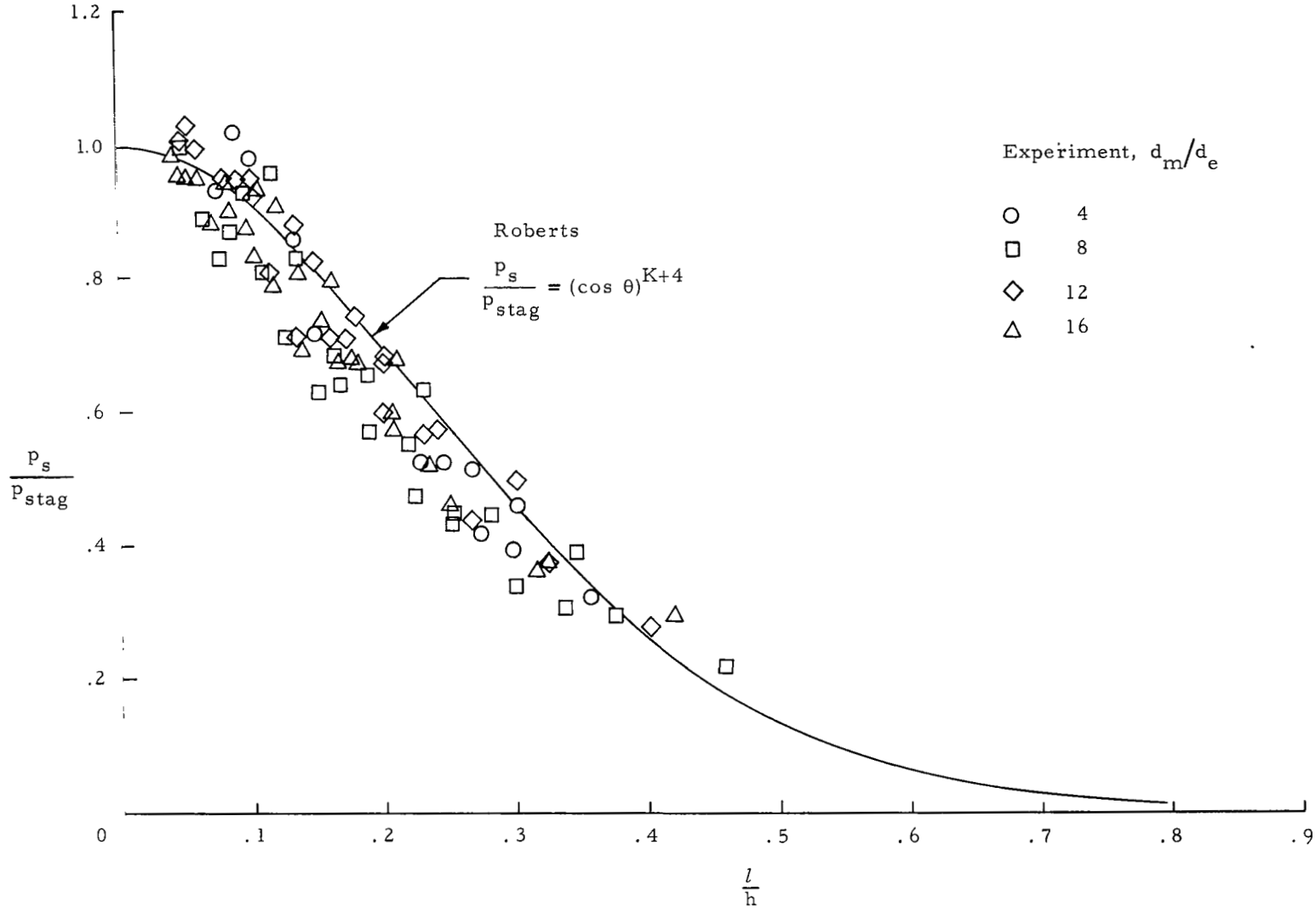

Figure 28.- Summary of distribution of impingement pressures along cylinders for $M_e = 5$ nitrogen jet having $d_e = 1.25$ in. (3.18 cm).

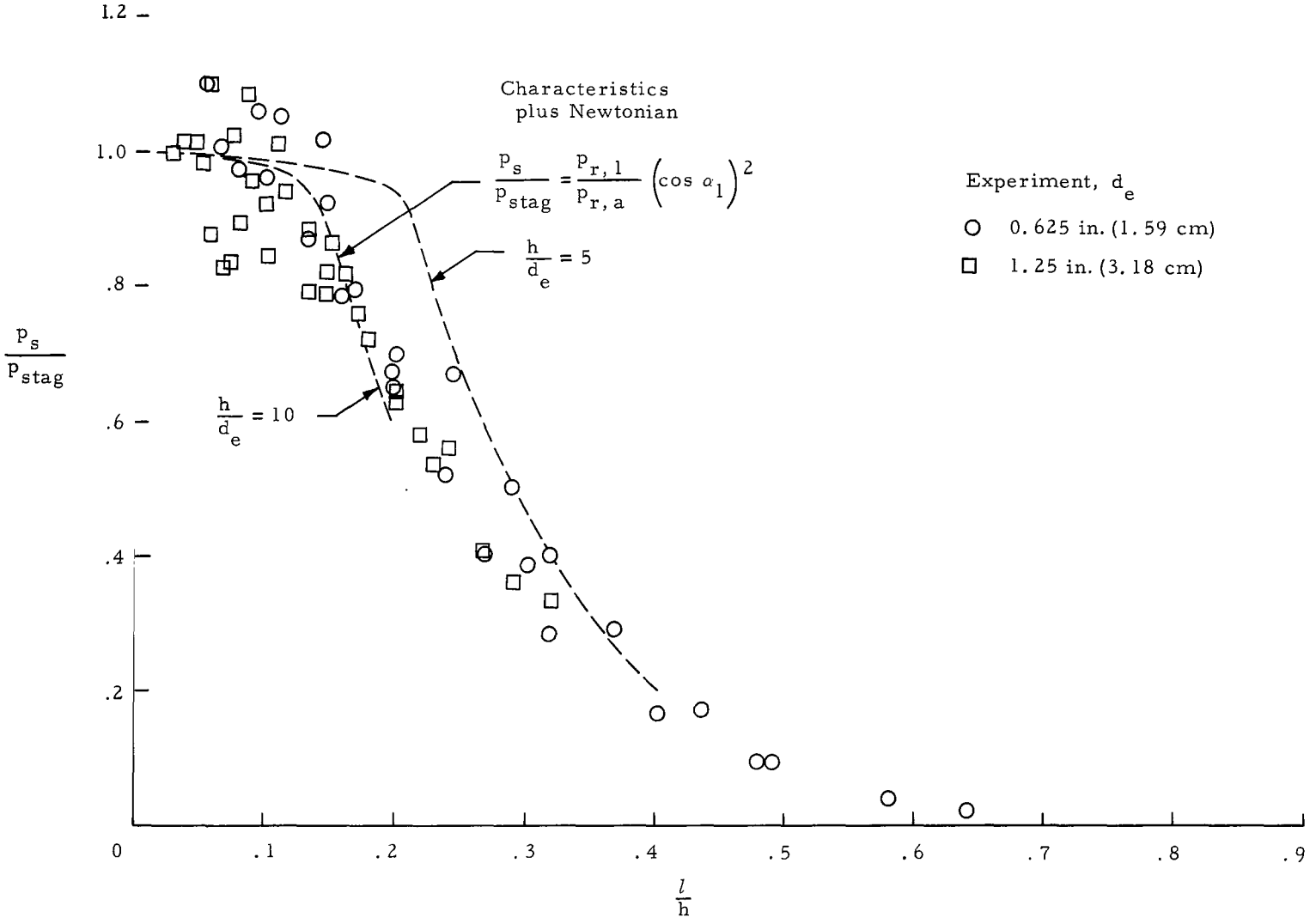

Figure 29.- Summary of distribution of impingement pressures along d_m = 10-in. (25.4-cm) cylinder for M_e = 7.09 helium jets.

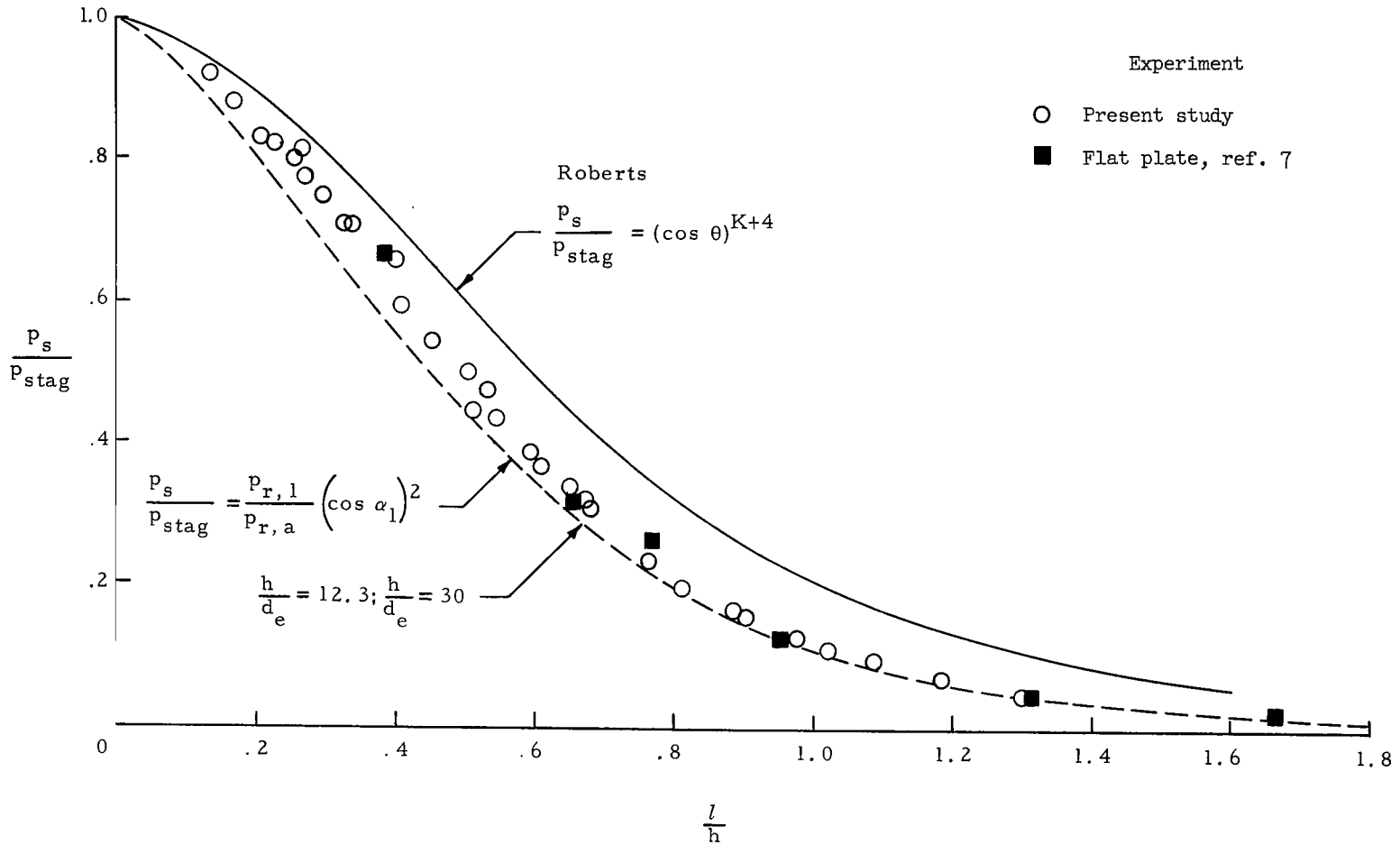

(a) Nitrogen, $\gamma = 1.4$.

Figure 30.- Summary of distribution of impingement pressures along d_m = 10-in. (25.4-cm) cylinder for sonic jets.

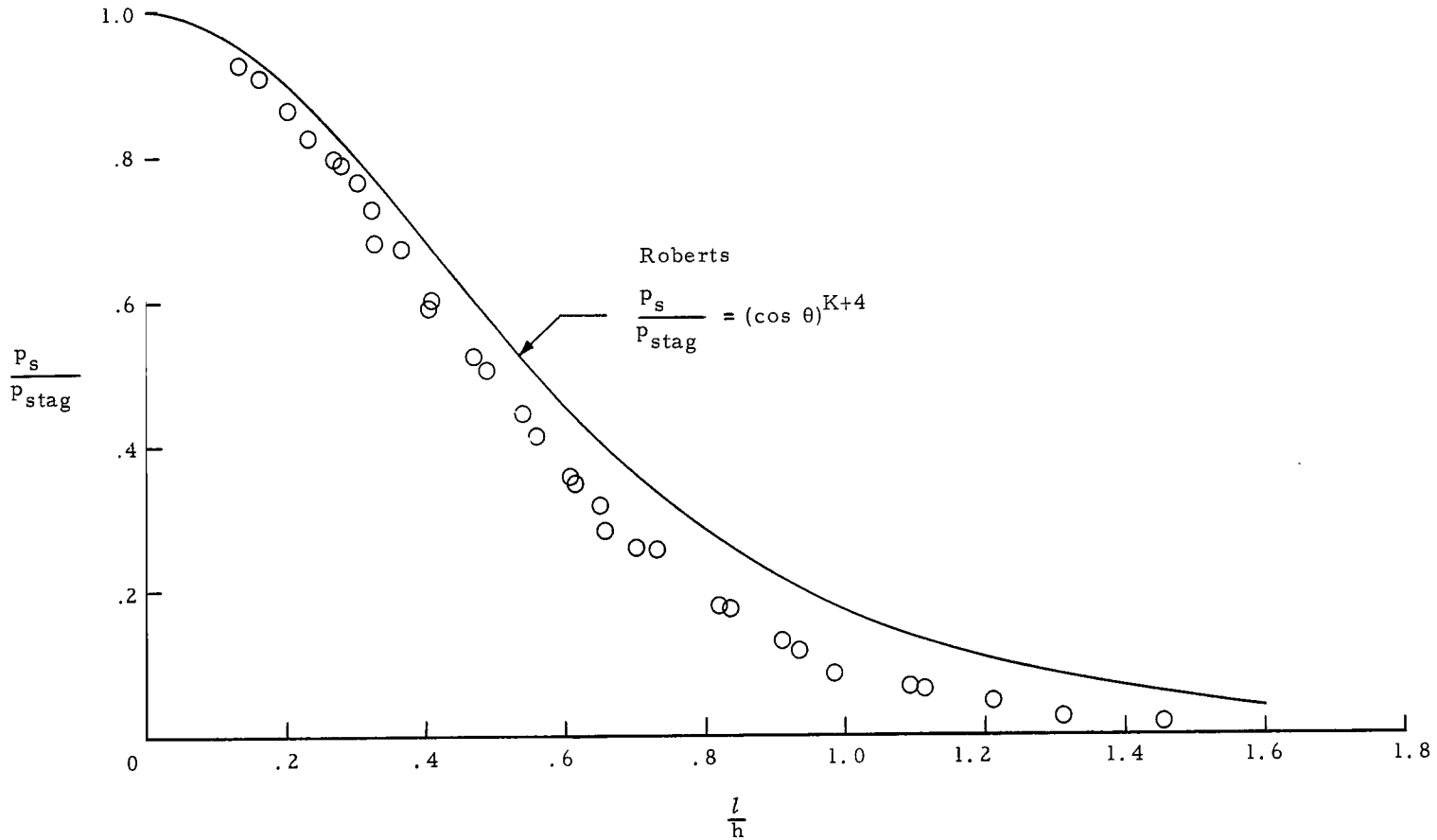

(b) Helium, $\gamma = 1.67$.

Figure 30.- Concluded.

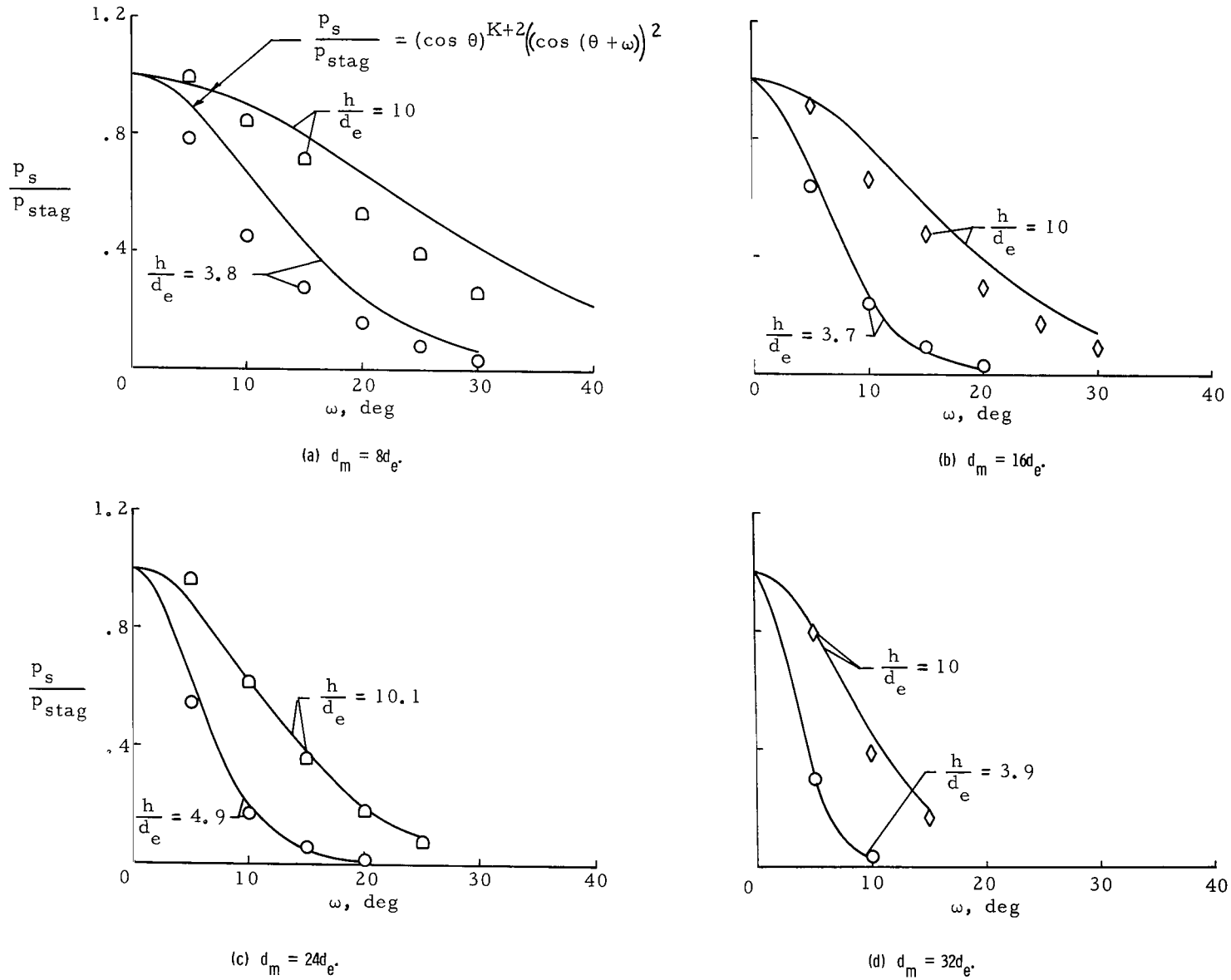

(a) $d_m = 8d_e$.

(b) $d_m = 16d_e$.

(c) $d_m = 24d_e$.

(d) $d_m = 32d_e$.

Figure 31.- Comparison of experimental and theoretical impingement pressure distributions around cylinders for $M_e = 5$ nitrogen jet having $d_e = 0.625$ in. (1.59 cm).

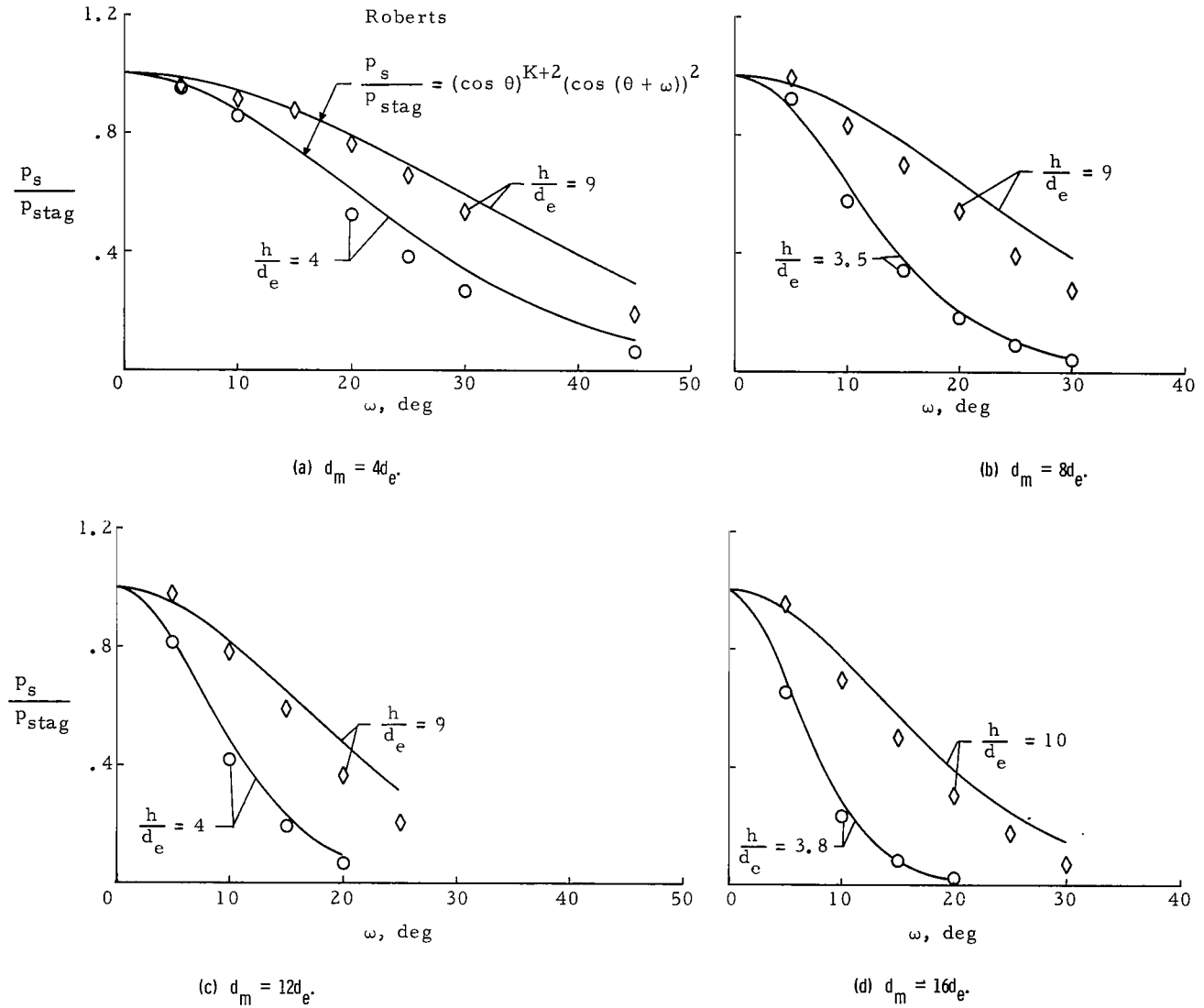

(a) $d_m = 4d_e$.

(b) $d_m = 8d_e$.

(c) $d_m = 12d_e$.

(d) $d_m = 16d_e$.

Figure 32.- Comparison of experimental and theoretical impingement pressure distributions around cylinders for $M_e = 5$ nitrogen jet having $d_e = 1.25$ in. (3.18 cm).

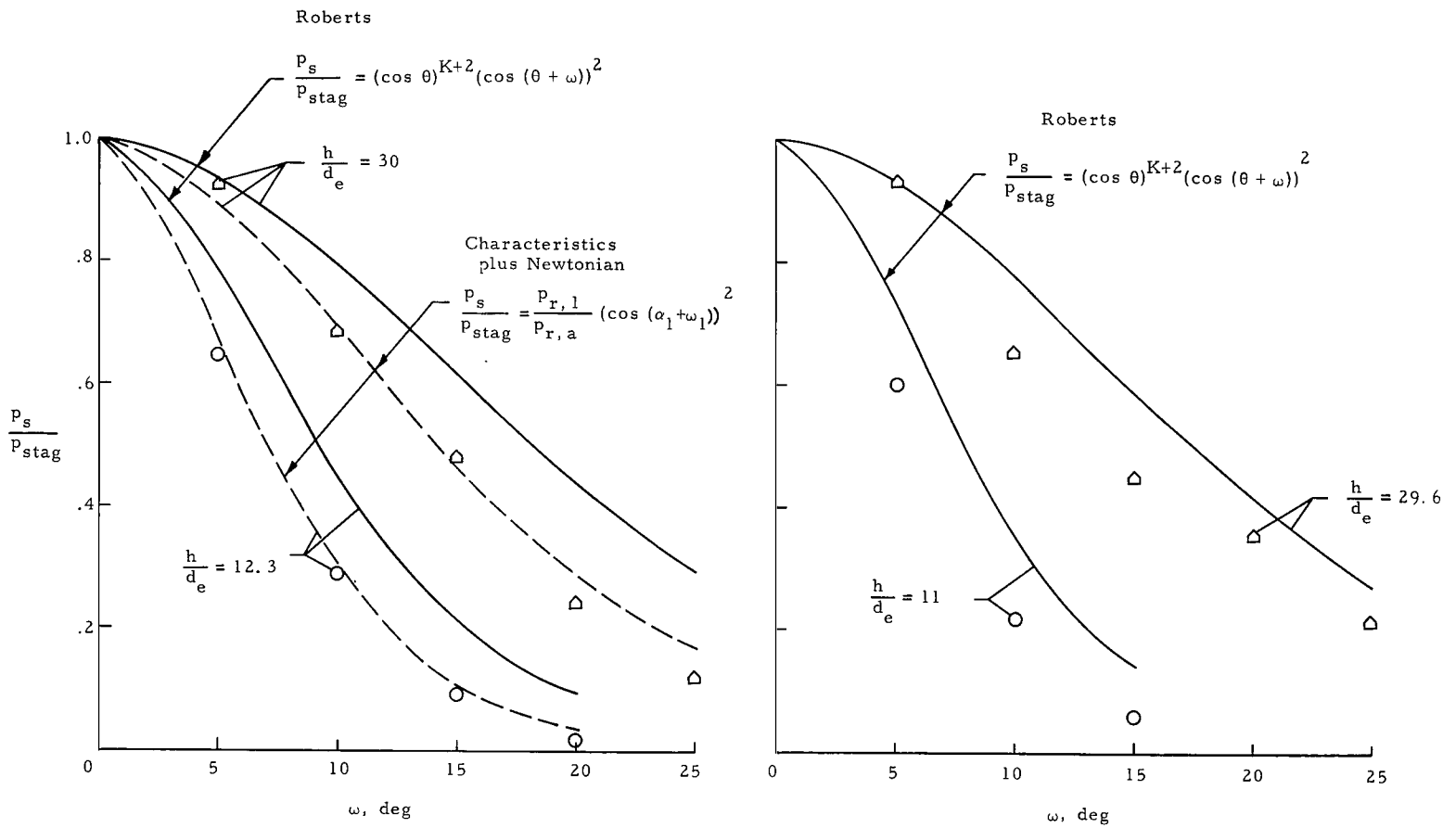

(a) Nitrogen, $\gamma = 1.4$.

(b) Helium, $\gamma = 1.67$.

Figure 33.- Comparison of experimental and theoretical impingement pressure distributions around d_m = 10-in. (25.4-cm) cylinder for sonic jets.

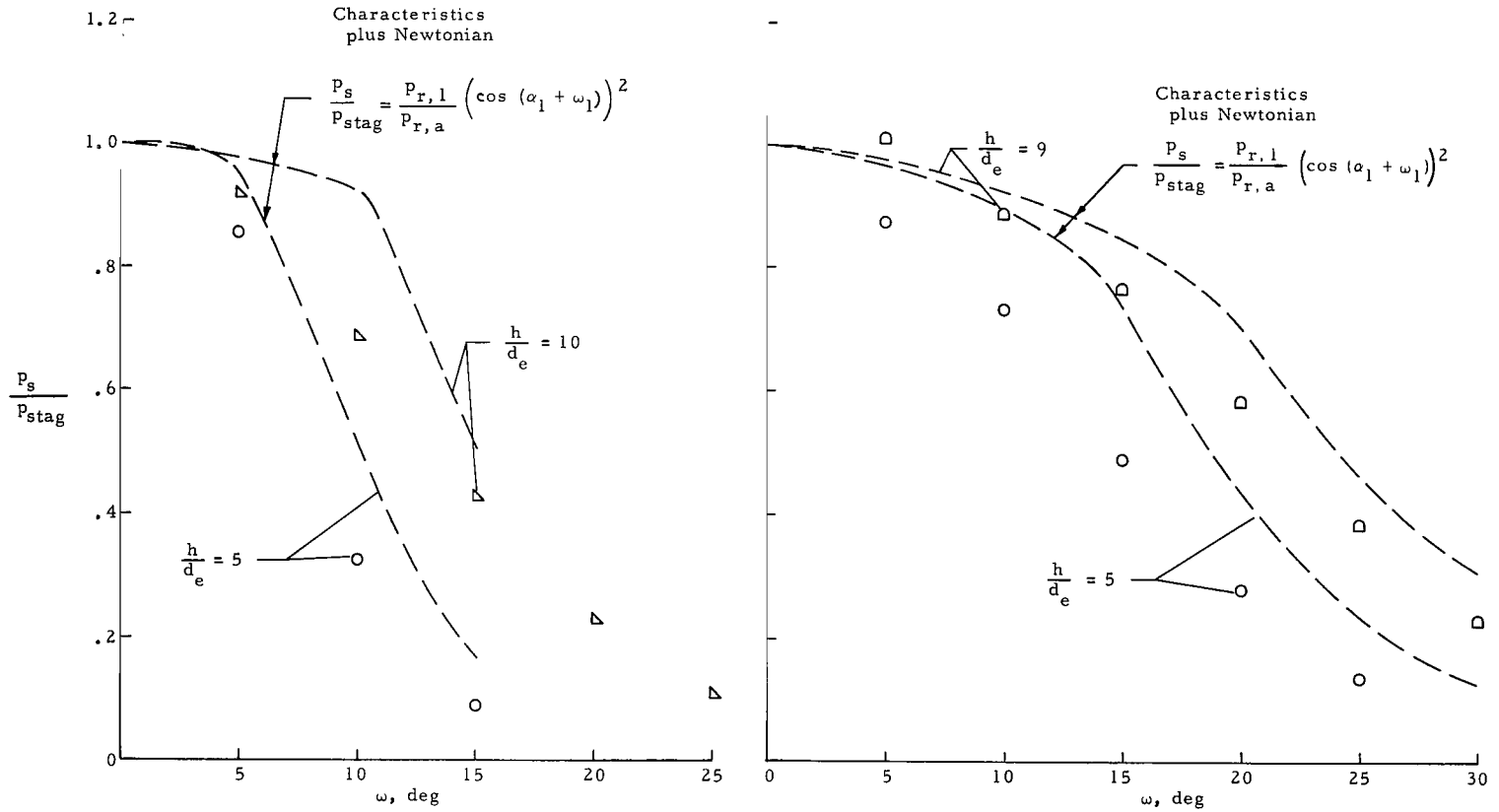

(a) d_e = 0.625 in. (1.59 cm).

(b) d_e = 1.25 in. (3.18 cm).

Figure 34.- Comparison of experimental and theoretical impingement pressure distributions around d_m = 10-in. (25.4-cm) cylinder for M_e = 7.09 helium jets.

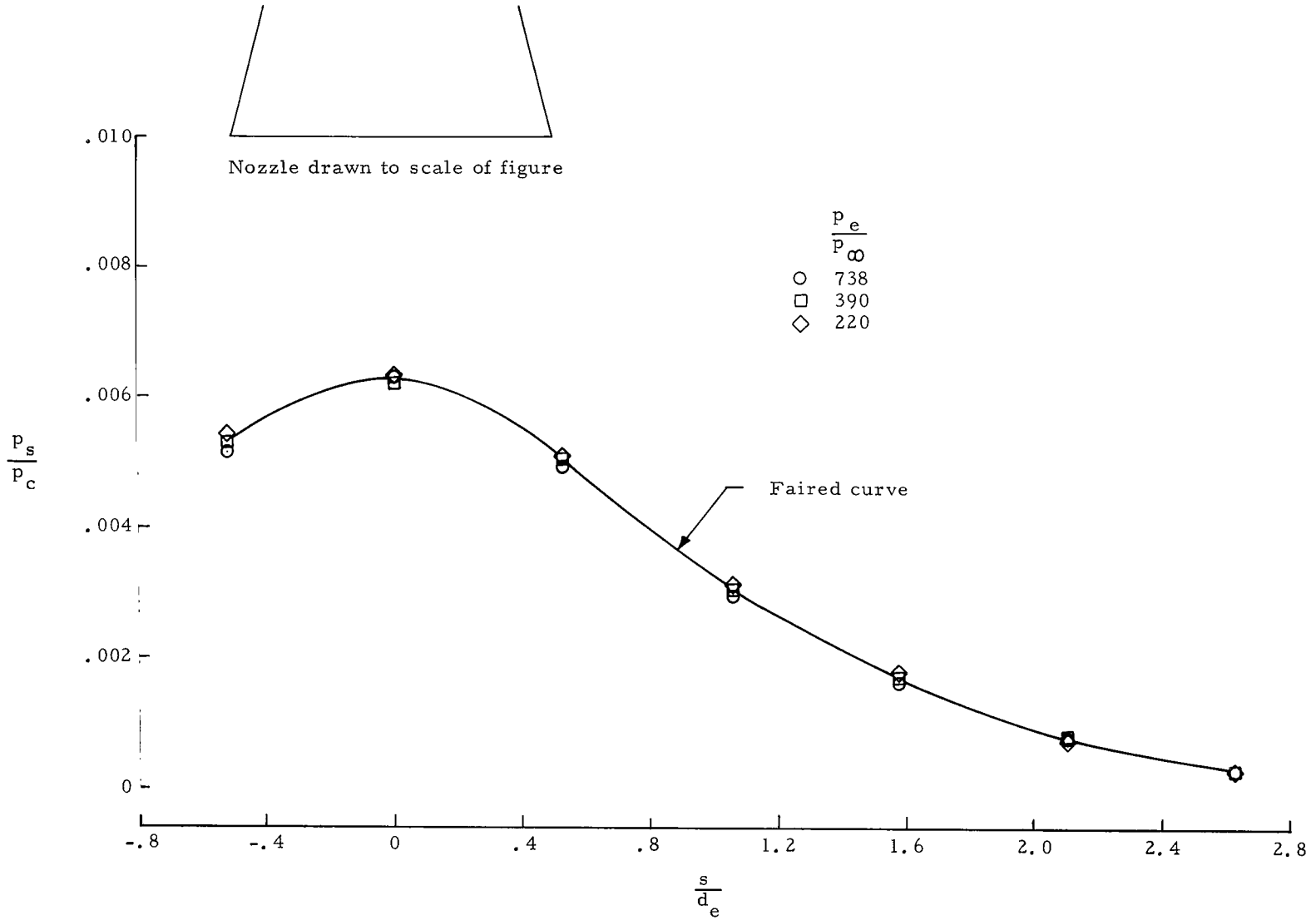

Figure 35.- Effect of ratio of jet-exit pressure to ambient pressure on the distribution of impingement pressures for $M_e = 5$ nitrogen jet. $d_m = 12d_e$; $h = 5d_e$; $d_e = 1.25$ in. (3.18 cm).

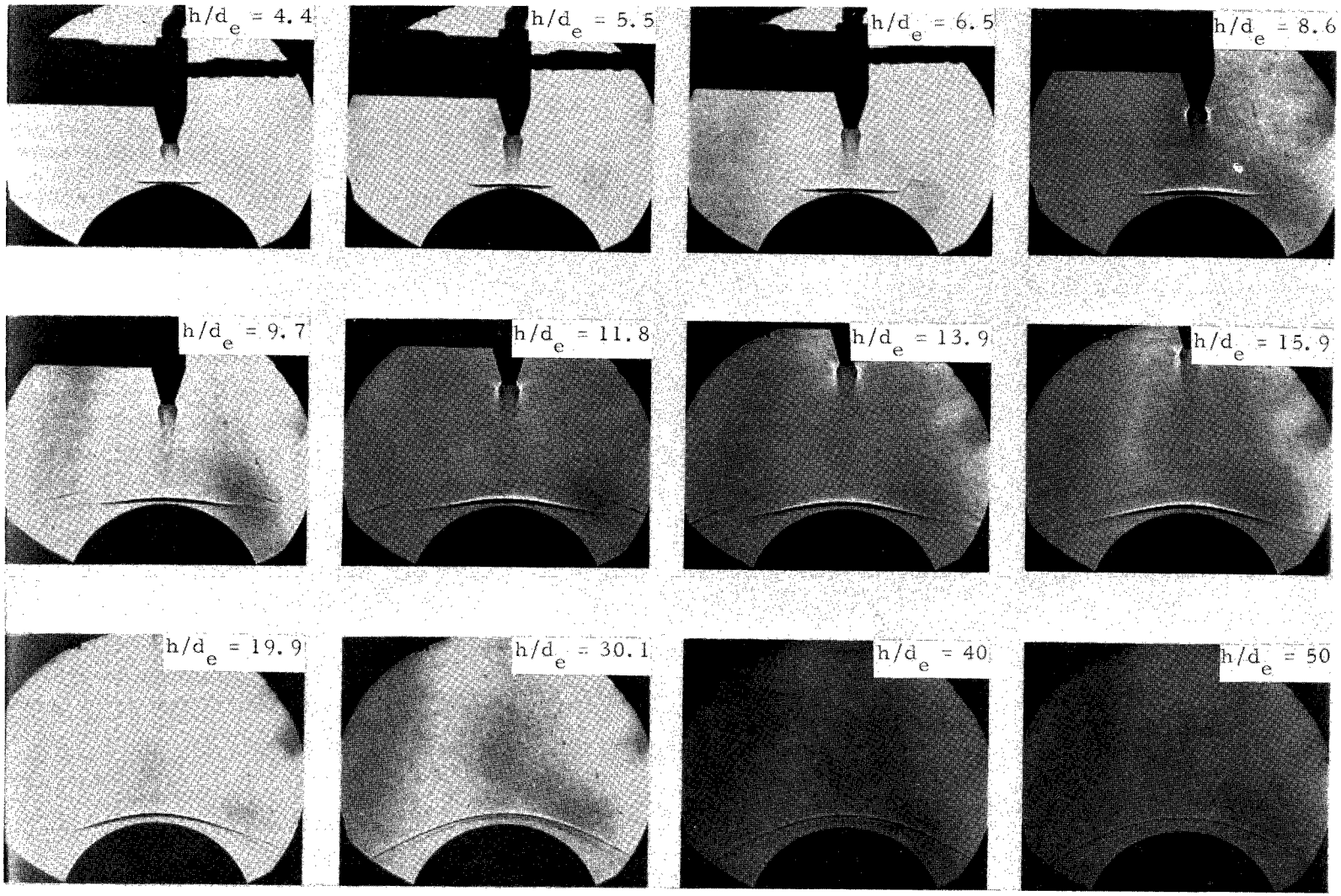

(a) d_e = 0.625 in. (1.59 cm). L-67-901

Figure 36.- Shadowgraphs of M_e = 5 nitrogen jets (γ = 1.4) exhausting onto d_m = 10-in. (25.4-cm) cylinder.

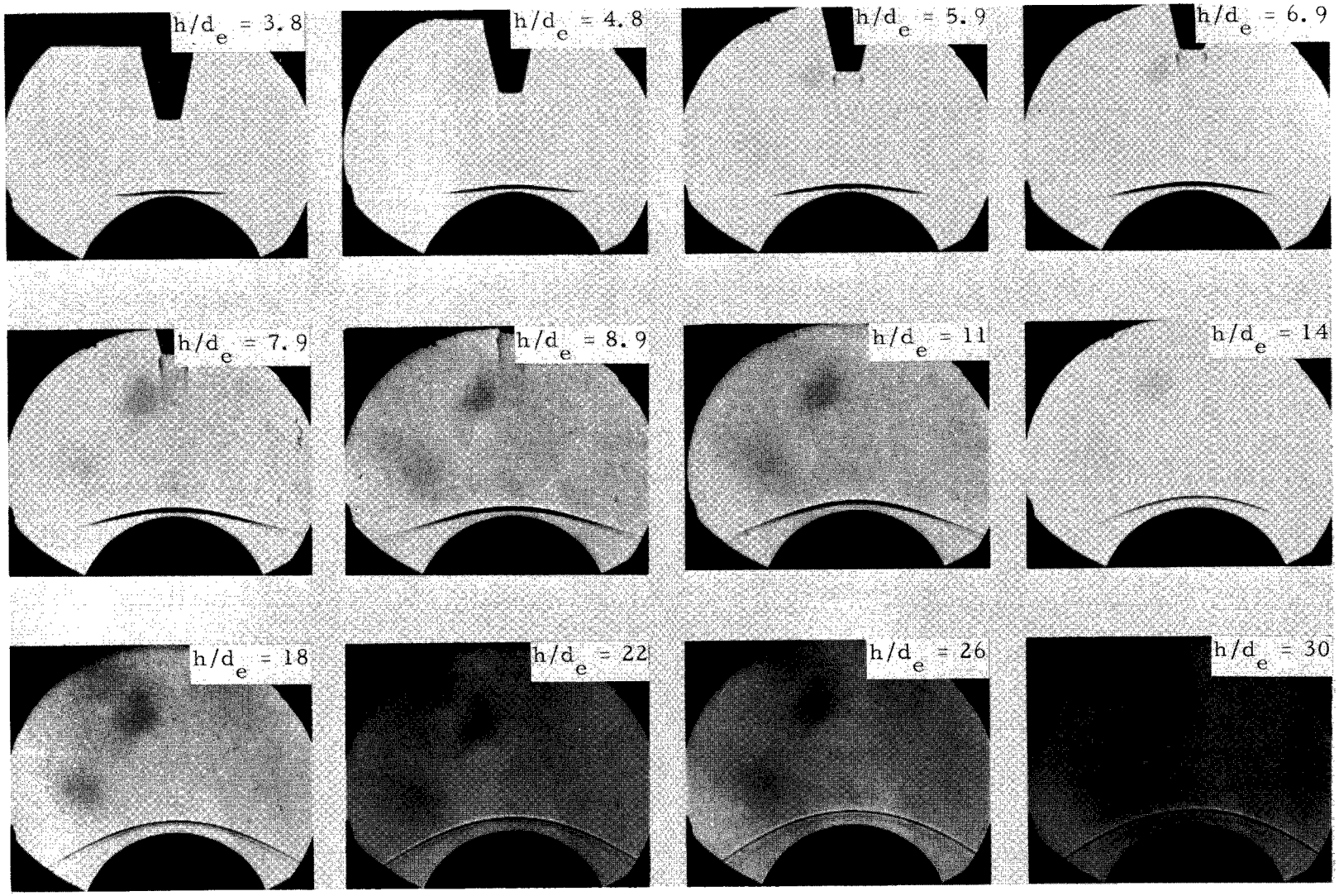

(b) d_e = 1.25 in. (3.18 cm).

L-67-902

Figure 36.- Concluded.

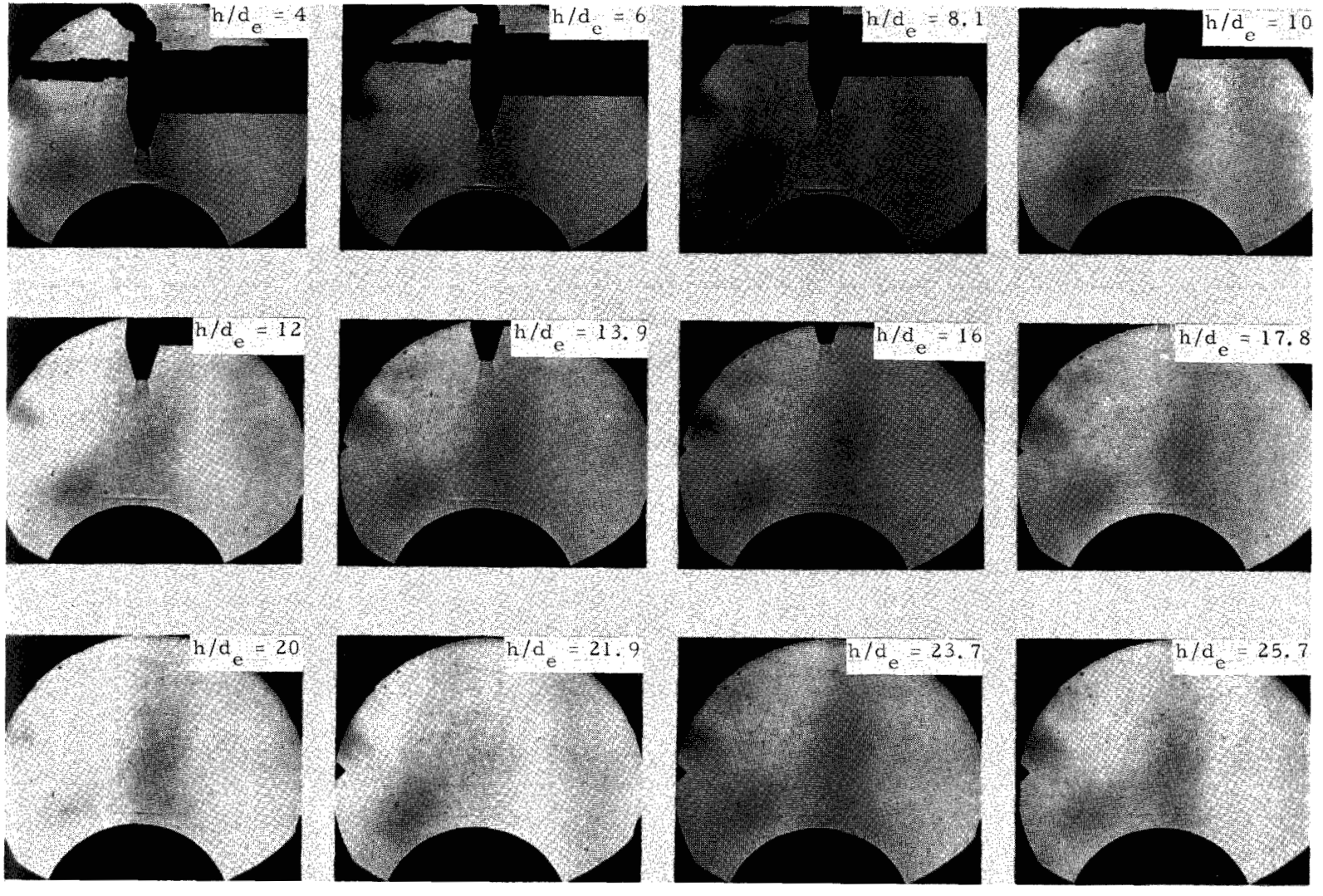

Figure 37.- Shadowgraphs of M_e = 7.09 helium jet (γ = 1.67) having d_e = 0.625 in. (1.59 cm) exhausting onto d_m = 10-in. (25.4-cm) cylinder. L-67-903

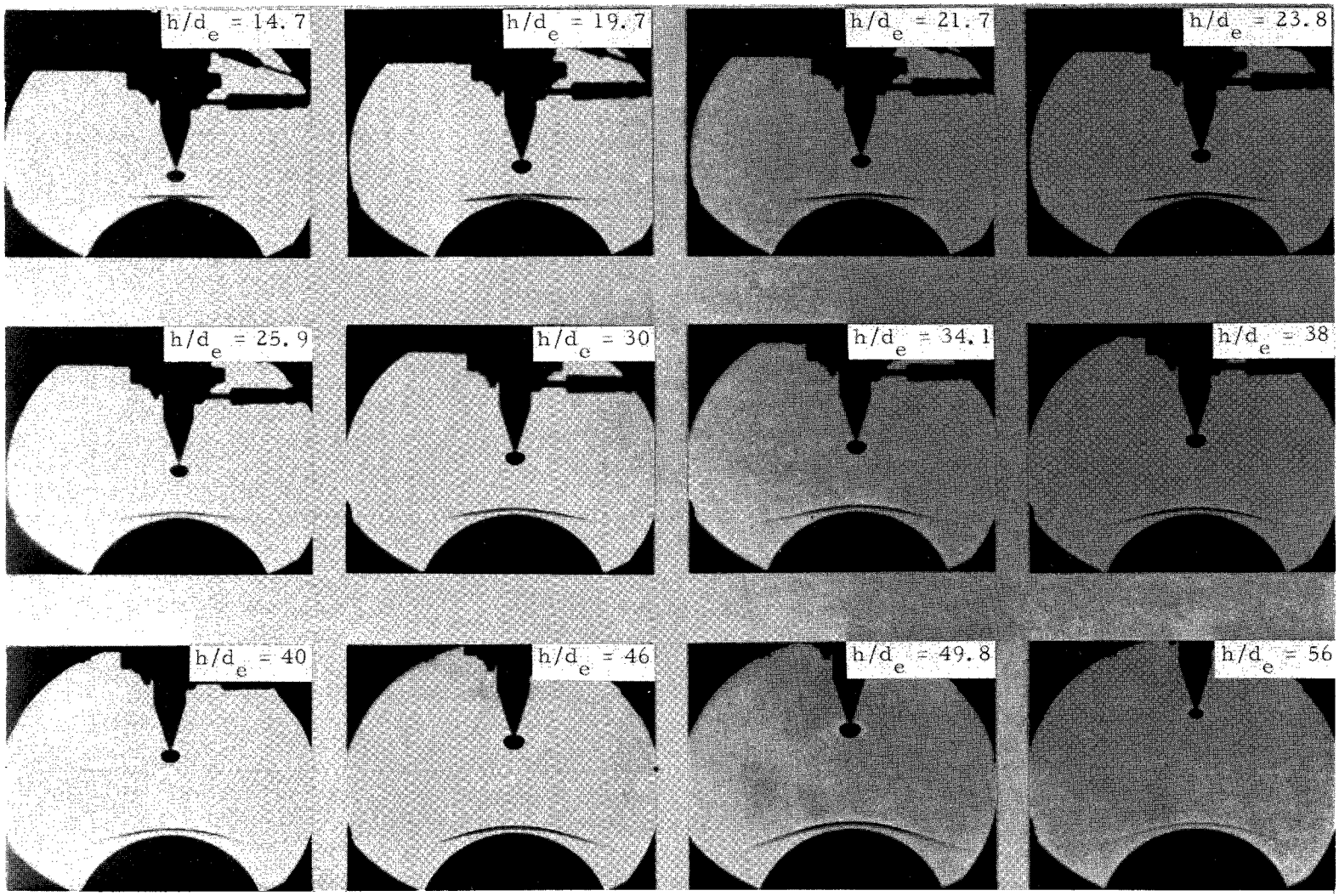

(a) Nitrogen, $\gamma = 1.4$. L-67-904

Figure 38.- Shadowgraphs of sonic jets exhausting onto d_m = 10-in. (25.4-cm) cylinder.

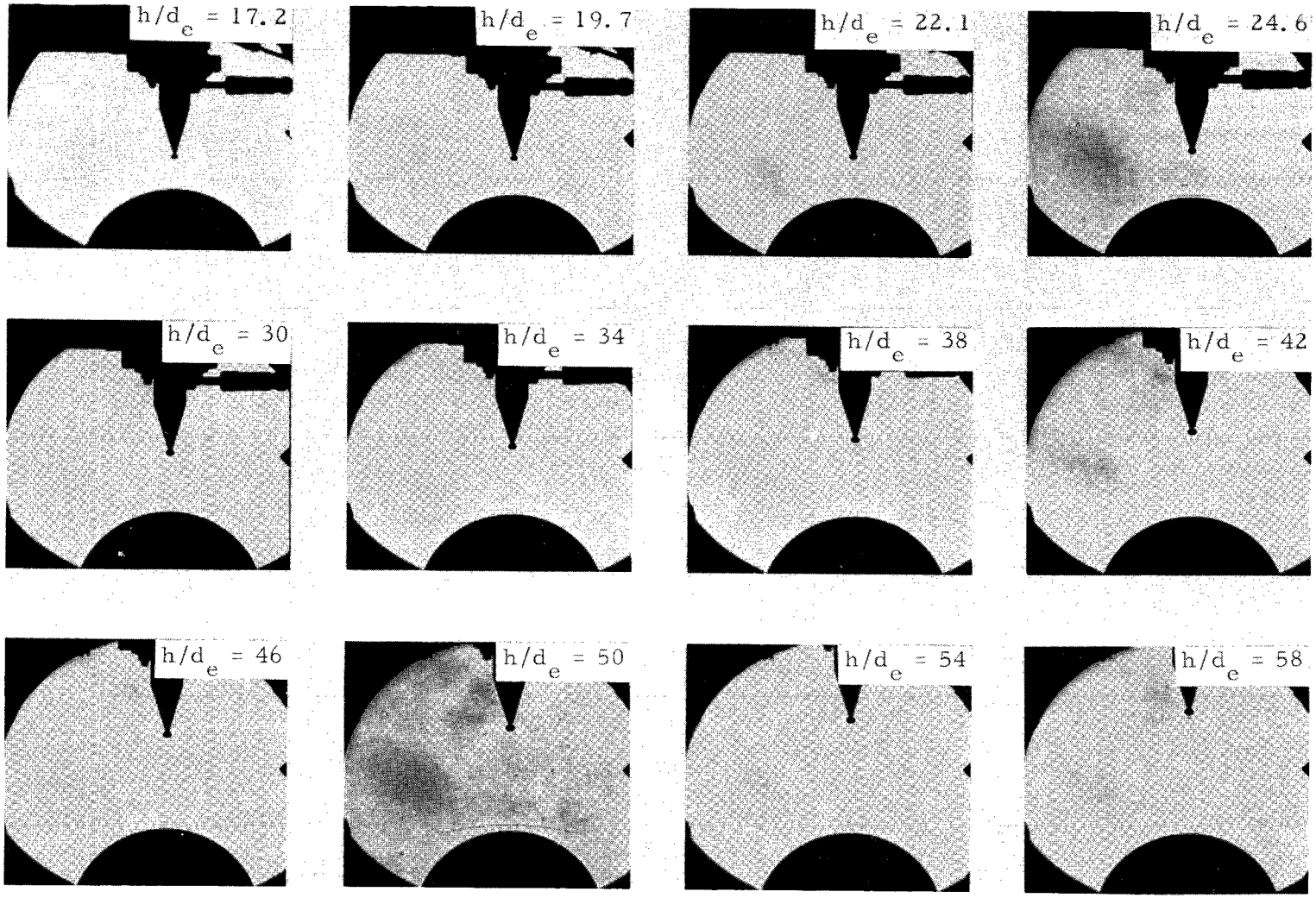

(b) Helium, $\gamma = 1.67$.

L-67-905

Figure 38.- Concluded.

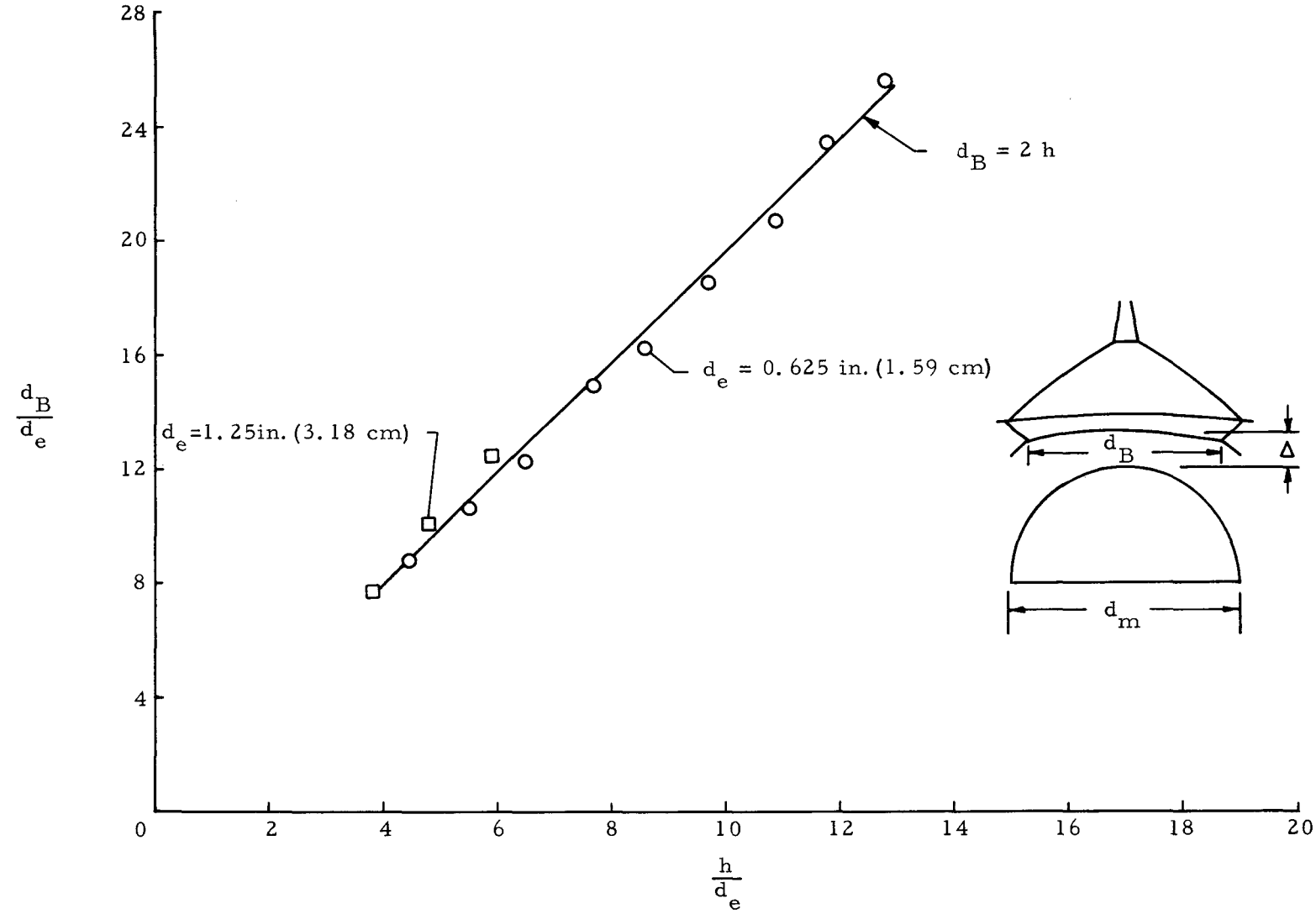

Figure 39.- Variation of shock bowl diameter with jet height for $M_e = 5$ nitrogen jets and d_m = 10-in. (25.4-cm) cylinder.

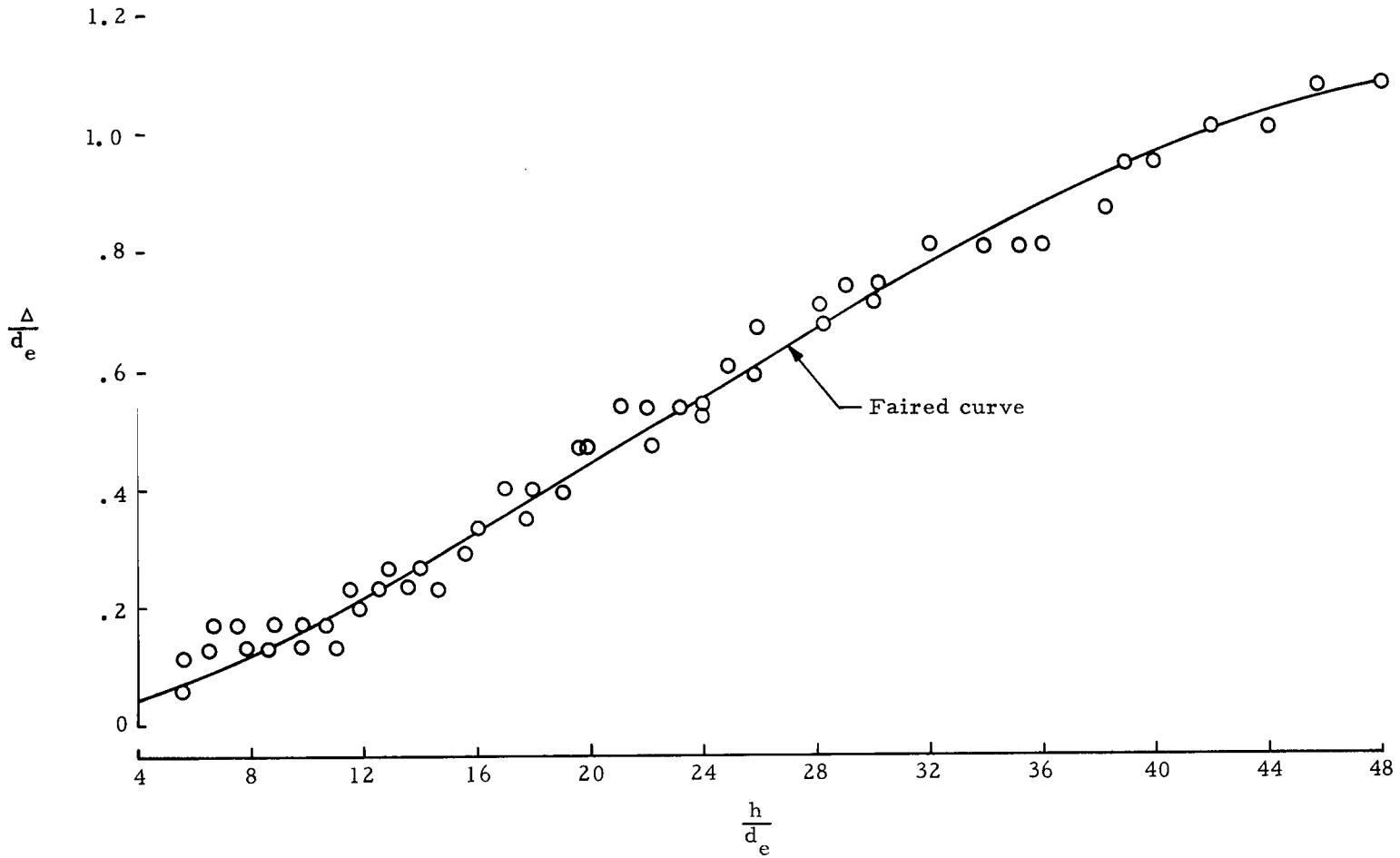

(a) d_e = 0.625 in. (1.59 cm).

Figure 40.- Variation of bow-shock standoff distance with jet height for M_e = 5 nitrogen jets and d_m = 10-in. (25.4-cm) cylinder.

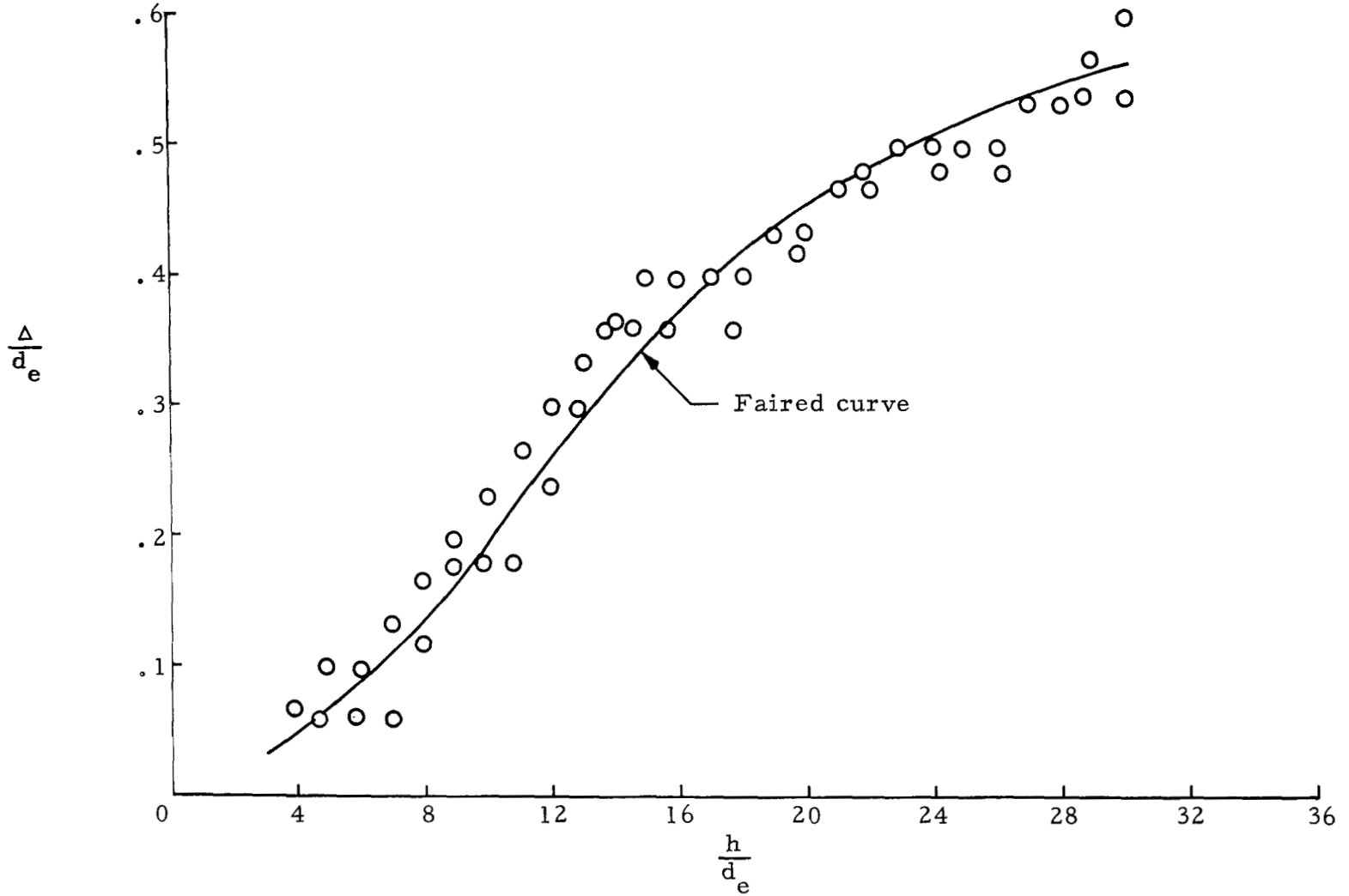

(b) d_e = 1.25 in. (3.18 cm).

Figure 40.- Concluded.

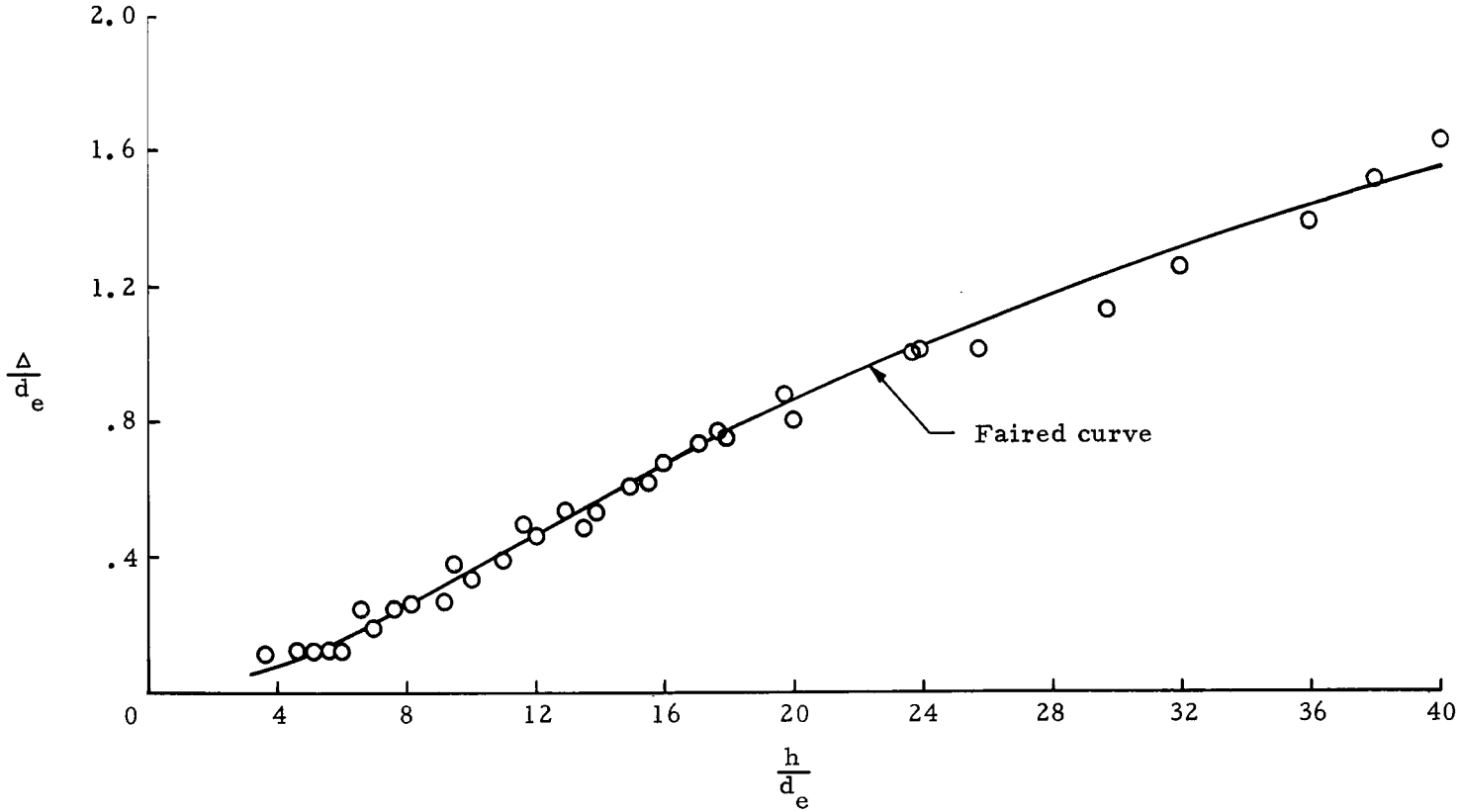

Figure 41.- Variation of bow-shock standoff distance with jet height for $M_e = 7.09$ helium jet having $d_e = 0.625$ in. (1.59 cm) and $d_m = 10$ in. (25.4 cm).

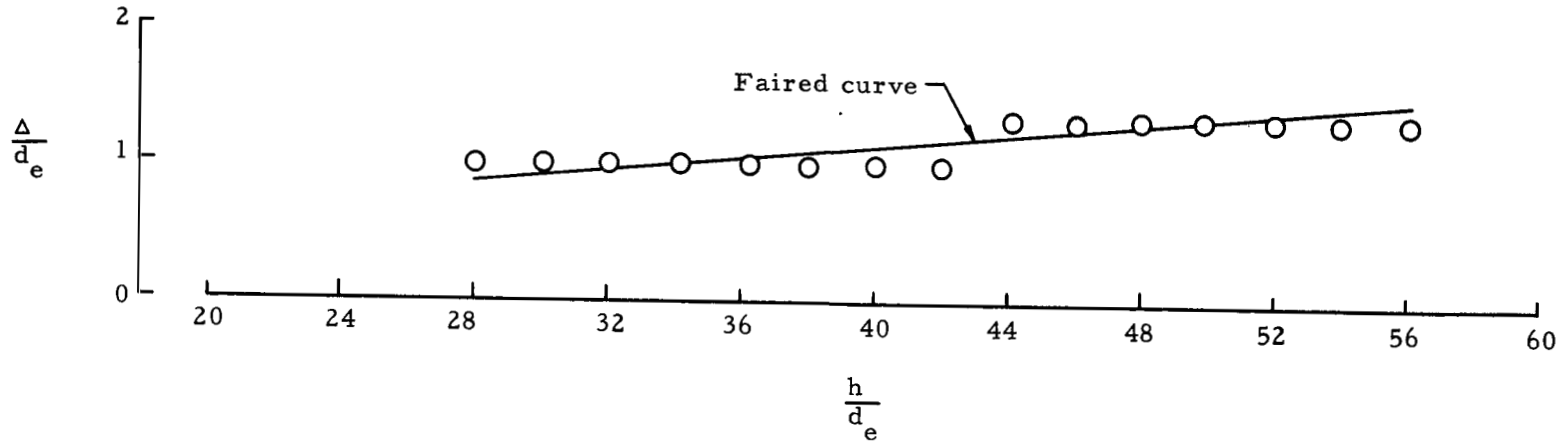

(a) Nitrogen, $\gamma = 1.4$.

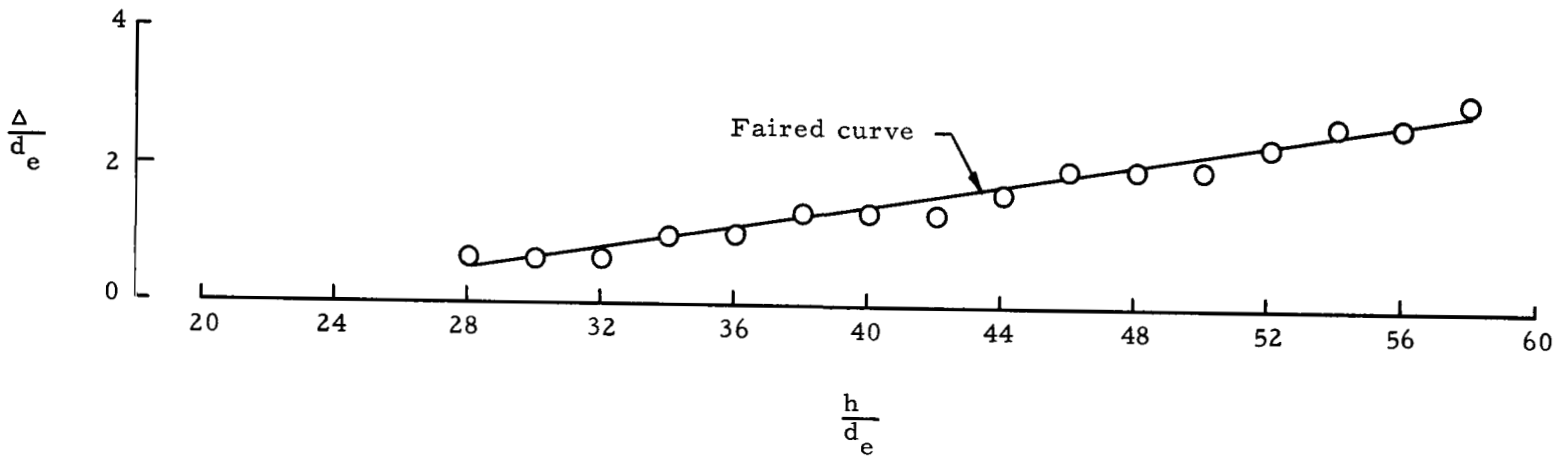

(b) Helium, $\gamma = 1.67$.

Figure 42.- Variation of bow-shock standoff distance with jet height for sonic jets and d_m = 10-in. (25.4-cm) cylinder.

"The aeronautical and space activities of the United States shall be conducted so as to contribute . . . to the expansion of human knowledge of phenomena in the atmosphere and space. The Administration shall provide for the widest practicable and appropriate dissemination of information concerning its activities and the results thereof."

—NATIONAL AERONAUTICS AND SPACE ACT OF 1958

NASA SCIENTIFIC AND TECHNICAL PUBLICATIONS

TECHNICAL REPORTS: Scientific and technical information considered important, complete, and a lasting contribution to existing knowledge.

TECHNICAL NOTES: Information less broad in scope but nevertheless of importance as a contribution to existing knowledge.

TECHNICAL MEMORANDUMS: Information receiving limited distribution because of preliminary data, security classification, or other reasons.

CONTRACTOR REPORTS: Scientific and technical information generated under a NASA contract or grant and considered an important contribution to existing knowledge.

TECHNICAL TRANSLATIONS: Information published in a foreign language considered to merit NASA distribution in English.

SPECIAL PUBLICATIONS: Information derived from or of value to NASA activities. Publications include conference proceedings, monographs, data compilations, handbooks, sourcebooks, and special bibliographies.

TECHNOLOGY UTILIZATION PUBLICATIONS: Information on technology used by NASA that may be of particular interest in commercial and other non-aerospace applications. Publications include Tech Briefs, Technology Utilization Reports and Notes, and Technology Surveys.

Details on the availability of these publications may be obtained from:

SCIENTIFIC AND TECHNICAL INFORMATION DIVISION

NATIONAL AERONAUTICS AND SPACE ADMINISTRATION

Washington, D.C. 20546